Topics in Guided-Wave Propagation Through Gyromagnetic Media

Part I — The Completely Filled Cylindrical Guide

By H. SUHL and L. R. WALKER

(Manuscript received January 26, 1954)

The characteristic equation for the propagation constants of waves in a filled circular guide of arbitrary radius is written in terms of magnetizing field and a carrier density, which are shown essentially to determine the dielectric and permeability tensors for a gas discharge plasma and for a ferrite. The complex structure of the spectrum of propagation constants and its dependence upon radius and the two parameters are analyzed by a semi-graphical method, supplemented by exact formulae in special regions. Thus the course of individual modes may be charted with fair accuracy.

1. INTRODUCTION

Any material medium which propagates electromagnetic disturbances possesses a local electric or magnetic structure and it is just the motion of the electric or magnetic carriers under the fields of the disturbance that determines how the propagation takes place. If a dc magnetic field be applied to the medium one may expect the local response to be altered and, consequently, to find changes in the character of the propagation. Gyromagnetic media are those for which such changes are sufficiently large to be experimentally significant. For plane waves and for optical frequencies the experimental effects and their explanation have been familiar for a great many years. The non-reciprocal rotation of the plane of polarization of light travelling parallel or antiparallel to an applied dc magnetic field, which is known as the Faraday effect, is such a phenomenon. So also is the fact that the medium becomes doubly refracting for arbitrary directions of propagation.

Interest in gyromagnetic media at longer wavelengths first arose in connection with radio propagation in the ionosphere. The ionosphere is essentially an ionic cloud and the earth supplies a magnetic field, which, for the charge densities involved, is sufficient to produce a large effect

upon propagation. Here, as in the earlier optical cases, the disturbances considered are essentially plane waves. In recent years, with the extensive development of microwave techniques, two gyromagnetic media have been investigated using guided waves. One of these is the gas discharge plasma, an ionic medium like the ionosphere, in which, however, the charge density may be varied over wide ranges in a controllable manner. The magnitude of the effects observed in such ionic media are governed by the relation of the applied frequency to the cyclotron frequency of the ions in the dc magnetic field. Goldstein and his associates[1] have studied the propagation of waves in a cylindrical waveguide within which a discharge is supported and to which a longitudinal magnetic field is applied. Among many effects which they have observed is a large Faraday rotation.

The other medium being actively investigated is the low-loss ferromagnetic medium, as exemplified by the ferrites. In this case the peculiarities of the medium have their origin in the precession of the magnetization of the ferrite about the applied field. This precession takes place with a frequency dependent upon the applied field strength and large changes in the nature of the propagation occur when the frequency of the r.f. applied field approaches this. Polder[2] worked out the effective properties of such a medium for plane waves and Hogan[3] has made various experimental studies of the propagation in cylindrical guides containing ferrite. Here, again, Faraday rotation and other non-reciprocal effects have been observed.

In this paper a variety of topics associated with the theory of guided waves in gyromagnetic media is considered, with the main emphasis laid on the ferrites. The exposition does not attempt to be systematic. Very few problems in this field admit of a thorough analytic treatment and, frequently, the more closely allied they are to the practical uses of ferrites in microwave devices the more fragmentary is the analysis. On the other hand since the problems can always be formulated it is always possible in specific cases to resort to a purely numerical solution. The problems considered here all arise in the effort to analyze the operation of various devices and different idealizations are utilized in particular cases.

In Part I the general properties of gyromagnetic media are discussed and the connection between the phenomenological constants of the medium and the underlying molecular model is derived for the ferrite and for the plasma. The assumptions necessary to render the ferrite problem tractable are discussed at some length. Maxwell's equations are written down for a general gyromagnetic medium and some of the salient features of their solution are noted. The propagation of circularly po-

larized waves in circularly cylindrical guide filled with ferrite or plasma is then considered. The characteristic equation connecting frequency and propagation constant is first derived. For the purpose of obtaining results which can be compared with experiment, a specific molecular model is chosen for the ferrite. In this way the ferrite itself is specified by a single parameter, its saturation magnetization, and its state by another, namely the applied field. The object of the calculation, then, is to find, for a given ferrite and a given guide radius, the mode spectrum of the wave guide and the variation of propagation constant with magnetic field. This is done by a semi-graphical method supplemented by exact analytic formulae in the neighborhood of certain critical points, series expansions in certain regions and some numerical computations in others. A sketch of a similar procedure applicable to the plasma is given.

It should be pointed out that the filled cylindrical waveguide is not a topic of the highest importance from the technical standpoint. It is for this reason that no effort is made here to obtain a comprehensive body of exact numerical information about the modes. One wishes, on the other hand, to exploit the simplifying features of the problem (as contrasted with the more useful case of a cylinder of ferrite not filling the guide) so that the discussion may be exhaustive, in the sense that the complete mode spectrum is exhibited.

In Part II we deal with cases of transverse magnetization. By that term we mean the following: the microwave fields propagate in a direction normal to the dc magnetization and they do not vary along the magnetization direction. They may then be separated into two independent sets of field components, of which only one explicitly depends on the dc magnetizing field. For these two fields wave impedances are defined which can be used for matching purposes. A few simple examples are then given. One special case, that of the "non-reciprocal helix" utilizing ferrite, is of importance in traveling-wave tube work and is discussed at length.[7] The slow-wave propagation along both a cylindrical and a "plane" helix are treated; magnetic loss is analyzed in some detail for the plane case, and general rules are given for its approximate determination in the cylindrical case.

In Part III perturbation theory and some miscellaneous topics are taken up. Suitable perturbation methods are developed for cases in which the wave guide fields are drastically modified over small volumes (as occurs if thin pencils or thin discs are inserted) and also for situations in which the local properties of the medium are but slightly disturbed over finite volumes. Among the miscellaneous topics dicusssed is the

propagation between infinite parallel planes filled with ferrite in a longitudinal magnetic field. The effect upon Faraday rotation of multiple reflections is considered.

2. THE PHYSICAL PROPERTIES

The propagation of electromagnetic waves in a medium is governed by Maxwell's equations which connect the space variations of $\underline{E}$ and $\underline{H}$, the electric and magnetic intensities with the time variations of $\underline{D}$ and $\underline{B}$, the electric displacement and magnetic induction. To characterize the particular medium relations may be given of the form $\underline{D} = \| \epsilon \| \underline{E}$ and $\underline{B} = \| \mu \| \underline{H}$ where $\| \epsilon \|$ and $\| \mu \|$ are the dielectric and permeability tensors. For disturbances whose amplitude is in some appropriate sense small, the elements of these tensors will be independent of rf amplitude, but will depend upon the dc state of the medium, upon the frequency of the signal and in unfavorable cases upon the wavelength of the latter. With the assumptions made in this paper the dependence upon wavelength will not arise.

The form of $\| \epsilon \|$ and $\| \mu \|$ may be known experimentally or it may be deduced from some molecular model of the medium. If the equations of motion of the parts of the medium are known under applied electric and magnetic fields, the displacement and magnetic induction resulting from this motion may be found explicitly. In isotropic media and in the absence of applied dc fields, each component of the displacement or of induction depends in the same way upon the associated component of $\underline{E}$ or $\underline{H}$. The tensors then become diagonal with equal elements. The application of a dc magnetic field, say in the z-direction, causes ions to circle about this field or magnetic dipoles to precess about it. It follows that a rf electric field in the ionic case or magnetic field in the ferrite, normal to the dc magnetic field, will produce a component of motion at right angles to itself and in time quadrature with it. From symmetry and from the equations of motion in a magnetic field the tensors may be expected to be now of the form

$$\begin{Vmatrix} a & -jb & 0 \\ jb & a & 0 \\ 0 & 0 & c \end{Vmatrix} \tag{1}$$

where a is an even function of magnetic field and b an odd function. c, in general, will be independent of the magnetic field.

That a and b at a given frequency and for a given sample of the medium are not independent but are related through the magnetizing dc field, H_0, is a fact of which we need not take cognizance when solving Maxwell's

equations subject to the appropriate boundary conditions. Their solution will determine the propagation constant β of a wave as a function of a and b, no matter what their interrelation. On the other hand, in a given experiment β is generally determined as a function of one parameter only: the magnetizing field H_0. Comparison of the family of calculated results $\beta = \beta(a, b)$, with the results $\beta = \beta(H_0)$, found experimentally will, of course, determine a and b as functions of H_0.

If, however, we have a prior knowledge of a and b in terms of H_0, either through postulating the correct dynamical model for the medium, or through independent experiments, we can utilize the functional form of a and b in our analysis of β, and thus arrive directly at β as a function of H_0. The distinction between the two methods is by no means academic; early introduction of such a functional form of a and b into the waveguide problem actually simplifies the analysis. Aside from this pragmatic consideration the latter method seems to us more appropriate for another reason: it is hardly the task of analysis of technical devices to check on the physical theories that give a and b as functions of H_0; such checks are made by experiments specifically designed to avoid the analytic complexities attending the solutions for most of the technically important structures.

Accordingly we adopt the more direct approach of expressing a and b in terms of H_0 (and, of course, in terms of the magnetic or electric carrier density of a given sample) throughout these papers, even in those few cases in which β can be expressed analytically as a function of a and b.

2.1 *Ferrites*

Most ferrites used in microwave applications are fully saturated in dc magnetic fields that are small compared with the dc field with which they are biased in operation. We shall therefore always postulate a fully saturated sample. Accordingly the magnetization vector $\underline{M}$ at a point in the sample will always be of constant magnitude, although its orientation will change in the ac field.

One equation of motion for M that takes this into account is

$$\frac{d\underline{M}}{dt} = \gamma[\underline{M} \times \underline{H}_T] - \frac{\gamma\alpha}{|\underline{M}|}[\underline{M} \times [\underline{M} \times \underline{H}_T]] \tag{2}$$

where $\underline{H}_T$ is a total effective magnetic field seen by the spins that make up $\underline{M}$, t is the time and γ is the gyromagnetic ratio appropriate to electron spins, whose g-factor is close to 2. The expression on the right hand side of (2) is in the nature of a torque; the force on $\underline{M}$ is always at right angles to $\underline{M}$, thus leaving its magnitude unchanged. The first term on

the right of (2) is quite well substantiated by quantum mechanical considerations. It is a vector normal to $\underline{M}$ and to the force $\underline{H}_T$ and is responsible for the precession. The second term is also a vector normal to $\underline{M}$, but is in the plane of $\underline{M}$ and $\underline{H}$ in a sense such as to reduce the angle of the precession. It thus represents a damping. Not much is known about the precise mechanism of the damping, so that its phenomenological representation by the second term of (2) is still in doubt.

$\underline{H}_T$, the total field acting on the electron spins, is made up of terms not all of which are of electromagnetic origin. It consists of the dc field $\underline{H}_0$ within the sample, the ac field $\underline{H}$, the anisotropy field, and the field ascribed to the quantum mechanical exchange forces between spins.

$\underline{H}_0$ in the sample must be calculated from the *applied* dc field $\underline{H}_{ext}$ by a purely magnetostatic calculation, which, in the case of sufficiently simple shapes, can be carried out with the help of the appropriate demagnetizing factors. Throughout this paper it is assumed that this problem has been solved, so that $\underline{H}_0$ is given. Furthermore it is assumed that $\underline{H}_{ext}$ and $\underline{H}_0$ are uniform. Boundary effects due to non-uniformities of $\underline{H}_0$ are neglected.

The microwave field $\underline{H}$ in the sample is one of the unknowns of the problem of propagation, and will appear in the solution of Maxwell's equations subject to the appropriate boundary conditions.

The anisotropy field, a property of a single crystal of ferrite, arises from the fact that through the medium of spin-orbit interaction, the electron spins can "see" the orbital wave-functions. Since these have the symmetry properties of the crystal, it is to be expected that the anisotropy field will be a vector function of $\underline{M}$, with the symmetry properties of the crystal. The samples of ferrite used in practice contain a great many small crystals randomly oriented, so that the net effect of the anisotropy field on microwave propagation must be obtained by means of an averaging procedure. The integrations involved are laborious and have not been carried out so far. We shall therefore neglect anisotropy altogether. Since anisotropy fields are usually of the order of a few hundred gauss, this will put our results in error below frequencies of about 3,000 mc/sec. (Corresponding to a precession frequency of $\gamma H_0 =$ 3,000 mc/sec., H_0 is about 1,100 gauss.)

The field between two spins ascribable to exchange forces will be zero when the two are parallel, and thus arises out of differences of spin orientation (that is, differences of $\underline{M}$) from place to place. In fact, analysis shows that this magnetic field is proportional to $\nabla^2\underline{M}$ for cubic crystals. Thus equation (2) really involves position coordinates as well as time. Hence the ac part $\underline{m}$ of $\underline{M}$ at a point will depend not only on the ac field

$\underline{H}$ at that point, but on values of $\underline{H}$ throughout the volume of the sample. Therefore $\underline{B}$, which is $\mu_0\underline{H} + \underline{m}$, will likewise be a functional of $\underline{H}$ over the whole sample. Fortunately it turns out that the spatial variation of $\underline{H}$ in a microwave structure is so much slower than that characteristic of the "spin waves" to which $\nabla^2\underline{M}$ gives rise that this effect is quite negligible at microwave frequencies. Only in the most immediate vicinity of gyromagnetic resonance could such effects become significant.

Thus, we shall regard $\underline{H}_T$ simply as the sum of the dc and ac magnetic fields, $\underline{H}_0 + \underline{H}$, and correspondingly $\underline{M}$ as the sum of the dc magnetization (directed along $\underline{H}_0$ in a saturated sample when anisotropy is neglected) plus an ac part $\underline{m}$. Equation (2) must now be solved for $\underline{m}$ in terms of $\underline{H}$. It is a non-linear equation, whose solution $\underline{m}$ will depend on $\underline{H}$ non-linearly, as will $\underline{B}$. Even if $\underline{m}$ could be determined in this way, Maxwell's equations would become non-linear, and hope of their solution remote. It is therefore necessary, and in the great majority of applications also quite sufficient, to assume that the ac quantities in (2) are so small that their products can be neglected and only linear terms taken into account. The terms $\underline{m}$ and $\underline{H}$ may now be assumed to vary as $\exp j\omega t$.

Under these circumstances, (2) becomes

$$\frac{d\underline{m}}{dt} = \gamma([\underline{m} \times \underline{H}_0] + [\underline{M}_0 \times \underline{H}]) - \frac{\alpha\gamma}{|M_0|}([\underline{M}_0 \times [\underline{m} \times \underline{H}_0]] + [\underline{M}_0 \times [\underline{M}_0 \times \underline{H}]]),$$

and is easily solved for $\underline{m}$ in terms of $\underline{H}$, and of the dc quantities H_0, M_0 which we shall assume to point in the z-direction. Each of the components m_x, m_y is a linear function of both H_x and H_y and when they are substituted in the components of the equation $\underline{B} = \mu_0\underline{H} + \underline{m}$, lead to expressions of the form (1) for $\underline{B}$ in terms of $\underline{H}$:

$$\begin{aligned} B_x &= \mu H_x - j\kappa H_y\,, \\ B_y &= j\kappa H_x + \mu H_y\,, \qquad \text{and} \\ B_z &= \mu_0 H_z\,. \end{aligned} \tag{3}$$

It is convenient to introduce two auxiliary quantities

$$\sigma = \frac{|\gamma|\,H_0}{\omega}; \qquad p = \frac{|\gamma|\,M_0}{\mu_0\omega},$$

and in terms of these one obtains the relations first derived by Polder:

$$\frac{\mu}{\mu_0} = 1 + p\,\frac{\sigma(1+\alpha^2) + j\alpha \operatorname{sgn} p}{\sigma^2(1+\alpha^2) - 1 + 2j\alpha\sigma \operatorname{sgn} p}, \qquad \text{and}$$
$$\frac{\kappa}{\mu_0} = \frac{-p}{\sigma^2(1+\alpha^2) - 1 + 2j\alpha\sigma \operatorname{sgn} p}, \tag{4}$$

where the function

$$\operatorname{sgn} p = +1 \qquad p > 0$$
$$= -1 \qquad p < 0$$

σ is the ratio of the natural precession frequency $\frac{1}{2\pi} \mid \gamma \mid H_0$ to the signal frequency. p is the ratio of a frequency $\frac{1}{2\pi} \mid \gamma \mid M_0/\mu_0$, associated with the saturation magnetization M_0, to the signal frequency. Note that σ and p always have similar signs: if H_0 is reversed, so is the saturation magnetization. Equations (4) are true only for a fully saturated sample. Therefore they hold good only for values of σ greater than the very small value corresponding to the amount of H_0 required to saturate the sample. In practice that value of H_0 is generally so small that this restriction is trivial. In the text a number of formulae will appear which apply "near $\sigma = 0$". These are to be understood as applying near the very small value of σ that corresponds to saturation.

Equation (4) has an interesting implication with regard to the loss parameter α. If α were zero, we would have

$$\frac{\mu}{\mu_0} = 1 - \frac{p\sigma}{1-\sigma^2}, \qquad \text{and}$$
$$\frac{\kappa}{\mu_0} = \frac{p}{1-\sigma^2}, \tag{5}$$

and these equations describe the loss-free case. If in equations (5), σ is replaced by $(\sigma + j\alpha \operatorname{sgn} p)$, the resulting expressions check (4) to order α. For small α, it follows that any propagation problem need be considered for the loss-free case (5) only.* The first order change due to loss in any formula so obtained can be deduced by differentiation of the formula

* A form of the damping term in Equation (2), no less justified experimentally than the one used above, is $-\frac{\alpha}{\mid \underline{M} \mid}\left(\underline{M} \times \frac{d\underline{M}}{dt}\right)$. When this expression is used the permeabilities are exactly functions of the variable, $\sigma + j\alpha \operatorname{sgn} p$.

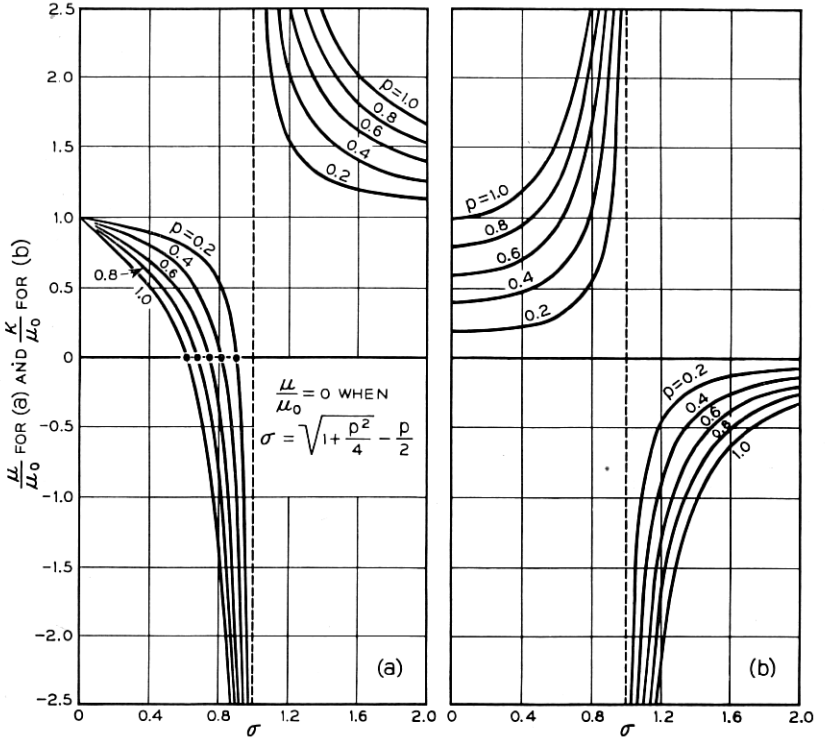

Figs. 1(a) and 1(b) — The relative permeabilities μ/μ_0 and κ/μ_0 versus σ.

with respect to σ, and multiplication by $j\alpha$ sgn p. Of course this procedure is invalid close to resonance ($\sigma = 1$), when terms in α^2 play an important part. Equations (5), which will hereafter be called the Polder equations, are plotted in Fig. 1. The quantity

$$\rho_H = \frac{\kappa}{\mu} = \frac{p}{1 - p\sigma - \sigma^2}$$

is shown in Fig. 1(c). It occurs in the waveguide theory, and also in the theory of other microwave circuits considered later on. The ratio $\mu/\mu_0 = \mu/\mu_z$ will be denoted by ν_H. At a fixed p, μ/μ_0 decreases from unity at $\sigma = 0$, through zero at $\sigma = -p/2 + \sqrt{p^2/4 + 1}$ to $-\infty$ at $\sigma = 1 - 0$, and then from $+\infty$ at $\sigma = 1 + 0$ steadily down to unity at $\sigma = \infty$. κ/μ_0 increases from p at $\sigma = 0$ to $+\infty$ at $\sigma = 1 - 0$, and then again from $-\infty$ at $\sigma = 1 + 0$ to zero at $\sigma = \infty$.

It has already been mentioned that the anisotropy fields are of the order of a few hundred gauss. For most ferrites the saturation magnetiza-

tion is about 1,000 gauss. It will therefore be consistent with the neglect of anisotropy to assume that the applied frequency is such that p is less than unity and this will be done hereafter.

2.2 *Ion clouds or plasmas*

Since these are considered in much less detail in these papers, their physical properties are stated only briefly here.

Instead of a tensor relationship between $\underline{B}$ and, $\underline{H}$ we now have one between the displacement vector $\underline{D}$ and the electric field E. If the magnetizing field is along the z axis, we have

$$\begin{aligned} D_x &= \epsilon E_x - j\eta E_y , \\ D_y &= j\eta E_x + \epsilon E_y , \text{ and} \\ D_z &= \epsilon_z E_z . \end{aligned} \tag{6}$$

If the medium consists of equal densities R of positive ions and electrons, and if collisions and thermal velocities are neglected, ϵ and η can be calculated for weak ac disturbances $\underline{E}e^{j\omega t}$ from the equation of motion

$$\dot{\underline{v}} = \frac{e}{m}\underline{E}e^{j\omega t} + \gamma[\underline{v} \times \underline{H}],$$

where $\underline{v}$ is the velocity vector of the electron and $\gamma = e\mu_0/m$, in the usual notation. When this equation is solved and the abbreviations

$$\omega_0 = |\gamma| H_0; \qquad \sigma = \frac{\omega}{\omega_0}; \qquad q = \frac{\omega_p}{\omega}; \qquad \omega_p = \frac{Re^2}{m\epsilon_0}$$

are introduced, one obtains, from the fact that the total current is $j\omega\epsilon_0\underline{E} + R\underline{v}$, the heavy ions being assumed stationary,

$$\begin{aligned} \epsilon &= \epsilon_0\left(1 + \frac{q^2}{\sigma^2 - 1}\right), \\ \eta &= \epsilon_0 \frac{q^2\sigma}{\sigma^2 - 1}, \text{ and} \\ \epsilon_z &= \epsilon_0(1 - q^2), \end{aligned} \tag{7}$$

where ϵ_0 is the dielectric constant of vacuum. The waveguide theory will involve the parameters

$$\begin{aligned} \nu_E &= \frac{\epsilon}{\epsilon_z} = 1 - \frac{\sigma^2 q^2}{(1 - \sigma^2)(1 - q^2)}, \text{ and} \\ \rho_E &= \frac{\eta}{\epsilon} = \frac{q^2\sigma}{\sigma^2 + q^2 - 1}. \end{aligned} \tag{8}$$

These results apply to stationary plasmas only. If the plasma were an electron stream moving along the wave-propagation direction, for example, the dielectric constants would depend on wavelength also, and the propagation problem would be much more involved.

The variations of ϵ and η with σ are shown in Fig. 2. ϵ/ϵ_0 for a given q^2 starts at $\sigma = 0$, $\epsilon = \epsilon_0 (1 - q^2)$, decreases through zero at $\sigma = \sqrt{1 - q^2}$ to $-\infty$ at $\sigma = 1 - 0$, starts again from $+\infty$ at $\sigma = 1 + 0$, and decreases to ϵ_0 at $\sigma = \infty$. $\eta = 0$ when $\sigma = 0$, decreases to $-\infty$ at $\sigma = 1 - 0$ and then decreases from $+\infty$ at $1 + 0$ to zero at $\sigma = \infty$.

We note that similar formulae apply to the electron-gas in semiconductors at temperatures sufficiently low and frequencies sufficiently high so that damping is not important. However, the formulae have to be

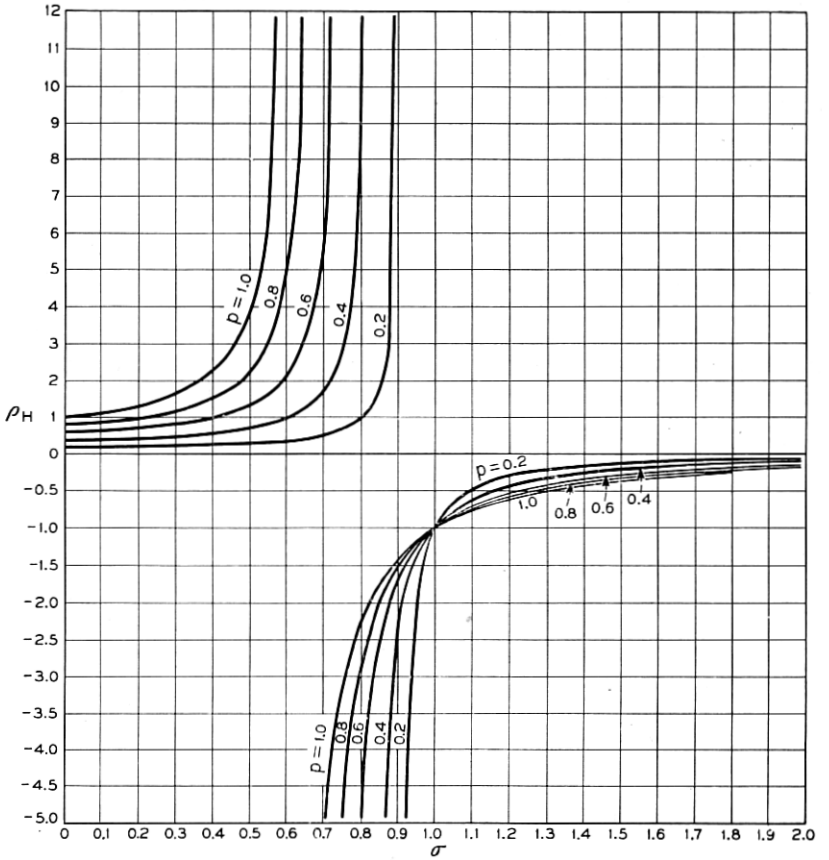

Fig. 1(c) — The ratio $\rho_H = \kappa/\mu$ versus σ.

generalized in some of those cases to take into account the existence of groups of electrons with different "effective masses" m.

3. THE SOLUTION OF MAXWELL'S EQUATIONS

Maxwell's equations will now be solved in a cylindrical waveguide filled with a hypothetical medium which contains the ferrite and the plasma as a special case. It will be supposed therefore that both its permeability and dielectric constant are tensors of the form previously considered.

3.1 *Field components*

The following notation will be found convenient. The projection of a vector $\underline{A}$ upon the plane normal to the z-axis will be written $\underline{A}_t$. If the components of $\underline{A}_t$ are α, β then an associated vector having components $(\beta, -\alpha)$ is devoted by $\underline{A}_t{}^*$. A similar notation is used for differential operators. Thus, if ∇ denotes $(\partial/\partial x, \partial/\partial y)$, ∇^* denotes $(\partial/\partial y, -\partial/\partial x)$†. Denoting scalar products by a dot, the following identities are evident

$$\underline{A}_t{}^* \cdot \underline{A}_t{}^* = \underline{A}_t \cdot \underline{A}_t ; \qquad (\underline{A}_t{}^*)^* = -\underline{A}_t ; \qquad \underline{A}_t \cdot \underline{A}_t{}^* = 0;$$
$$\underline{A}_t \cdot \underline{B}_t{}^* = -\underline{A}_t{}^* \cdot \underline{B}_t ;$$

and

$$\underline{A}_t \cdot \underline{B}_t{}^* = z\text{-component of } [\underline{A} \times \underline{B}].$$

Also if $\underline{k}$ is a unit vector along the positive z-axis, $\underline{k} \times \underline{A} = -\underline{A}_t{}^*$. Similar relations hold for differential operators. If one denotes the starring operation by the symbol P then clearly

$$P^2 = -1; \qquad P^{-1} = -P; \qquad \frac{1}{P + a} = \frac{1}{1 + a^2}(a - P),$$

where a is a number.

Maxwell's equations may now be written, for that case in which the dependence of any component upon t and z is of the form $e^{j(\omega t - \beta z)}$, in the form:

$$\begin{aligned} \nabla^* H_z + j\beta \underline{H}_t{}^* &= j\omega\epsilon \underline{E}_t + \omega\eta \underline{E}_t{}^*, \\ \nabla \cdot \underline{H}_t{}^* &= j\omega\epsilon_z E_z , \\ \nabla^* E_z + j\beta \underline{E}_t{}^* &= -j\omega\mu \underline{H}_t - \omega\kappa \underline{H}_t{}^*, \text{ and} \\ \nabla \cdot \underline{E}_t{}^* &= -j\omega\mu_z H_z , \end{aligned} \tag{9}$$

where use is made of equations (3) and (6).

† The operator ∇^* is called "flux" by Schelkunoff. Strictly, one should write ∇_t and $\nabla_t{}^*$, rather than ∇ and ∇^*, but this is needlessly cumbersome.

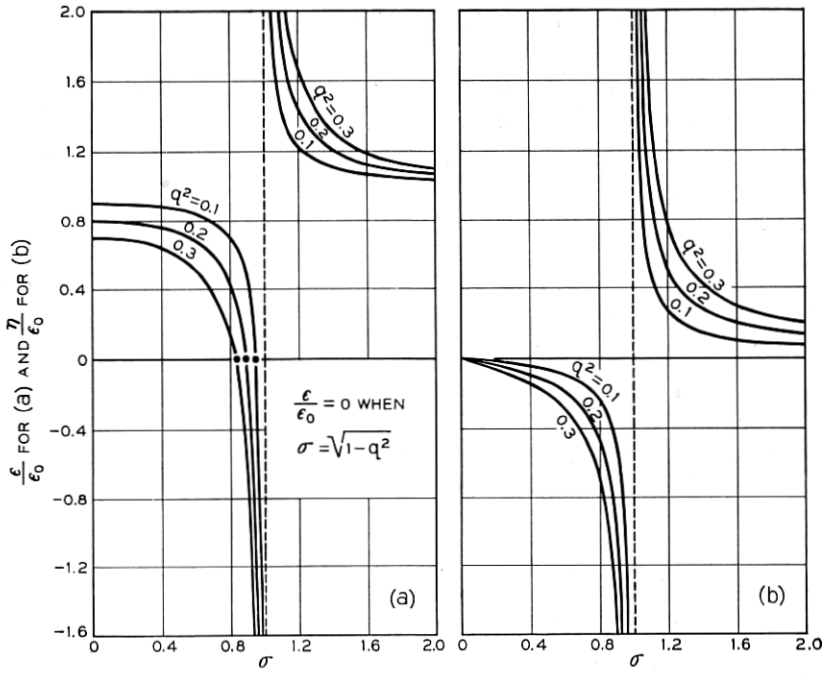

Figs. 2(a) and 2(b) — The relative dielectric constants ϵ/ϵ_0 and η/ϵ_0 versus σ.

It is desirable to remove scale factors as far as possible. A unit of length given by

$$\frac{1}{\beta_0} = \frac{1}{\omega\sqrt{\mu_z\epsilon_z}}$$

will be used to measure lengths. This unit is $\lambda_0/2\pi$, where λ_0 is the wavelength in an unbounded, unmagnetized medium. It will be assumed that β is in future measured in units of β_0. Finally all magnetic fields will be multiplied by $\sqrt{\mu_z/\epsilon_z}$ to give them the dimensions of electric fields. Using the definitions of the ν's and ρ's given in Section 2, Maxwell's equations may be put into the form:

$$\nabla^* H_z + j\beta \underline{H}_t^* = \nu_E(j\underline{E}_t + \rho_E \underline{E}_t^*), \tag{10a}$$

$$\nabla \cdot \underline{H}_t^* = jE_z, \tag{10b}$$

$$\nabla^* E_z + j\beta \underline{E}_t^* = -\nu_H(j\underline{H}_t + \rho_H \underline{H}_t^*), \tag{10c}$$

and

$$\nabla \cdot \underline{E}_t^* = -iH_z. \tag{10d}$$

$\underline{E}_t$ and $\underline{H}_t$ may now be eliminated yielding two simultaneous second order equations for E_z and H_z. These, in turn, may be combined to produce two independent second order equations each of which is satisfied by an appropriate linear combination of E_z and H_z. These equations may be solved and E_z and H_z expressed as linear combinations of the solutions. The transverse fields are then written in terms of E_z and H_z and, finally, the boundary conditions are applied leaving a transcendental equation in β^2.

Operating on (10a) and (10c) with $\nabla\cdot$ and taking account of (10b), (10d), one finds that

$$\begin{aligned} j\beta\nabla\cdot\underline{H}_t^* &= \nu_E(j\nabla\cdot\underline{E}_t + j\rho_E H_z) \quad = -\beta E_z\,, \text{ and} \\ j\beta\nabla\cdot\underline{E}_t^* &= -\nu_H(j\nabla\cdot\underline{H}_t + j\rho_H E_z) = \beta H_z \end{aligned} \tag{11}$$

Operating on (10a) and (10c) with $\nabla^*\cdot$, using $\nabla^*\cdot\nabla^* = \nabla^2$ and so on, one obtains, using (10b) and (10d),

$$\begin{aligned} \nabla^2\underline{H}_z + j\beta\nabla\cdot H_t &= \nu_E(-H_z + \rho_E\nabla\cdot\underline{E}_t), \text{ and} \\ \nabla^2\underline{E}_z + j\beta\nabla\cdot E_t &= -\nu_H(E_z + \rho_H\nabla\cdot\underline{H}_t). \end{aligned} \tag{12}$$

Now, elimination of $\nabla\cdot E_t$ and $\nabla\cdot H_t$ between (11) and (12) yields

$$\begin{aligned} \nabla^2 H_z + \nu_E\left(1 - \rho_E{}^2 - \frac{\beta^2}{\nu_E\nu_H}\right)H_z &= j\beta(\rho_E + \rho_H)E_z\,, \text{ and} \\ \nabla^2 E_z + \nu_H\left(1 - \rho_H{}^2 - \frac{\beta^2}{\nu_E\nu_H}\right)E_z &= -j\beta(\rho_E + \rho_H)H_z\,, \end{aligned} \tag{13}$$

equations which demonstrate that pure TE or TM fields no longer exist, as the result of the presence of ρ's. H_z or E_z might now be eliminated between these equations giving a single equation in ∇^2 and $(\nabla^2)^2$, but it is more convenient to find those linear combinations of E_z and H_z which satisfy a first order equation in ∇^2. Writing such a linear combination as

$$\psi = E_z + j\Lambda H_z\,, \tag{14}$$

and adding $j\Lambda$ times the first of equations (13) to the second, it is found that this is an equation in ψ alone of the form

$$\nabla^2\psi + \chi^2\psi = 0, \tag{15}$$

provided that Λ is a root of the quadratic

$$\Lambda^2 - \frac{\nu_E\left(1 - \rho_E{}^2 - \frac{\beta^2}{\nu_E\nu_H}\right) - \nu_H\left(1 - \rho_H{}^2 - \frac{\beta^2}{\nu_E\nu_H}\right)}{\beta(\rho_E + \rho_H)}\Lambda - 1 = 0. \tag{16}$$

The value of χ^2 is then given by

$$\chi_{1,2}^{\ 2} = \nu_E \left(1 - \rho_E^{\ 2} - \frac{\beta^2}{\nu_E \nu_H}\right) - \beta(\rho_E + \rho_H)\Lambda_{2,1}\,, \tag{17a}$$

or

$$\chi_{1,2}^{\ 2} = \nu_H \left(1 - \rho_H^{\ 2} - \frac{\beta^2}{\nu_E \nu_H}\right) + \beta(\rho_E + \rho_H)\Lambda_{1,2}\,, \tag{17b}$$

where Λ_1 and Λ_2 are the roots of (16) and $\chi_1^{\ 2}$, $\chi_2^{\ 2}$ are the corresponding χ^2. The labelling of the roots is not important, but consistency must be maintained. From (14) E_z and H_z must satisfy

$$E_z + j\Lambda_1 H_z = \psi_1\,,$$

and

$$E_z + j\Lambda_2 H_z = \psi_2$$

so that

$$E_z = \frac{\Lambda_2\psi_1 - \Lambda_1\psi_2}{\Lambda_2 - \Lambda_1}\,, \tag{18a}$$

and

$$H_z = j\,\frac{\psi_1 - \psi_2}{\Lambda_2 - \Lambda_1}\,. \tag{18b}$$

Solutions of (15) may now be sought in cylindrical coordinates. To satisfy the boundary conditions in circular guide it will be necessary to assume the solutions to vary as $e^{jn\theta}$, where θ is the polar angle and n is any integer, positive, negative or zero. Equation (15) then becomes

$$\frac{1}{r}\frac{\partial}{\partial r}\left(r\,\frac{\partial\psi_{1,2}(r)}{\partial r}\right) + \left(\chi_{1,2}^{\ 2} - \frac{n^2}{r^2}\right)\psi_{1,2}(r) = 0,$$

if r is the radius. Solutions which are regular within the guide will have the form of constant multiples of $J_n(\chi_{1,2}r)$, where J_n is the n^{th} order Bessel function. The solutions of (15) are, then,

$$\psi_{1,2} = A_{1,2}J_n(\chi_{1,2}r)e^{jn\theta}, \tag{19}$$

where the A's are constants. E_z and H_z can be found now from (18), but further equations must be found to express $\underline{E}_t$ and $\underline{H}_t$. Using P to denote the starring operation, (10a) and (10c) may be re-written as

$$(j\nu_F P - \rho_E\nu_E)\underline{E}_t + j\beta\underline{H}_t = -\nabla\underline{H}_z\,,$$

and

$$-j\beta \underline{E}_t + (j\nu_H P - \rho_H \nu_H)\underline{H}_t = \nabla E_z ,$$

which yield

$$\{[\nu_E\nu_H(1 + \rho_E\rho_H) - \beta^2] - j\nu_H\nu_E(\rho_H + \rho_E)P\}\underline{E}_t = -j\beta\nabla E_z - \nu_H(jP - \rho_H)\nabla H_z ,$$

and

$$\{[\nu_E\nu_H(1 + \rho_E\rho_H) - \beta^2] - j\nu_H\nu_E(\rho_H + \rho_E)P\}\underline{H}_t = \nu_E(jP - \rho_E)\nabla E_z - j\beta\nabla H_z$$

The term in parentheses may be removed by using the rule for inverting such expressions in P which was given earlier. This process gives

$$\Omega\underline{E}_t = \left[\left(1 + \rho_E\rho_H - \frac{\beta^2}{\nu_E\nu_H}\right) + j(\rho_H + \rho_E)P\right] [- j\beta\nabla E_z - \nu_H(jP - \rho_H)\nabla H_z], \tag{20a}$$

and

$$\Omega\underline{H}_t = \left[\left(1 + \rho_E\rho_H - \frac{\beta^2}{\nu_E\nu_H}\right) + j(\rho_H + \rho_E)P\right] [\nu_E(jP - \rho_E)\nabla E_z - j\beta\nabla H_z], \tag{20b}$$

where

$$\Omega = \nu_E\nu_H\left[\left(1 + \rho_E\rho_H - \frac{\beta^2}{\nu_E\nu_H}\right)^2 - (\rho_E + \rho_H)^2\right],$$

$$= \nu_E\nu_H\left[\frac{\beta^2}{\nu_E\nu_H} - (1 + \rho_E)(1 + \rho_H)\right]\left[\frac{\beta^2}{\nu_E\nu_H} - (1 - \rho_E)(1 - \rho_H)\right].$$

It may be noted that for plane waves in the unbounded medium along the z axis, which have $E_z = H_z = 0$, Ω must vanish and that the propagation constants for such plane waves are evidently given by

$$\beta^2 = \nu_E\nu_H(1 \pm \rho_E)(1 \pm \rho_H). \tag{21}$$

The values of E_z and H_z given by (18) may now be substituted in (20) and the operator P removed. This gives, finally,

$$(\Lambda_1 - \Lambda_2)\Omega\underline{E}_t = j\left[\left(1 + \rho_E\rho_H - \frac{\beta^2}{\nu_E\nu_H}\right)(\beta\Lambda_2 - \rho_H\nu_H) + \nu_H(\rho_H + \rho_E)\right]\nabla\psi_1 - \left[(\beta\Lambda_2 - \rho_H\nu_H)(\rho_E + \rho_H) + \nu_H\left(1 + \rho_E\rho_H - \frac{\beta^2}{\nu_E\nu_H}\right)\right]\nabla^*\psi_1 \tag{22a}$$

minus the same expression with suffixes 1 and 2 interchanged.

$$(\Lambda_1 - \Lambda_2)\Omega \underline{H}_t = \left[\left(1 + \rho_E\rho_H - \frac{\beta^2}{\nu_E\nu_H}\right)(\Lambda_2\nu_E\rho_E - \beta) - \nu_E\Lambda_2(\rho_E + \rho_H)\right]\nabla\psi_1$$
$$- j\left[\nu_E\Lambda_2\left(1 + \rho_E\rho_H - \frac{\beta^2}{\nu_E\nu_H}\right) - (\rho_E + \rho_H)(\Lambda_2\nu_E\rho_E - \beta)\right]\nabla^*\psi_1 \qquad (22b)$$

minus the same expression with suffixes 1 and 2 interchanged.

Equations (22a) and (22b) may be written in a variety of equivalent forms by making use of the relations between Λ_1 and Λ_2. The manipulations which have been used in deriving (22a) and (22b) assume the use of rectangular coordinates, but the results are valid in polar coordinates if $\underline{E}_t$ means (E_r, E_θ) and ∇ means $\left(\frac{\partial}{\partial r}, \frac{1}{r}\frac{\partial}{\partial\theta}\right)$. That this is the case may be seen from the consideration that the rotation, $-\theta$, which carries the vector (E_x, E_y) into the vector (E_r, E_θ) also transforms $\left(\frac{\partial}{\partial x}, \frac{\partial}{\partial y}\right)$ into $\left(\frac{\partial}{\partial r}, \frac{1}{r}\frac{\partial}{\partial\theta}\right)$.*

3.2 *The characteristic equation*

The boundary conditions of the problem are that $E_z = 0$ and $E_\theta = 0$ at $r = r_0$, the radius of the guide. E_z is given by [see (18)].

$$(\Lambda_2 - \Lambda_1)E_z = [\Lambda_2 A_1 J_n(\chi_1 r) - \Lambda_1 A_2 J_n(\chi_2 r)]e^{jn\theta}, \qquad (23)$$

and vanishes at $r = r_0$ if

$$A_1 = \frac{J_n(\chi_2 r_0)}{\Lambda_2}; \qquad A_2 = \frac{J_n(\chi_1 r_0)}{\Lambda_1}.$$

Hence the relations hold:

$$\psi_{1,2} = \frac{1}{\Lambda_{2,1}} J_n(\chi_{2,1} r_0) J_n(\chi_{1,2} r) e^{jn\theta}.$$

From (22a) it follows that

$$(\Lambda_1 - \Lambda_2)\Omega E_\theta = \frac{J_n(\chi_2 r_0)e^{jn\theta}}{\Lambda_2}\left[-\frac{n}{r}\left\{\left(1 + \rho_E\rho_H - \frac{\beta^2}{\nu_E\nu_H}\right)(\beta\Lambda_2 - \rho_H\nu_H)\right.\right.$$
$$\left.+ \nu_H(\rho_H + \rho_E)\right\} J_n(\chi_1 r) + \left\{(\beta\Lambda_2 - \rho_H\nu_H)(\rho_E + \rho_H)\right.$$
$$\left.\left. + \nu_H\left(1 + \rho_E\rho_H - \frac{\beta^2}{\nu_E\nu_H}\right)\right\}\chi_1 J_n'(\chi_1 r)\right]$$

* In Appendix III the field components in polar coordinates are written out fully for the ferrite and plasma cases with some changes in notation which are introduced in Sections 4.11 and 4.2.

minus the same expression with the suffixes interchanged. Hence

$$
\begin{aligned}
&(\Lambda_1 - \Lambda_2)\Omega E_\theta(r_0) \\
&= \frac{J_n(\chi_1 r_0)J_n(\chi_2 r_0)e^{jn\theta}}{r_0}\left[(\Lambda_1 - \Lambda_2)n\nu_H\left(\frac{\rho_H\beta^2}{\nu_E\nu_H} + \rho_E(1 - \rho_H{}^2)\right)\right. \\
&\quad + \left\{\beta(\rho_E + \rho_H) - \Lambda_1\nu_H\left(1 - \rho_H{}^2 - \frac{\beta^2}{\nu_E\nu_H}\right)\right\}\frac{\chi_1 r_0 J_n'(\chi_1 r_0)}{J_n(\chi_1 r_0)} \\
&\quad \left. - \left\{\beta(\rho_E + \rho_H) - \Lambda_2\nu_H\left(1 - \rho_E{}^2 - \frac{\beta^2}{\nu_E\nu_H}\right)\right\}\frac{\chi_2 r_0 J_n'(\chi_2 r_0)}{J_n(\chi_2 r_0)}\right],
\end{aligned}
\tag{24}
$$

where use has been made of the relation $\Lambda_1\Lambda_2 = -1$. Therefore the characteristic equation for β^2 is obtained by equating the term in square brackets to zero. Because of the quadratic relation satisfied by Λ and the relation between Λ and χ, it is possible to write the characteristic equation in a great variety of ways. It will be convenient to introduce a function

$$
F_n(x) = F_{-n}(x) = \frac{xJ_n'(x)}{J_n(x)}. \tag{25}
$$

Using the F-function and replacing the Λ's by χ's the characteristic equation may be written:*

$$
\begin{aligned}
n\nu_H(\chi_2{}^2 - \chi_1{}^2)\left[\frac{\rho_H\beta^2}{\nu_E\nu_H} + \rho_E(1 - \rho_H{}^2)\right]\frac{1}{\beta(\rho_E + \rho_H)} &= \frac{\chi_2{}^2}{\Lambda_2}F_n(\chi_1 r_0) \\
&\quad - \frac{\chi_1{}^2}{\Lambda_1}F_n(\chi_2 r_0).
\end{aligned}
\tag{26}
$$

The asymmetry of this equation between ρ_H, ν_H and ρ_E, ν_E arises from the fact that the boundary conditions involve electric field components alone.

It may be noted that if the basic solution had been taken to vary as $\cos n\theta$ or $\sin n\theta$, the expression for E_θ would have been a linear combination of $\sin n\theta$ and $\cos n\theta$ that could not have vanished at the walls for all θ.

In passing we remark that for a guide of arbitrary cross-section, the

* The characteristic equations given in Reference 4 were specializations to the ferrite and plasma cases of the form in square brackets. They have also been derived by Kales[5] and Gamo[6]. These authors have given expressions for some, though not all, of the varieties of cut-off point derived in this paper and classified them as TE or TM according to the field configuration at cut-off. By contrast, they are classified here by their association with quasi-TE or quasi-TM limit modes which reduce to the usual TE and TM modes in the unmagnetized medium.

boundary value problem may be put into the form, of which (26) is a special case,

$$\nabla^2 f_1 + \chi_1^2 f_1 = 0,$$

and

$$\nabla^2 f_2 + \chi_2^2 f_2 = 0,$$

$$j\left(\frac{\chi_2^2}{\Lambda_2}\frac{\partial f_1}{\partial N} - \frac{\chi_1^2}{\Lambda_1}\frac{\partial f_2}{\partial N}\right) = \frac{\nu_H(\chi_2^2 - \chi_1^2)}{\beta(\rho_E + \rho_H)}\left[\frac{\rho_H\beta^2}{\nu_E\nu_H} + \rho_E(1 - \rho_H^2)\right]\frac{\partial f_1}{\partial S},$$

where $\partial/\partial N$ and $\partial/\partial S$ are normal and tangential derivatives at the guide surface, where, in addition, $f_1 = f_2$.

4. DISCUSSION OF THE PROPAGATION CONSTANTS

At this point we specialize the characteristic equation (26) to one or other of the two media.

4.1. *The ferrite* ($\rho_E = 0$, $\nu_E = 1$)

4.11. After some rearrangement the characteristic equation becomes

$$\frac{1}{\chi_1^2}\left[\frac{F_n(\chi_1 r_0)}{\lambda_1} - n\right] = \frac{1}{\chi_2^2}\left[\frac{F_n(\chi_2 r_0)}{\lambda_2} - n\right], \tag{27}$$

where $\lambda_{2,1} = \beta\,\Lambda_{1,2}$ and the λ satisfy

$$\lambda_{1,2}^2 - \frac{(1 - \nu_H)\left(1 - \dfrac{\beta^2}{\nu_H}\right) + \nu_H\rho_H^2}{\rho_H}\lambda_{1,2} - \beta^2 = 0. \tag{28}$$

The χ's are given by

$$\chi_{1,2}^2 = \left(1 - \frac{\beta^2}{\nu_H}\right) - \rho_H\lambda_{1,2}. \tag{29}$$

From Polder's equations for ρ_H and ν_H, (28) may be written

$$\lambda_{1,2}^2 - [p + \sigma(1 - \beta^2)]\lambda_{1,2} - \beta^2 = 0, \tag{30}$$

or

$$\lambda_1\lambda_2 = -\beta^2, \tag{31a}$$

$$\lambda_1 + \lambda_2 = p + \sigma(1 - \beta^2),$$

$$= p + \sigma + \sigma\lambda_1\lambda_2. \tag{31b}$$

If β^2 be eliminated between equations (28) and (29), $\chi_{1,2}^2$ may be ex-

pressed solely in terms of $\lambda_{1,2}$, ρ_H and ν_H in the form

$$\chi_{1,2}^2 = \frac{1 - \lambda_{1,2}^2}{\dfrac{1}{1 - \dfrac{\nu_H}{\rho_H}\lambda_{1,2}} - 1}.$$

Again using Polder's formulae, this becomes

$$\chi_{1,2}^2 = \frac{1 - \lambda_{1,2}^2}{1 - \sigma\lambda_{1,2}}. \tag{32}$$

With these expressions for the χ, the characteristic equation takes the form

$$G(\lambda_1, \sigma, r_0) = G(\lambda_2, \sigma, r_0), \tag{33}$$

where

$$G(\lambda, \sigma, r_0) = \frac{1 - \sigma\lambda}{1 - \lambda^2}\left[\frac{1}{\lambda} F_n\left(r_0\sqrt{\frac{1 - \lambda^2}{1 - \sigma\lambda}}\right) - n\right]. \tag{34}$$

Equations (31b) and (33) may now be considered for a fixed σ and p as determining associated pairs of values for λ_1 and λ_2. Such a pair in turn determines $\beta^2 = -\lambda_1\lambda_2$. Since β^2 must be positive for propagation λ_1, λ_2 must have opposite signs. The convention will be adopted that λ_1 is positive and λ_2 is negative. Equation (31b) will hereafter be called the Polder relation and Equation (33) the G-equation.

An important fact of which frequent use will be made is that the transformation

$$\lambda_1 \to -\lambda_2, \qquad \lambda_2 \to -\lambda_1, \qquad \sigma \to -\sigma, \qquad p \to -p$$

leaves the Polder relation and β^2 unchanged and converts n to $-n$ in the G-equation. It follows that it is necessary to consider positive n only, provided we allow the pair σ, p to take on negative as well as positive values. This corresponds to the physical fact that a right-circular wave in a backward-directed magnetizing field behaves like a left-circular wave in a forward field.

The discussion in this paper is confined to the first azimuthal mode number $n = \pm 1$. Accordingly the symbol F will replace F_1 in what follows.

Before commencing the graphical analysis of the G function it is advantageous to consider briefly the function $F(x) = xJ_1'(x)/J_1(x)$, which we require for real and for purely imaginary x. By logarithmic differentia-

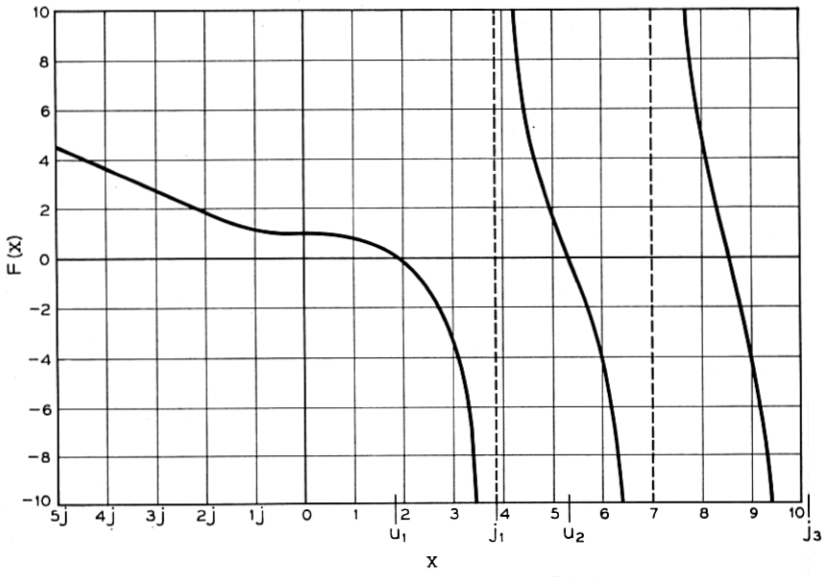

Fig. 3 — The function $F(x) = \dfrac{xJ_1'(x)}{J_1(x)}$.

tion of the infinite product for $J_1(x)$, $F(x)$ is found to be given by

$$F(x) = 1 - 2\sum_{n=1}^{\infty} \frac{x^2}{j_n^2 - x^2},$$

where the j_n's are the zeros of $J_1(x)$.

Thus, $F(x)$ is real if x^2 is, which is always the case here. For positive x, $F(x)$ is an always decreasing function of x, which has an infinite number of first order zeros and poles. The zeros are those of $J_1'(x)$ and will be denoted by u_n . The poles are the zeros of $J_1(x)$. It may be recalled from the properties of Bessel functions that for large n these zeros and poles are essentially equally spaced with a separation $\pi/2$. When x is a pure imaginary, equal to jy, $F(x)$ becomes $yI_1'(y)/I_1(y)$. This is a steadily increasing function of y, always positive, and behaving like $y - \frac{1}{2}$ for large y. The function F is shown in Fig. 3. Further formulae pertaining to F are given in Appendix I. The inverse function $F^{-1}(x)$, which is also of some importance, is a multivalued function of x, whose behavior is readily understood from the figure for $F(x)$. We are now ready to proceed with the graphical analysis of the G-equation.

In a rectangular coordinate system with λ as abscissa and σ as ordinate, a contour map is sketched of the function

$$G = \frac{1 - \sigma\lambda}{1 - \lambda^2}\left[\frac{1}{\lambda} F\left(r_0 \sqrt{\frac{1 - \lambda^2}{1 - \sigma\lambda}}\right) - 1\right]$$

for all values of λ, σ from $-\infty$ to $+\infty$, r_0 being kept fixed. This can be done as accurately as desired by first drawing the contours $\chi^2 = \frac{1 - \lambda^2}{1 - \sigma\lambda}$ = constant (Fig. 4), along each of which G simply behaves like $A/\lambda + B$ and is easily evaluated with the help of a table of F. However,

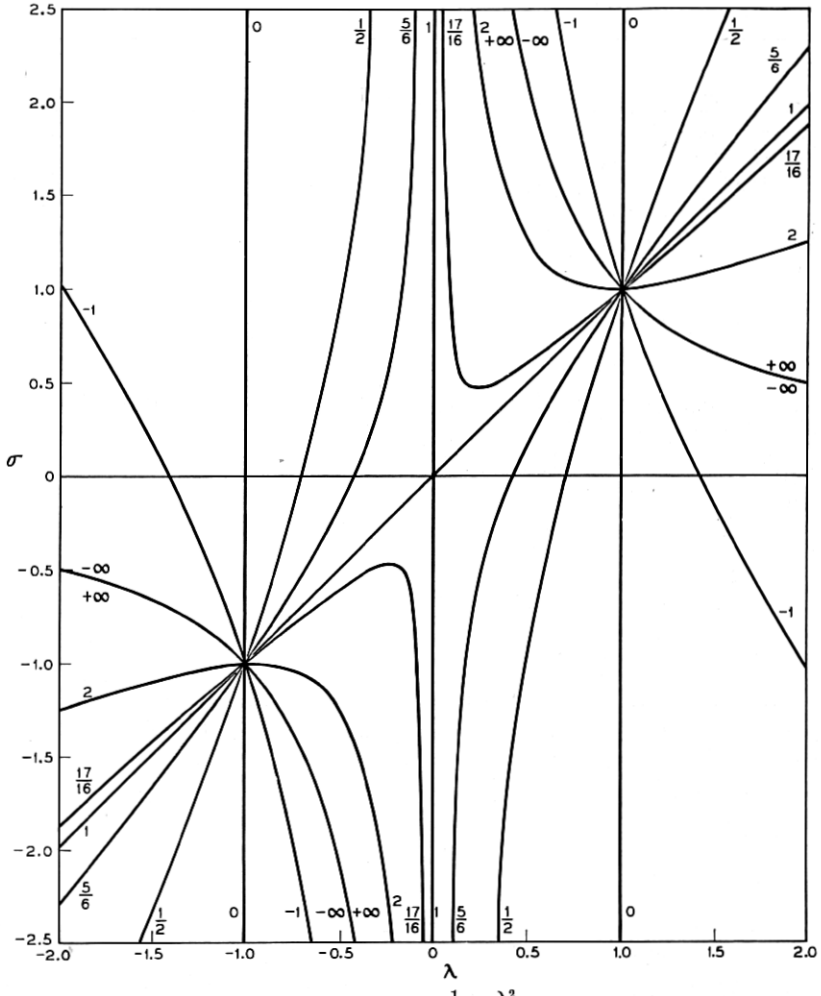

Fig. 4 — Curves of constant $\chi^2 = \frac{1 - \lambda^2}{1 - \sigma\lambda}$ in the $\sigma - \lambda$ plane.

many features of the G-contours are already determined by the position of the contours $G = \infty$, and $G = 0$, across which G changes sign (from $\pm\infty$ to $\mp\infty$ or from ± 0 to ∓ 0). Because of their special role in the subsequent analysis it is desirable to introduce a scheme for their enumeration. The infinity and zero curves in the right-hand half-plane will be denoted by I and 0, respectively, those in the left-hand half-plane by I' and $0'$. All but two of the I-curves arise from the poles j_n of F. Their equations are

$$\frac{1 - \lambda^2}{1 - \sigma\lambda} = j_n^2/r_0^2 \qquad n = 1, 2, \cdots$$

Each of these curves has two branches, one in the half-plane $\lambda > 0$, one in $\lambda < 0$ and these are called I_n, I_n' respectively. All I_n curves pass through $\lambda = 1$, $\sigma = 1$, all I_n' curves pass through $\lambda = -1$, $\sigma = -1$. The lines $\lambda = 0$, $\lambda = -1$ are also infinity curves to be denoted by I_A, I_B' respectively (As $\lambda \to +1$, G tends to a finite value).

Zero curves of G are given by

$$F\left(r_0\sqrt{\frac{1 - \lambda^2}{1 - \sigma\lambda}}\right) = \lambda,$$

or in a more readily computable form by

$$\sigma = \frac{1}{\lambda} - \frac{r_0^2(1 - \lambda^2)}{\lambda[F^{-1}(\lambda)]^2}. \tag{35}$$

The branches of $F^{-1}(\lambda)$ may be labelled according to the scheme: "0" for $-\infty < [F^{-1}(\lambda)]^2 < j_1^2$; "1" for $j_1^2 < [F^{-1}(\lambda)]^2 < j_2^2$ and so on. The nth branch of $F^{-1}(\lambda)$ gives rise to an 0_n curve for $\lambda > 0$ and to an $0_n'$ curve for negative λ. All $0_n'$ curves pass through $\lambda = -1$, $\sigma = -1$; all save one of the 0_n curves pass through $\lambda = 1$, $\sigma = 1$. The exceptional one, seen to be 0_0, is associated with the "0" branch of $F^{-1}(\lambda)$ on which $F^{-1}(1) = 0$. For fixed σ, G tends to zero as $\lambda \to \infty$, hence the vertical lines $\lambda = \pm\infty$ are also zero curves, to be denoted by 0_∞ and $0_\infty'$ respectively.

In a sense the two branches of $\sigma\lambda = 1$ are also zero curves, to be called 0_c and $0_c'$. 0_c and $0_c'$ are zero curves only when viewed from "one side." In the right half-plane, for $\lambda < 1$ as $\sigma\lambda \to 1 - 0$ and for $\lambda > 1$ as $\sigma\lambda \to 1 + 0$, the argument of F tends to infinity and remains real. Therefore G passes through all values an indefinite number of times and $\sigma\lambda = 1$ is a limit line of all contours, $G =$ constant. For $\lambda < 1$ as $\sigma\lambda \to 1 + 0$ and for $\lambda > 1$ as $\sigma\lambda \to 1 - 0$, the argument of F is

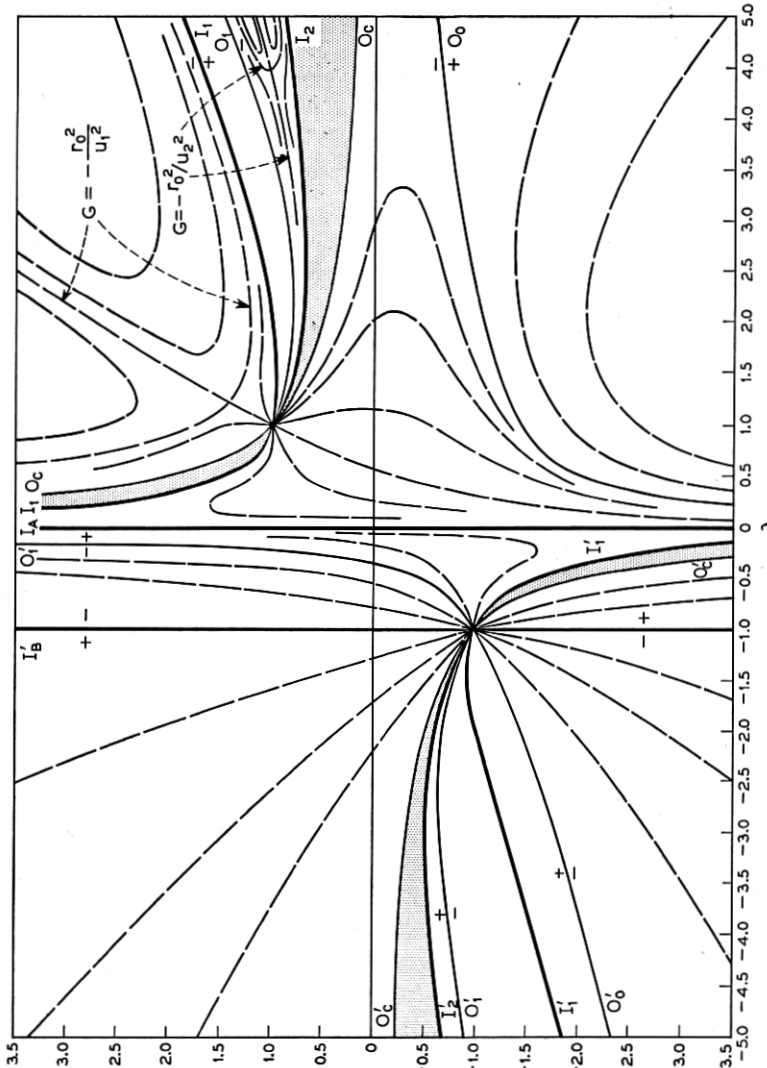

Fig. 5 — Contours of constant $G(\lambda, \sigma)$ for $r_0 = 2.2$. Scales distorted to show saddle points. G assumes any given value infinitely often in the shaded regions.

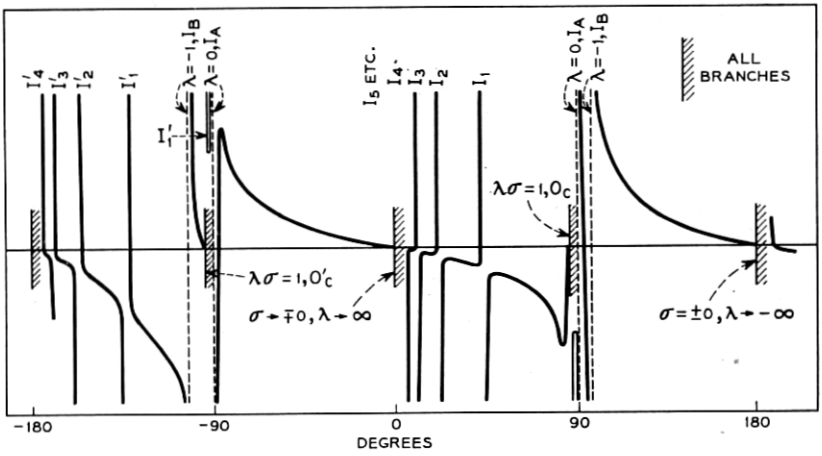

Fig. 6 — Qualitative behavior of $G(\lambda, \sigma)$ at large distances from the origin as a function of arc tan σ/λ. r_0 is about 2.

imaginary and F tends to infinity. However $F \Big/ \dfrac{1-\lambda^2}{1-\sigma\lambda}$ tends to zero so that G tends to zero.

To complete the picture of the G-function given by the form and position of the 0 and I curves it is necessary to see how it behaves at large distances from the origin. This is indicated in Fig. 5 and also by Fig. 6. The latter shows the value of G at large distances as a function of direction. In general, along the line $\sigma = c\lambda + d$ (c finite), G will tend to $-c$ for all d. For $c = r_0^2/j_n^2$ (which is the slope of the asymptotes to the I_n curves), G again tends to a constant. Now, however, the constant depends upon d and assumes all values from $-\infty$ to $+\infty$ as a function of d. In the first quadrant the sign of variation of the limiting value of G with direction c is opposite to that of its variation with d near $c = r_0^2/j_n^2$. Consequently local maxima and minima arise as a function of direction between successive I_n-curves. This suggests the existence of saddle points, which may be verified directly. In the third quadrant, the dependence of G upon c and d does not give such maxima and minima, and indeed no saddle points are found there. Finally it is necessary to consider the behavior of G as σ tends to infinity, while λ remains finite, corresponding to $(1/c) \to 0$. If λ remains fixed, then for $\lambda > -1$, $G \to \mp\infty$ as $\sigma \to \pm\infty$; and for $\lambda < -1$, $G \to \pm\infty$ as $\sigma \to \pm\infty$. As $\lambda \to 0$, the curves of constant G are asymptotic to $\lambda\sigma = \left(1 - \dfrac{r_0^2}{u_n^2}\right) - B\lambda$, where B goes from $-\infty$ to $+\infty$ with G. Interleaved with these families of curves are the curves

$G = \pm\infty$, which are $\lambda\sigma = \left(1 - \frac{r_0^2}{j_n^2}\right) + 0(\lambda^2)$. More detailed information on these matters will be found in Appendix II.

From the G-diagram it would be possible to determine pairs of λ-values with opposite signs, which, for a definite σ-value satisfy the characteristic equation, but, for a given p such pairs would not necessarily satisfy the Polder relation (31b). It is necessary to have a procedure which takes account of the latter systematically. Such a method may be based upon the fact that if, for σ and p positive, the Polder relation is solved for λ_1 in terms of λ_2 it can be thought of as a rather simple mapping of the whole λ_2-quadrant upon a part of the λ_1-quadrant ($\lambda_1 > 0$). Similarly for σ and p negative there is an analogous mapping of the λ_1-quadrant onto the λ_2-quadrant.

Considering first the case $\sigma, p > 0$, the Polder relation may be written in the forms

$$\lambda_1 = \frac{\sigma + p - \lambda_2}{1 - \sigma\lambda_2} = \frac{1}{\sigma} + \frac{\sigma + p - 1/\sigma}{1 - \sigma\lambda_2} = T(\lambda_2). \tag{36}$$

From (36) it may be seen that the curves $\lambda_2 = $ const. transform into a bundle of hyperbolae passing through the intersection of $\sigma = 1/\lambda_1$ and $\sigma = \lambda_1 - p$; that is, through λ_{10}, σ_0, where

$$\sigma_0 = -p/2 + \sqrt{\frac{p^2}{4} + 1}, \qquad \lambda_{10} = p/2 + \sqrt{\frac{p^2}{4} + 1}.$$

These hyperbolae have the vertical asymptotes $\lambda_1 = -1/\lambda_2$, and intersect $\sigma = 0$ at $\lambda_1 = p - \lambda_2$. For a fixed positive σ less than σ_0, λ_1 decreases from $1/\sigma$ to $\sigma + p$ as λ_2 increases from $-\infty$ to 0, but when σ is greater than σ_0, λ_1 increases from $1/\sigma$ to $\sigma + p$ under the same circumstances. Thus the whole λ_2-quadrant is transformed upon that part of the λ_1-quadrant which lies between the hyperbola $\lambda_1 = 1/\sigma$ and the straight line $\lambda_1 = \sigma + p$. It follows that points in the λ_1-quadrant which are, for a given p, excluded from this region, cannot be the site of acceptable solutions of the G-equation.

Since as has already been stated, the Polder relation is unchanged by the substitution $\lambda_1 \to -\lambda_2$, $\lambda_2 \to -\lambda_1$, $\sigma \to -\sigma$, and p to $-p$, it follows that for σ and p negative a similar mapping of the λ_1-quadrant upon part of the λ_2-quadrant takes place. The transforms of the lines $\lambda_1 = $ const. and so forth may easily be found by using these substitutions in the formulae already given.

Reference to Fig. 1(a) and (b) will show that $\pm\sigma_0$ are the values of σ at which μ reverses sign. Therefore we may expect σ_0 to play a special role

in the propagation theory, as also does $\sigma = 1$. The following scheme exists: for $0 < \sigma < \sigma_0$, κ and μ are both positive; for $\sigma_0 < \sigma < 1$, $\kappa < 0$ and $\mu < 0$, for $\sigma > 1$, κ is negative and μ positive. If σ is changed to $-\sigma$, μ goes into μ, and κ into $-\kappa$.

The procedure which will now be used to discuss the solution of the characteristic equation, observing the Polder relations, begins by writing the equation, for σ, p positive, in the form

$$G(\lambda_1, \sigma, r_0) = G(T(\lambda_1), \sigma, r_0)$$

We are already in possession of a contour map of the left hand side of this equation in the quadrant $\sigma > 0$, $\lambda > 0$, and of the function $G(\lambda_2, \sigma, r_0)$ in the quadrant $\lambda < 0$, $\sigma > 0$. The latter surface has now to be transformed into one in the λ_1-quadrant by the relation

$$\lambda_2 = T(\lambda_1) = (\sigma + p - \lambda_1)/(1 - \sigma\lambda_1)$$

(or equally well, $\lambda_1 = T(\lambda_2)$. This may be effected by considering the transformation of curves $G(\lambda_2, \sigma, r_0) =$ constant, onto the λ_1-quadrant. For the I' curves whose analytical expression in terms of σ and λ_2 is very simple, the corresponding explicit expression of the transformed curve in λ_1 and σ is simple. Contours other than I' are most easily transformed by replotting $G(\lambda_2, \sigma, r_0) =$ const. in the hyperbola-mesh formed by the lines $T(\lambda_2)$. However, information about particular points and about asymptotic behavior of these transformed curves is available in analytic form and is stated in Appendix II. The two surfaces so obtained will intersect in various curves, along whose projections on the $\lambda - \sigma$ plane both Polder relation and G-equation are satisfied. For each such projection λ_1 is a function of σ, λ_2 is then known in terms of σ and p, and finally $\beta^2 = -\lambda_1\lambda_2$ is known. In most cases the general course of these curves can be found without resort to much numerical analysis. Each of the curves is associated with a definite mode and it follows that the classification of the modes can be carried out fairly easily. The approximate location of the solution curves relies upon the fact that if the position of the infinity curves of both surfaces is known, continuity considerations will frequently assure the existence of an intersection within certain regions. Moreover, the neighborhood of certain special points on these solution curves can be investigated analytically. These are points at which one or both of the G-functions may be approximated by a simpler expression; included among these is the point at infinity.

It is clear that for σ and p negative the whole procedure outlined above may be carried out in a similar way, with the $\sigma > 0, \lambda > 0$ quadrant now being transformed on to the $\sigma < 0, \lambda < 0$ quadrant.

It is possible to translate such solution curves into $\beta^2 - \sigma$ curves in a direct graphical manner if a mesh of constant β^2 lines is drawn in the first quadrant. From (30) these are given by

$$\lambda_1^2 - [p + \sigma(1 - \beta^2)]\lambda_1 - \beta^2 = 0,$$

or

$$\frac{1 - \lambda_1^2}{1 - \left[\sigma + \dfrac{p}{1 - \beta^2}\right]\lambda_1} = 1 - \beta^2.$$

The contour, $\beta = b$, is just the contour $\chi^2 = 1 - b^2$ displaced along the σ-axis by an amount, $-p/(1 - b^2)$. The contours of constant β all pass through the point $\sigma = \sigma_0$, $\lambda = \sigma_0 + p$ and are shown in Fig. 7. Their

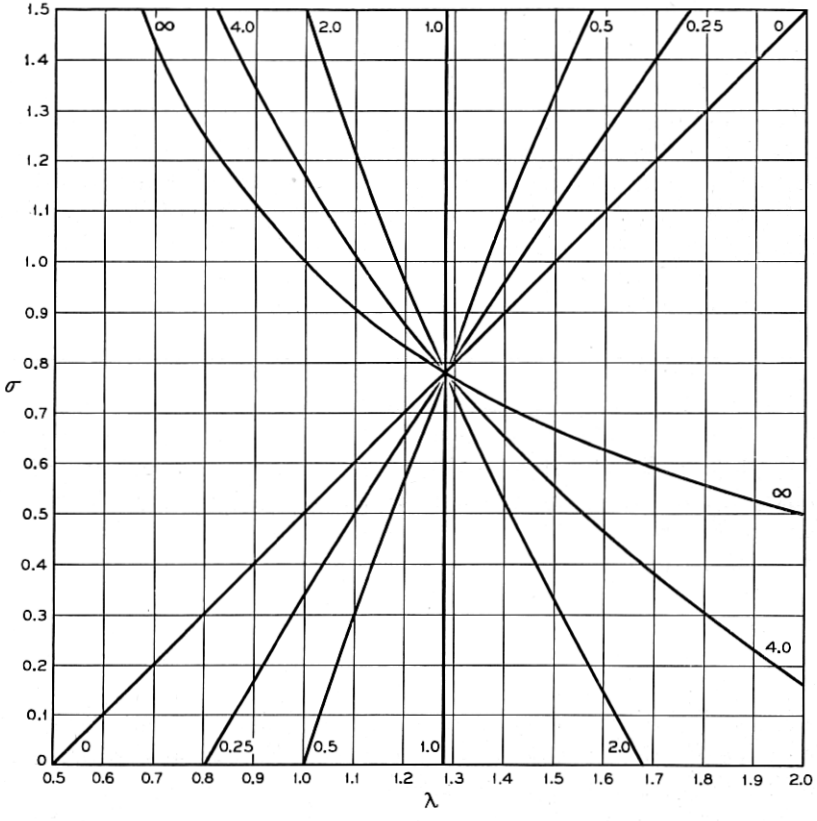

Fig. 7 — Contours of constant $\beta^2 = \lambda \dfrac{\lambda - p - \sigma}{1 - \sigma\lambda}$ for $p = 0.5$.

$[\beta^2(\lambda, \sigma, p) = \beta^2(-\lambda, -\sigma, -p)]$

course in the third quadrant is immediately found by reflection in the origin.

When $p = 0$ the magnetization of the ferrite vanishes and it is clear that we should then obtain just the modes of a guide filled with isotropic material ($\mu = \mu_z$; $\kappa = 0$). Superficially it might appear that, since the equations (31b) and (33) depend upon σ, even for $p = 0$, this result might not be attained. We now show that β^2 is indeed independent of σ for $p = 0$. It may first be noted that in this case if $\sigma \neq 1$, the Polder relation (31b) transforms

$$\frac{1 - \lambda_1^2}{1 - \sigma\lambda_1} \text{ into } \frac{1 - \lambda_2^2}{1 - \sigma\lambda_2} \text{ and } \lambda_1 \text{ into } \frac{\sigma - \lambda_2}{1 - \sigma\lambda_2}.$$

The G-equation reads

$$\frac{1 - \lambda_2\sigma}{1 - \lambda_2^2}\left[\frac{1}{\lambda_2} F\left(r_0 \sqrt{\frac{1 - \lambda_2^2}{1 - \sigma\lambda_2}}\right) - 1\right] = \frac{1 - \lambda_2\sigma}{1 - \lambda_2^2}\left[\frac{1 - \sigma\lambda_2}{\sigma - \lambda_2} F\left(r_0 \sqrt{\frac{1 - \lambda_2^2}{1 - \sigma\lambda_2}}\right) - 1\right].$$

Since $\lambda_1 \neq \lambda_2$ we must have

$$F\left(r_0 \sqrt{\frac{1 - \lambda_2^2}{1 - \sigma\lambda_2}}\right) = 0 \quad \text{or} \quad \infty,$$

or

$$\frac{1 - \lambda_{1,2}^2}{1 - \sigma\lambda_{1,2}} = \frac{u_n^2}{r_0^2} \quad \text{or} \quad \frac{j_n^2}{r_0^2}.$$

Thus $\lambda_{1,2}$ are roots of

$$\lambda^2 - \sigma\frac{u_n^2}{r_0^2}\lambda + \left(\frac{u_n^2}{r_0^2} - 1\right) = 0,$$

or else of

$$\lambda^2 - \sigma\frac{j_n^2}{r_0^2}\lambda + \left(\frac{j_n^2}{r_0^2} - 1\right) = 0,$$

In the first case

$$-\lambda_1\lambda_2 = \beta^2 = 1 - \frac{u_n^2}{r_0^2},$$

and in the second

$$-\lambda_1\lambda_2 = \beta^2 = 1 - \frac{j_n^2}{r_0^2}.$$

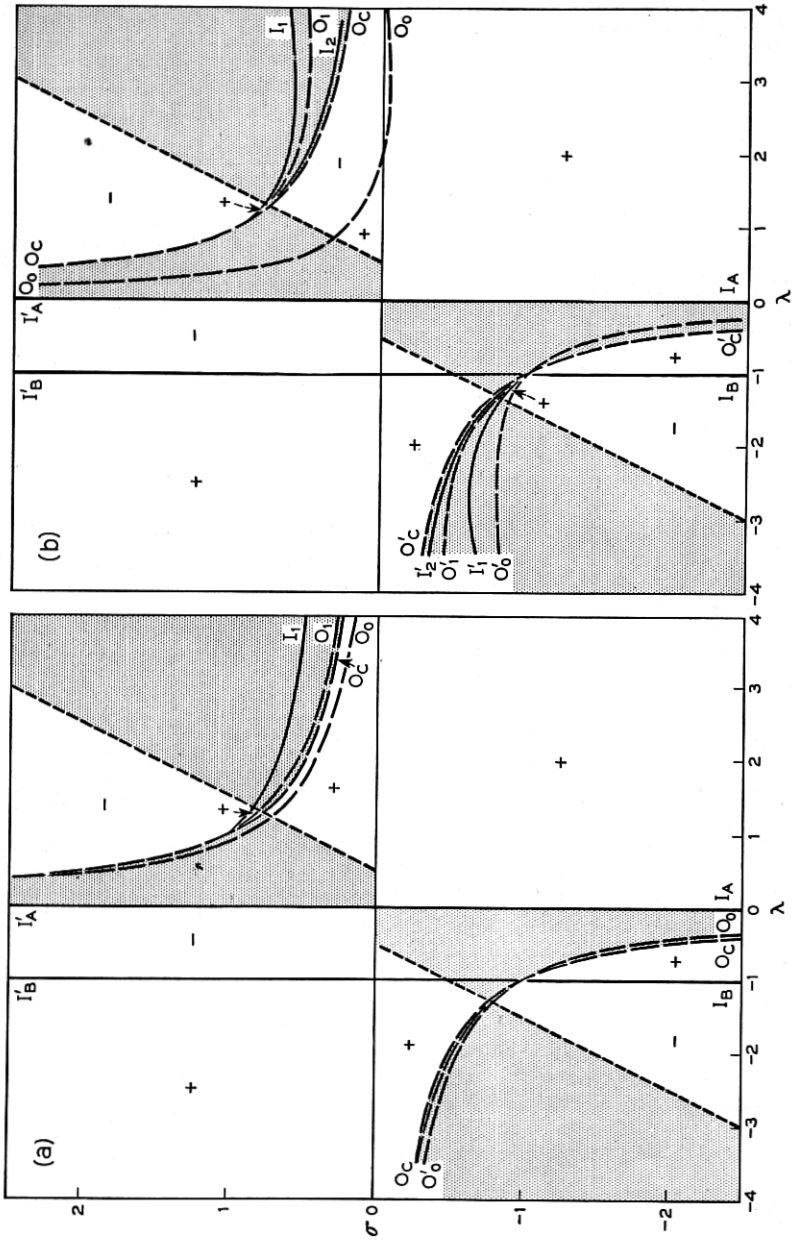

Fig. 8 — The division of the parts of the $\lambda - \sigma$ plane allowed by the Polder relation, Equation (31b), into regions of positive and negative G by the first few 0 and I curves. Excluded regions are shaded. $|p|$ is about 0.5. Fig. 8(a), $0 < r_0 < 1$; Fig. 8(b), $1 < r_0 < u_1$; Fig. 8(c), $r_0 = u_1$; Fig. 8(d), $u_1 < r_0 < j_1$; Fig. 8(e), $j_1 < r_0 < u_2$.

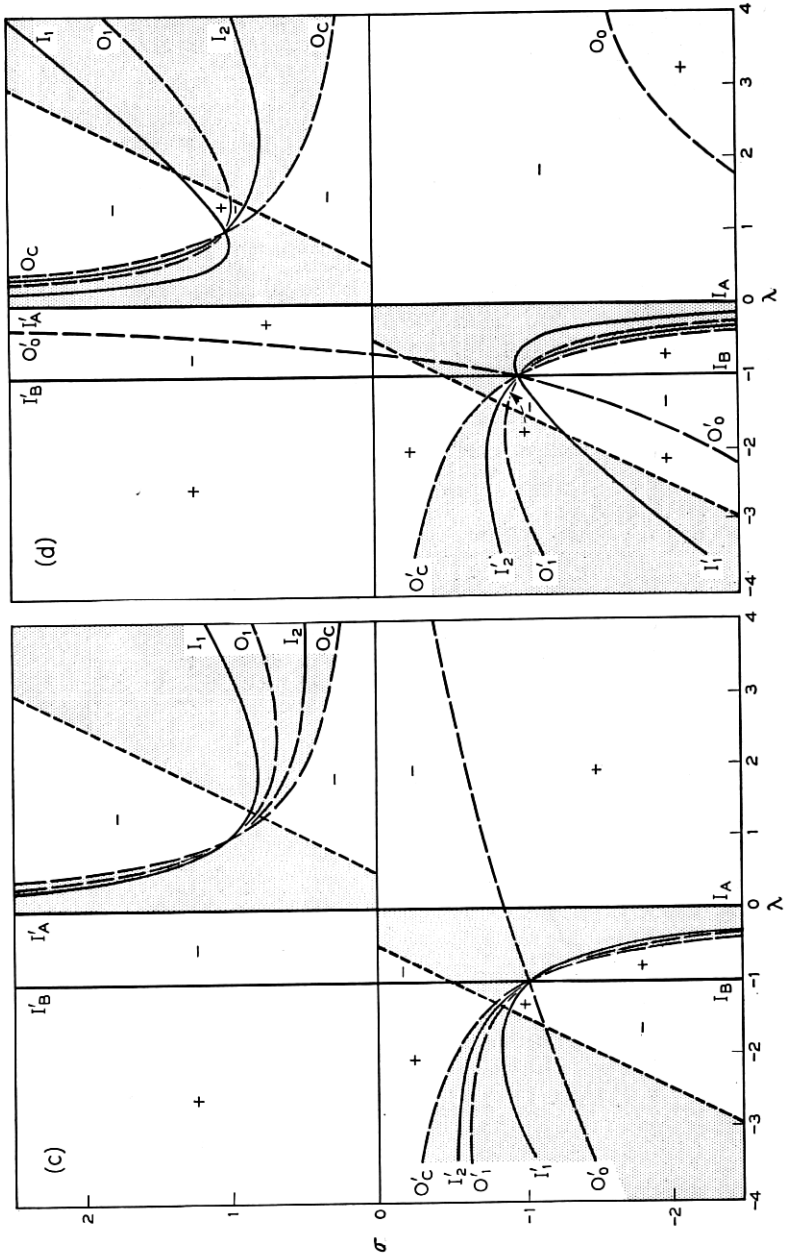

Fig. 8(c) and (d) — See Fig. 8.

Thus, when $\sigma \neq 1$, the β^2 values, for $p = 0$, are evidently independent of σ and are just those of an isotropic medium. When $\sigma = 1 (\mu = \kappa = \infty)$, $p = 0$, β^2 is indeterminate and for p small, there is a small region near $\sigma = 1$, of width $\sim p$, in which β^2 differs appreciably from the isotropic value. The convergence of an expansion of β^2 in powers of p[(61) and (62)] shows a marked dependence on σ.

4.12. The scheme of analysis described above will now be illustrated in detail by a discussion for a radius r_0 between u_1 and j_1, which, if the ferrite were unmagnetized, would propagate the TE_{11}-mode alone.

Figs. 8(c) and 8(d) show the division of the $\lambda - \sigma$ plane into regions of positive and negative $G(\lambda, \sigma)$ by the various I and 0 curves. A few contours of constant G are plotted to indicate the behavior of the function in more detail. That part of the $\lambda - \sigma$ plane which is excluded by the

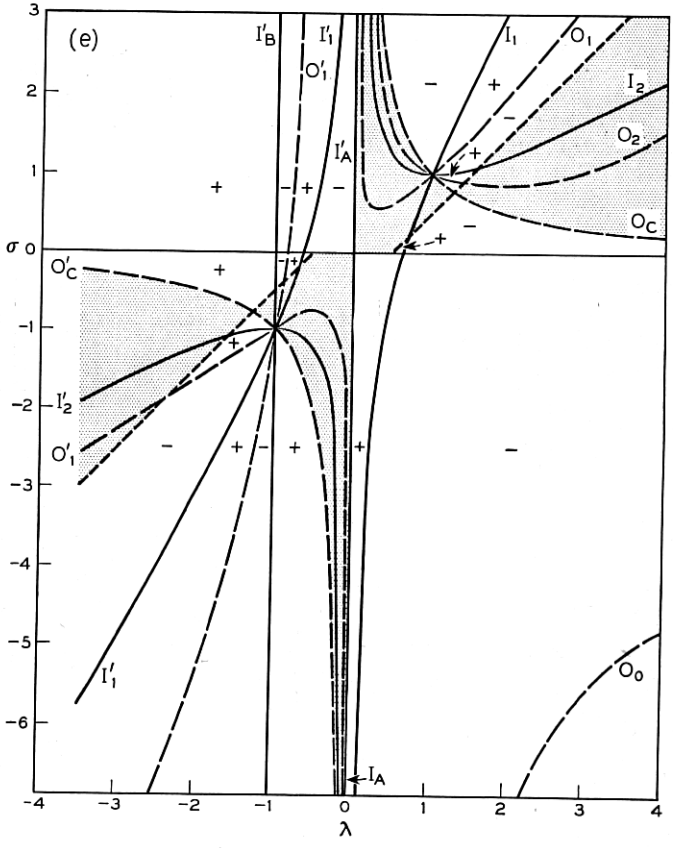

Fig. 8(e) — See Fig. 8.

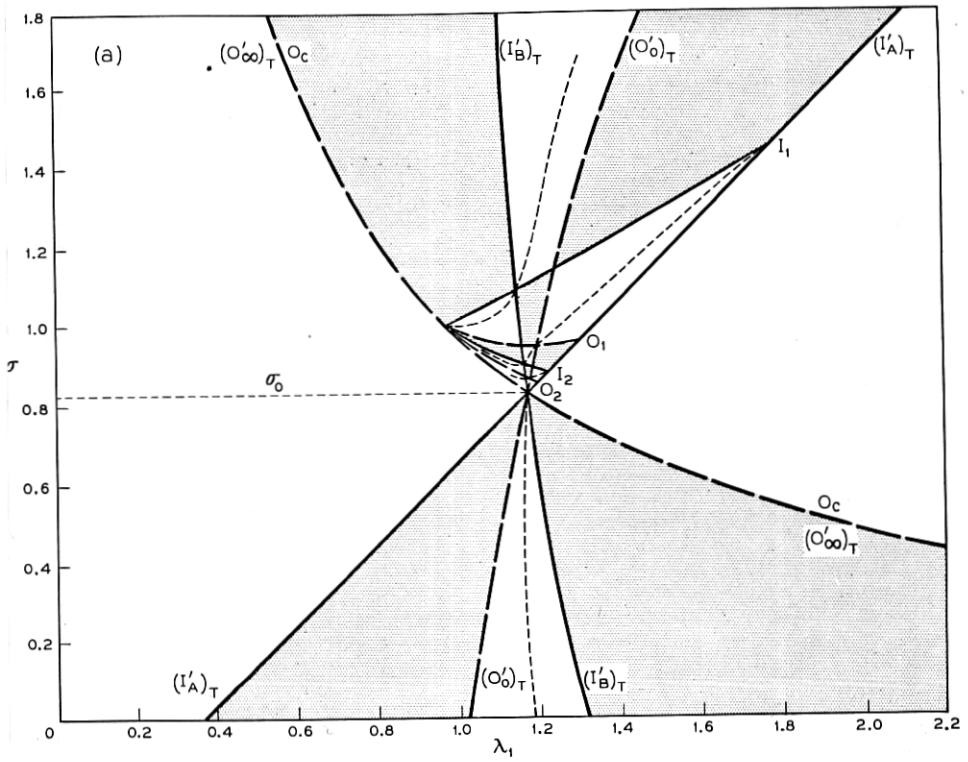

Fig. 9 — Geometrical exploration of the solution curves. The permitted areas of the $\lambda - \sigma$ plane are divided by the O, I, $(O)_T$, $(I)_T$ curves into regions in which $G(\lambda, \sigma)$ and $G(T(\lambda), \sigma)$ have like or unlike signs. Shaded regions are those of unlike signs. Solution curves (shown schematically by dotted lines) must lie in regions of like signs. Only the first few O and I curves are shown. Fig. 9(a) and (b), $r_0 \sim 3.0$; Fig. 9(c) and (d), $r_0 \sim 5.0$; Fig. 9(e) and (f), $u_2 < r_0 < j_2$; Fig. 9(g), $r_0 < u_1$. $|p| < 1$, throughout. The horizontal dashed line marks $|\sigma| = |\sigma_0|$.

Polder relation is indicated, for $p = \frac{1}{2}$, by shading. For other p-values the straight portion of the boundary of the excluded region is simply translated along the λ-axis.

In Fig. 9(a) the allowed region of the first quadrant is shown again, together with the transforms $(I_A')_T$, $(0_1')_T$, and $(I_B')_T$ of the only critical curves I_A', $0_1'$ and I_B' occurring in the second quadrant for the present radius. Regions in which $G(\lambda_1, \sigma)$ and $G(T(\lambda_1), \sigma)$ have opposite sign are shaded; the common signs in the remaining parts of the quadrant are as indicated. (In this diagram p is taken to be $\frac{3}{8}$).

From the disposition of the surfaces $G(\lambda_1, \sigma)$ in the region between 0_1

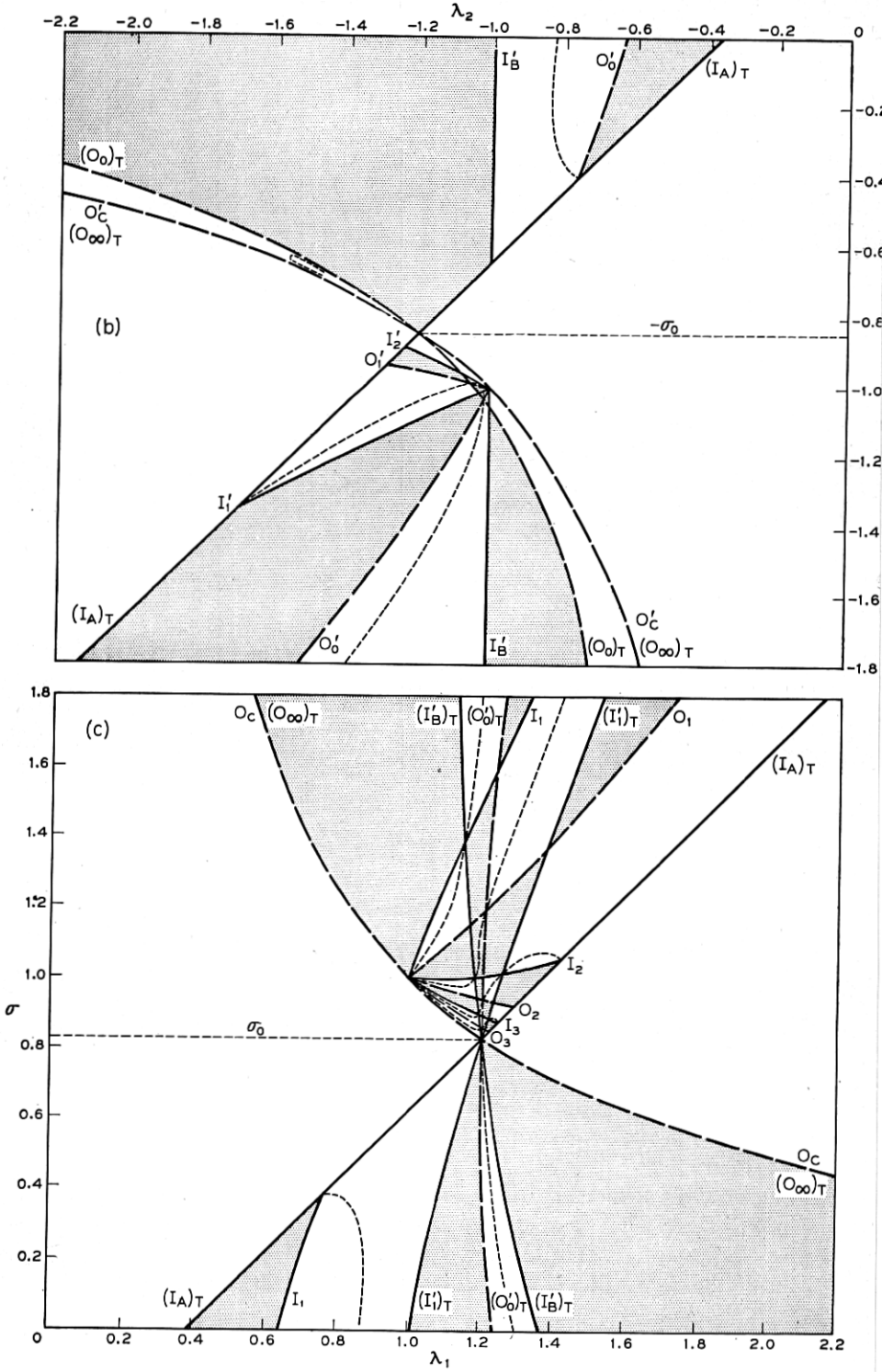

Fig. 9(b) and (c) — See Fig. 9.

and I_1 and of the surface $G(T(\lambda_1), \sigma)$ between $(0_\infty')_T$ and $(I_B')_T$ it is evident that along any contour such as $G(\lambda_1, \sigma) = K$, $G(T(\lambda_1), \sigma)$ will take on all positive values from 0 to ∞ and, in particular, K. Since this is true for any K, it follows that the region between 0_1, I_1, $(I_B')_T$ contains a solution curve. Two points on this curve are immediately obvious: the intersections of $(I_B')_T$, I_1 and the point (1, 1) on $(0_\infty')_T$, 0_c. The first is the intersection of the curves

$$\lambda = 1 + \frac{p}{1 + \sigma}, \qquad \frac{j_1^2}{r_0^2} = \frac{1 - \lambda^2}{1 - \sigma\lambda}.$$

At the point (1, 1), λ_2 is $-\infty$, λ_1 is unity and β^2 is therefore infinite. Armed with this knowledge we now investigate analytically the behavior of β^2 near $\sigma = 0$ directly from the original G-equation and Polder relations. Writing $\lambda_1 = 1 + c\epsilon$ and $\sigma = 1 + \epsilon$, $(1 - \lambda^2)/(1 - \sigma\lambda)$ is to zero

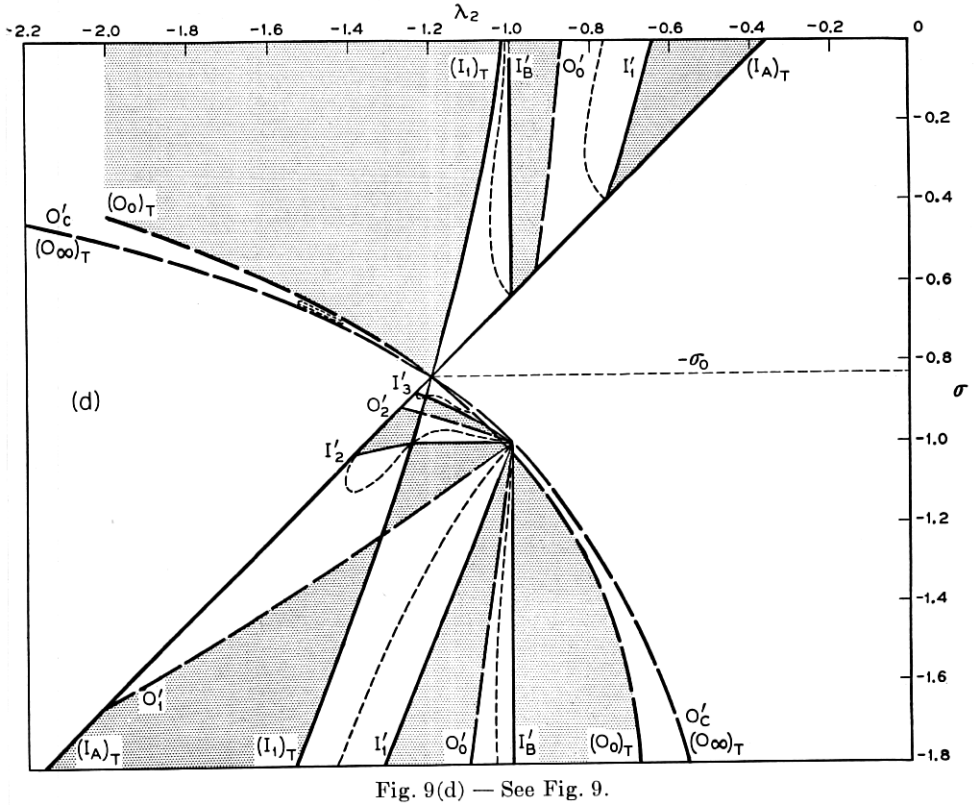

Fig. 9(d) — See Fig. 9.

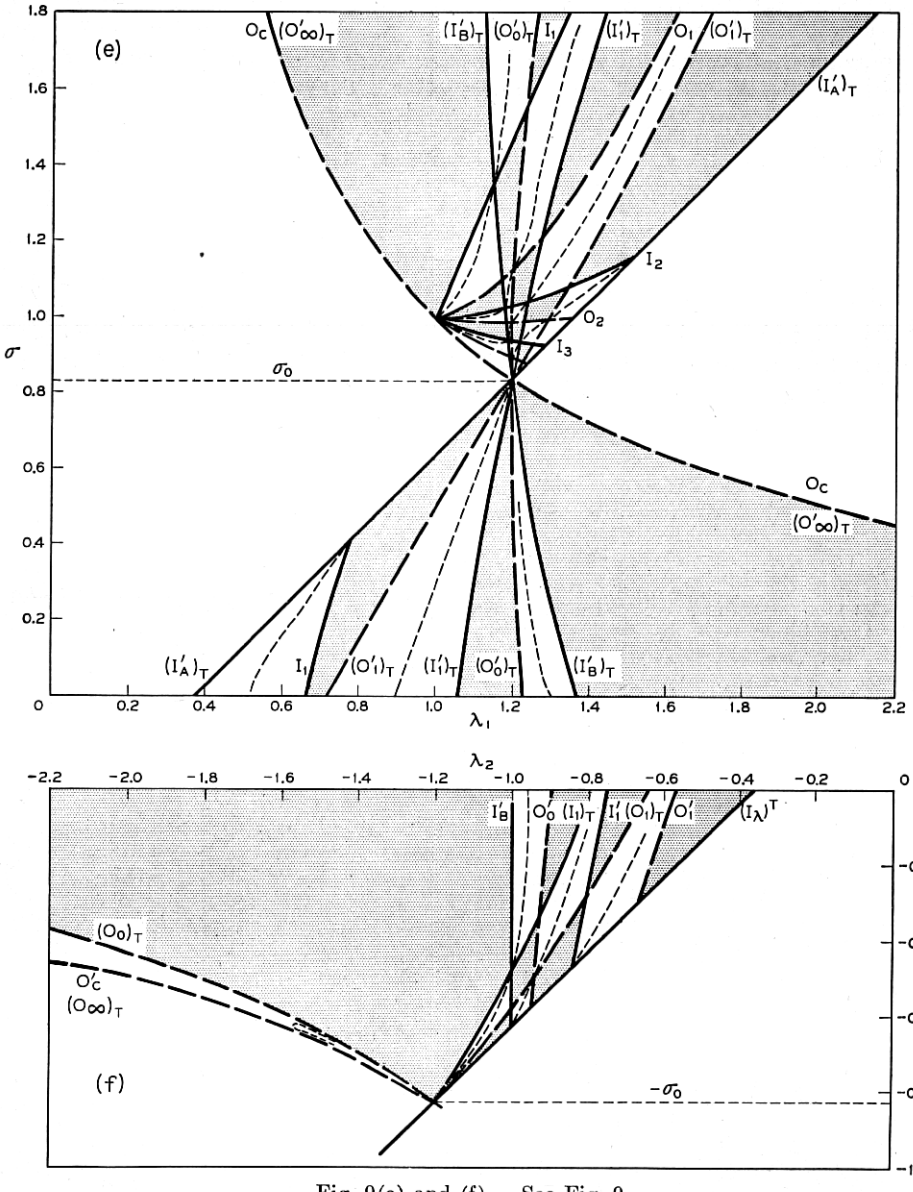

Fig. 9(e) and (f) — See Fig. 9.

order just $2c/1 + c$. Thus, $G(\lambda_1, \sigma)$ to zero order is

$$\frac{1+c}{2c}\left[F\left(r_0\sqrt{\frac{2c}{1+c}}\right) - 1\right].$$

But we have, in this case, $G(\lambda_2) = 0$, so that

$$\frac{2c}{1+c} = \frac{z_1^2}{r_0^2},$$

where z_1 is the smallest non-zero root of $F(z) = 1$. From the Polder relation, the leading term of λ_2 is $-p/(1+c)\epsilon$, and consequently the leading term of β^2 is

$$\frac{p}{(1+c)\epsilon} = \frac{p\left(1 - \frac{z_1^2}{2r_0^2}\right)}{\sigma - 1}.$$

This analysis is readily extended to the next order term, which is stated in Section (4.17).

From analogous considerations concerning the variation of one G-

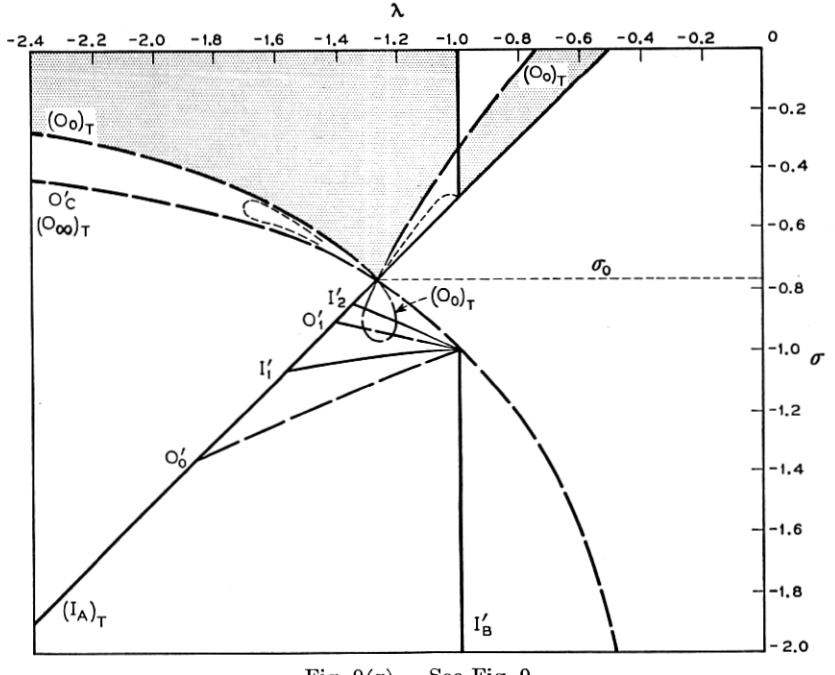

Fig. 9(g) — See Fig. 9.

function through all possible values of the other in the region bounded by I_1, $(I_B')_T$, $(0_1')_T$ we deduce that the solution curve just discussed continues into that region and persists as $\sigma \to \infty$. For, the asymptote of $(0_1')_T$ is $\sigma = \frac{r_0^2}{u_1^2}\lambda$, and between it and $\lambda = 1$, which is the asymptote of $(I_B')_T$, $G(T(\lambda_1), \sigma)$ takes on all values between 0 and $-\infty$; in particular, the limited range of values assumed by $G(\lambda_1, \sigma)$ in this region. The behavior of the solution curve for large σ may be deduced by using the asymptotic formulae for curves $G(\lambda_1, \sigma) = g$ and $G(T(\lambda_1)\sigma) = g$ which are given in the appendix. These are

$$\sigma = -g\lambda_1 - gF\left(\frac{r_0}{\sqrt{-g}}\right),$$

and

$$\sigma = \frac{r_0^2}{u_1^2}\lambda_1 - \left[p + 2\left(1 + \frac{gu_1^2}{r_0^2}\right)\frac{1 - \frac{r_0^2}{u_1^2}}{1 - u_1^2}\right].$$

It is clear that g at a point of intersection is given by $-r_0^2/u_1^2$ plus terms of order $1/\lambda_1$; substituting this value in the second equation gives the solution curve correctly to order $1/\lambda_1$ in the form.

$$\sigma = \frac{r_0^2}{u_1^2}\lambda_1 - p.$$

When the solution curve has such a linear asymptote it is convenient to calculate β^2 from the formula

$$\beta^2 = 1 + \frac{p}{\sigma} - \frac{\lambda}{\sigma} + \text{terms of order higher than } 1/\sigma$$

which is readily obtained from (30). In the present case

$$\beta^2 = \left(1 - \frac{u_1^2}{r_0^2}\right)\left(1 + \frac{p}{\sigma}\right) + \text{higher terms in } 1/\sigma. \tag{38}$$

As $\sigma \to \infty$, β^2 tends to the value appropriate to the TE_{11}-mode in an isotropic medium ($\mu \to \mu_z = \mu_0$, $\kappa \to 0$ as $\sigma \to \infty$). Thereby the whole solution curve is classified as specifying part of a TE_{11}-limit mode.

The remaining section of the TE_{11}-limit mode in the upper half-plane is again found in the region between $(0_1')_T$ and $(I_B')_T$ for $\sigma < \sigma_0$. Any line $\sigma =$ constant $< \sigma_0$ cuts these two curves at two values of λ_1. As λ_1 varies between these values, $G(T(\lambda_1), \sigma)$ varies from 0 to $-\infty$; it is, thus,

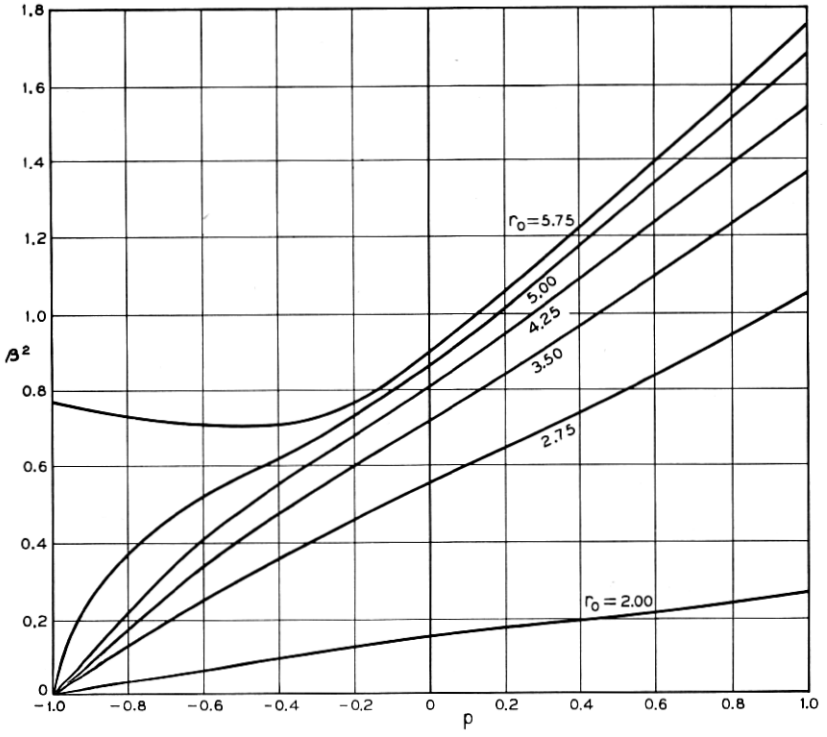

Fig. 10(a) — β^2 versus p for small values of σ — the TE_{11}-limit mode.

clearly equal to the finite (negative) $G(\lambda_1, \sigma)$ somewhere between. This situation persists up to $\sigma = \sigma_0 - 0$ and a solution curve therefore exists between $\sigma = 0$ and $\sigma = \sigma_0$. It meets $\sigma = 0$ for λ_1 satisfying

$$\frac{1}{1-\lambda_1^2}\left[\frac{1}{\lambda_1}F(r_0\sqrt{1-\lambda_1^2}) - 1\right] = \frac{1}{1-\lambda_2^2}\left[\frac{1}{\lambda_2}F(r_0\sqrt{1-\lambda_2^2}) - 1\right],$$

and

$$\lambda_1 + \lambda_2 = p. \tag{39}$$

These equations have been solved numerically; the corresponding $\beta^2 = -\lambda_1\lambda_2$ is shown in Fig. 10(a). For r_0 between u_1 and j_1 a value derived for β^2 from the first three terms of an expansion of β^2 in powers of p, equation (61), turns out to be in very good agreement with the numerical calculation up to $p = 1$, for $\sigma = 0$ and presumably is good for small σ.

At σ_0 (the point at which μ becomes negative), the solution curve is "cutoff". However, the corresponding β^2 is not zero. As σ_0 is approached from below $G(\lambda_1, \sigma) \to 0$ and so $G(\lambda_2, \sigma)$ tends to zero. Thus, λ_2 tends to

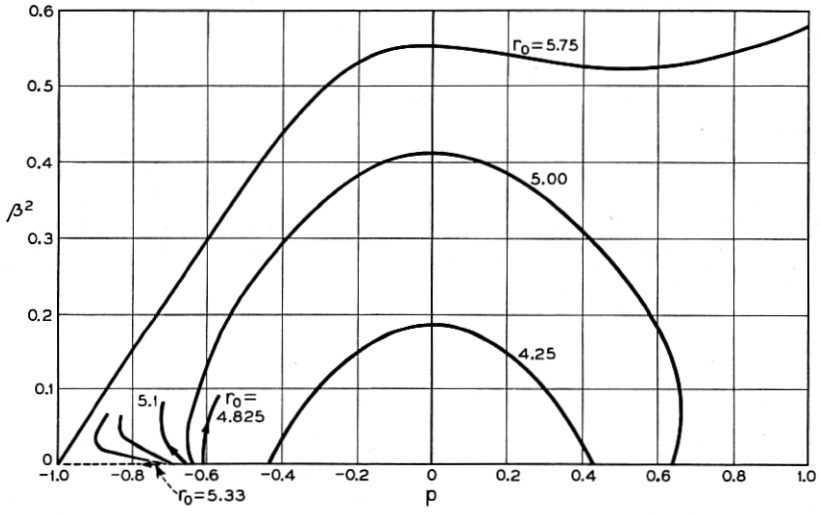

Fig. 10(b) — β^2 versus p for small values of σ — the TM_{11}-limit mode.

the negative root λ_{20} (unique for the present radius) of

$$F\left(r_0\sqrt{\frac{1-\lambda_2^2}{1-\sigma_0\lambda_2}}\right) = \lambda_2 .$$

The associated β^2 is $-\lambda_{20}\lambda_{10} = -\dfrac{\lambda_{20}}{\sigma_0}$ and is shown in Fig. 11(a). The way in which β^2 approaches this value as $\sigma \to \sigma_0$ can be found and is one of the more subtle examples of behavior of a mode near a special point. Writing $\sigma = \sigma_0 - \delta\sigma$, $\lambda_1 = \lambda_{10} - \delta\lambda_1$, we observe that, since $\sigma_0 + p - \dfrac{1}{\sigma_0} = 0$, the Polder relation in the form

$$\lambda_1 = \frac{1}{\sigma} + \frac{\sigma + p - 1/\sigma}{1 - \sigma\lambda_2}$$

fully determines $\dfrac{d\lambda_1}{d\sigma}$; any variation due to $\delta\lambda_2$ vanishes at $\sigma = \sigma_0$. $\delta\lambda_2$ can be determined from the G-equation. Near $\sigma\lambda = 1 - 0$ $(\lambda > 1)$, $G(\lambda_1, \sigma)$ is given by

$$-\frac{r_0}{\lambda_1}\sqrt{\frac{1-\sigma\lambda_1}{\lambda_1^2 - 1}},$$

which near σ_0, λ_{10} may be written

$$-\sqrt{\delta\sigma}\,\frac{r_0}{\lambda_{10}}\sqrt{\frac{\lambda_{10}\dfrac{d\sigma}{d\lambda_1}+\sigma_0}{\lambda_{10}^2-1}}\,.$$

The perturbed $G(\lambda_2, \sigma)$ which (since $G(\lambda_{20}, \sigma_0) = 0$) is $\dfrac{\partial G}{\partial \lambda_{20}}\,\delta\lambda_2 + 0(\delta\sigma)$ equals the preceeding expression and gives

$$\delta\lambda_2 = -\sqrt{\delta\sigma}\,\frac{r_0}{\lambda_{10}}\sqrt{\frac{\lambda_{10}\dfrac{\delta\sigma}{\delta\lambda_1}+\sigma_0}{\lambda_{10}^2-1}}\left(\frac{\partial G}{\partial\lambda_{20}}\right)^{-1}.$$

Accordingly, $\delta\beta^2 = -\lambda_{10}\,\delta\lambda_2 + 0(\delta\sigma)$, a result which shows that β^2 tends to its terminal value along the vertical. It is clear analytically and graphically that this mode persists as $p \to 0$, and must be identified with the only isotropic mode for this radius, namely TE_{11}. No other branches exist below $\sigma = \sigma_0$, since $G(\lambda_1, \sigma)$ and $G(T(\lambda_1), \sigma)$ have opposite signs except in the region just considered.

The two solution curves considered so far are not the only ones; in fact the infinity of sheets of the surface $G(\lambda_1, \sigma)$ in the region bounded by I_1, O_c and $(I_A')_T$, Fig. 9(a), intersect the transformed sheets $G(T(\lambda_1)\sigma)$ in infinitely many more curves. In the blank areas of that region the G-functions have equal sign, and all these areas must be carriers of solution curves, since in every one of them every single contour $G(\lambda_1, \sigma) = g$

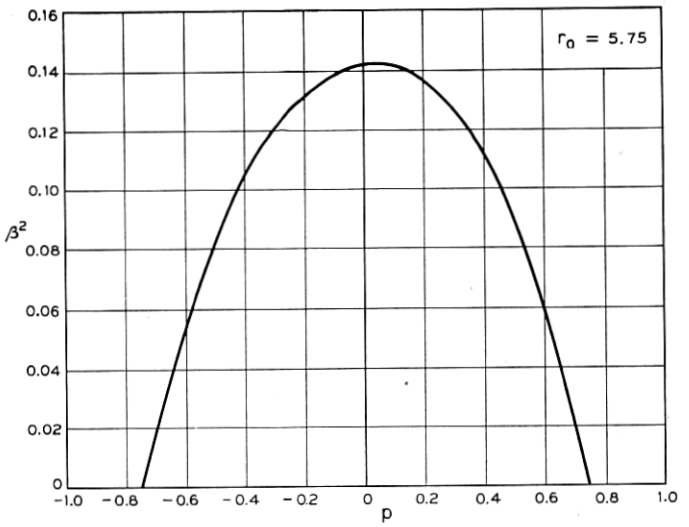

Fig. 10(c) — β^2 versus p for small values of σ — the TE_{12}-limit mode.

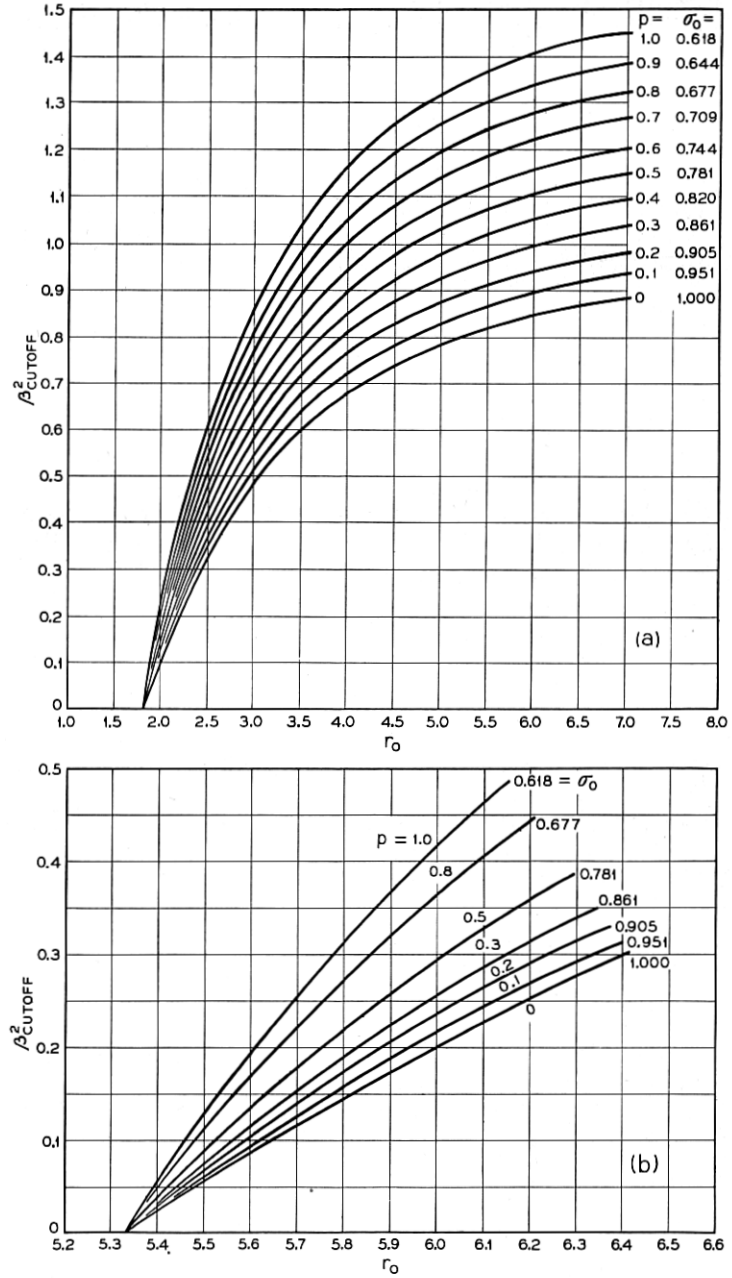

Fig. 11 — β^2 at the type 2′ cutoff as a function of r_0 for various p. $2_0'$ cutoff, TE_{11}-limit mode; (b), $2_1'$ cutoff, TM_{11}-limit mode. The presence of a curve for $p = 0$ is clarified in the text.

crosses all contours of $G(T(\lambda_1), \sigma)$, in particular $G(T(\lambda_1), \sigma) = g$. All the additional solution curves arising in this way start at $\sigma = 1, \lambda_1 = 1$; the n^{th} of them threads its way from one blank region to another, first through the intersection of I_{n+1} with $(I_B')_T$, then through the intersection of 0_n with $(0_1')_T$, and finally comes to an end at the intersection of I_n with $(I_A')_T$. At the end point ($\sigma = 1, \lambda_1 = 1$), λ_2 and, therefore, β^2 are infinite, (just as for the TE_{11} solution curve). At the end point (I_n, $(I_A')_T$), λ_2, and, therefore, β^2 are zero. The σ and λ_1 values corresponding to the latter are obtained from the equations

$$\frac{1 - \lambda_{1n}^2}{1 - \sigma_n \lambda_{1n}} = \frac{j_n^2}{r_0^2}; \qquad \lambda_{1n} = \sigma_n + p. \tag{40}$$

It is possible to derive the slope $\delta\beta^2/\delta\sigma$ of the $\beta^2 - \sigma$ curves at these cut-off points. Near cut-off, the infinity I_n of $G(\lambda_1, \sigma)$ is matched by the infinity I_A' of $G(\lambda_2, \sigma)$. The G-equation therefore degenerates to

$$\frac{1}{\lambda_2} F(r_0) = \frac{j_n}{r_0 \sqrt{\dfrac{1 - \lambda_1^2}{1 - \sigma\lambda_1}} - j_n} \cdot \frac{1}{\lambda_{1n}} \cdot \frac{r_0^2}{j_n^2}.$$

Writing $\sigma = \sigma_n - x\lambda_2$, $\lambda_1 = \lambda_{1n} - y\lambda_2$, expansion of the right hand side of this equation to order $1/\lambda_2$ furnishes one relation between x and y; the Polder equation furnishes another. The two can be solved for x, and so, since to first order

$$\delta\beta^2 = -\lambda_{1n}\lambda_2 = \lambda_{1n} \frac{\sigma - \sigma_n}{x} = \lambda_1 \frac{\delta\sigma}{x}$$

$\delta\beta^2/\delta\sigma$ may be found. It is found that for convenience in computation, the results of this calculation are best presented parametrically. Equations (46–8) represent equations (40) and $\delta\beta^2/\delta\sigma$ in this way. Fig. 12 (a) and (b) show the result of some computations. Near $\sigma = 1$, $\beta^2 = \infty$, these added solution curves behave rather like the TE_{11} curve. The leading term in the expansion of β^2 in powers of $\dfrac{1}{\sigma - 1}$ is now

$$\frac{p\left(1 - \dfrac{z_{n+1}^2}{r_0^2}\right)}{\sigma - 1}$$

for the solution curve ending at $I_n - (I_A')_T$. Here z_{n+1} is the $(n+1)^{\text{th}}$ root of $F(z) = 1$, not counting 0.

It will turn out later that the infinity of solution curves just discussed represents an incipient form of the whole mode spectrum; the reservoir

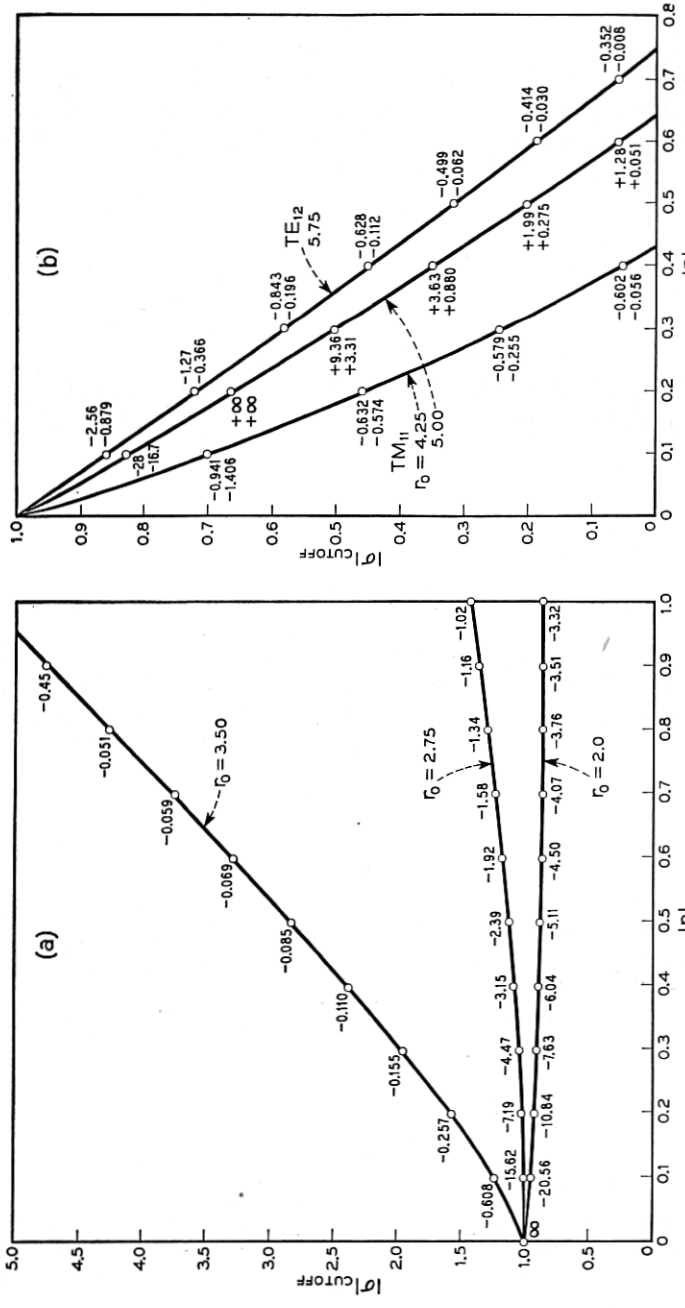

Fig. 12 — Type 1 cutoff. $|\sigma|$ versus $|p|$ for some values of r_0. (a) refers to the TM_{11}-limit mode in its incipient stage; the number attached to the points are values of $\frac{d\beta^2}{d\sigma}$ sgn p at the cutoff. (b) refers to the fully developed TM_{11}-limit and TE_{12}-limit modes in the region $|\sigma| < |\sigma_0|$: the upper attached number is $\frac{d\beta^2}{d\sigma}$ sgn p and the lower attached number $\frac{d\beta^2}{dp}$ sgn p.

from which higher modes are drawn as the guide radius is increased. That the propagation of modes which for larger guide radii correspond to higher TM and TE modes is possible for limited ranges of σ might be ascribed to the larger μ-values in those ranges, which cause the wave to see an effectively larger guide. This explanation is convincing only when $\sigma > 1$. When $\sigma_0 < \sigma < 1$, μ is negative, and the propagation must then be the result of an interplay between μ and κ. In passing we remark that we are here dealing with the propagation analog of so-called "shape resonances," which physicists sometimes encounter in resonance experiments on small spheres of ferrite in cavities.

We now turn to a discussion of the solution curves for $\sigma < 0$ which lie in the third quadrant. Fig. 9(b) shows the partition of the region allowed by the Polder relation (again for $p = \frac{3}{8}$) into positive and negative regions by the various I', $0'$, $(I)_T$ and $(0)_T$ curves. Regions in which $G(\lambda_2, \sigma)$ and $G(T(\lambda_2), \sigma)$ have opposite signs are shaded. For $\sigma < -\sigma_0$, the question whether a given region of like signs is the site of a solution curve may, with one exception, be answered by the same type of geometrical argument as used for $\sigma > 0$. The singular area is that part of the region bounded by I_B' and 0_c in which the G-functions are both positive. Here both $G(\lambda_2, \sigma)$ and $G(T(\lambda_2), \sigma)$ are zero on 0_c; $G(\lambda_2, \sigma)$ goes to ∞ on I_B', whereas $G(T(\lambda_2), \sigma)$ is finite throughout the region. No intersection can be predicted, then, by the earlier argument. It can indeed be shown (for all r_0) that there is no such intersection. For, in the case $p = 0$, the solution curves are I_n' or $0_n'$ curves as demonstrated in Section (4.11). The region under consideration contains no such curves, and hence no solution curves. Thus, for $p = 0$, since $G(\lambda_2, \sigma)$ goes to infinity on I_B', the surface $G(T(\lambda_2), \sigma)$ must lie entirely below the surface $G(\lambda_2, \sigma)$. Consider now, for fixed σ and increasing p, a point on the $G(T(\lambda_2), \sigma)$ surface whose height remains unchanged. For such a point $T(\lambda_2, p, \sigma)$ remains fixed and from the Polder relation this means an increasingly negative λ_2. Since it can be shown that $G(\lambda_2, \sigma)$ goes monotonically from 0 to ∞ as λ_2 becomes more negative, it follows that $G(T(\lambda_2), \sigma)$ continues to be below $G(\lambda_2, \sigma)$ for all p.

All other regions of common sign do carry solution curves. That corresponding to the TE_{11}-limit mode begins at $\sigma = -1$, $\lambda_2 = -1$, passes through the intersection of $(0_0)_T$ and $0_0'$ and persists for indefinitely large σ. The asymptotic formula (38), for β^2 at large σ also holds as $\sigma \to -\infty$, if the signs of both σ and p are taken to be negative. The behavior of β^2 near $\sigma = -1$ may be found by the same means used at $\sigma = 1$. The resulting expression* is to order $\frac{1}{\sigma + 1}$, essentially the same

* See Section 4.17 for a more exact formula.

as the earlier (37) except that the smallest root of $F(z) = -1$ replaces that of $F(z) = 1$. The remaining solution curves confined to the region bounded by $0_0'$, 0_c, $(I_A)_T$ portray the incipient modes already encountered in the first quadrant. Their behavior near $\sigma = -1$ also follows (58), associated with the higher roots of $F(z) = -1$. Their end points, the intersections of I_n' with $(I_A)_T$, are still given by the parametric representation (46–8), due regard being paid to the signs of σ_n and p.

The remaining branch of the TE_{11}-limit mode, lying above $\sigma = -\sigma_0$, is found in the triangle between $(I_A)_T$, $\sigma = 0$ and I_B. Its end points are given by (39) with p negative and by the intersection of I_B' with $(I_n)_T$ which is $\sigma = -(1 + p)$, $\lambda_2 = -1$, $\lambda_1 = 0$. Thus the cut-off in contrast to the analogous branch for $\sigma > 0$, is given by $\beta^2 = 0$, $\sigma = -(1 + p)$. (When $p < -1$, the branch does not exist at all.) We note that a left-circular plane wave is cut off at exactly the same value of σ as the TE-mode is in this particular case (see, however, the following sections). The slope at cut-off is determined by expanding the G functions near their infinities at I_n and I_B' and utilizing the Polder relation. The slope is found to be

$$\frac{d\beta^2}{d\sigma} = \frac{F(r_0)}{p(1 - F(r_0))}. \tag{41}$$

A further solution curve lies in the region between 0_c and $(0_0)_T$ for $\sigma > -\sigma_0$. It has no analogue in a guide with isotropic material and will be discussed later.

In the discussion of the mode spectrum for radii between u_1 and j_1 three distinct types of cut-off point have already been encountered. When larger radii are treated it is found that no other types arise.* In Section 4.17 formulas relevant to the three types are given. An examination of the field components in the neighborhood of the cut-off points is of some interest. Cut-off points of type one (intersections of I_n and $(I_A')_T$ or I_n' and $(I_A)_T$), at which $\beta^2 = 0$, have $E_z = 0$ and the field is of a pure TE-type. The medium behaves transversely as though it had a permeability, $\mu - \kappa^2/\mu$. Although the field is purely TE at cut-off the mode terminating at such a point may in the limit of vanishing magnetization be either a TE- or a TM-mode. This impartiality extends to cut-off points of the other types. Cut-off points of type II $[(0_n')_T - 0_c$ or $(0_n)_T - 0_c']$ occur at $\sigma = \pm\sigma_0$, where $\mu = 0$ and here β^2 does not vanish. In such cases one of the χ's is finite and the corresponding contributions to the field pattern quite normal. The other, however, tends

* There is an exception to this statement. This is the type designated in Section 4.17 as $2_{0\infty}$ which cuts off an isolated mode having no TE or TM analogue.

to an infinite imaginary value and the associated fields are confined very closely to the guide walls. The wall currents are very large and essentially longitudinal. Type III cut-off points $[I_B - (I_A)_T]$ at which $\mu = -\kappa$ have $\beta^2 = 0$, but the fields are not of a purely TE- or TM-type. They consist essentially of a rotating, transverse, H, which is uniform over the guide. The components H_z, E_θ and E_r are smaller by one order of $\sigma - \sigma_{\text{cut-off}}$ and E_z, two orders smaller.

It should be stressed again that, in general, the modes are never of pure TE or TM type. Nevertheless, for the sake of brevity, we shall refer to them as such; calling them TE-modes or TM-modes according to their limit as the magnetization is removed.

4.13. We now consider the behavior of the modes as a function of radius. The reader will be aided by Figs. 8(a) to (e) and 9(a) to (g). In preparation for this it is necessary to examine the movement of the I_n, I_n' and 0_n, $0_n'$ curves when r_0 is varied. It will be recalled that the equation for the I_n curves and their reflections, I_n', in the origin, is

$$\frac{1 - \lambda^2}{1 - \sigma\lambda} = \frac{j_n^2}{r_0^2}.$$

The contours $\chi(\lambda, \sigma) = C$, where $\chi^2 = (1 - \lambda^2)/(1 - \sigma\lambda)$ have already been plotted in Fig. 4. The I_n, I_n' curves are among these, and, clearly, for a fixed n, the associated χ^2 decreases as r_0 increases. The course of a given pair (I_n, I_n') may then be seen directly from Fig. 4. The qualitative behavior of the pair changes radically only when r_0 passes through the value j_n. Before it does so, I_n lies, for λ between 0 and 1, above $\sigma = \lambda$ and tends to $\sigma = \infty$ as λ tends to zero. At $r_0 = j_n$, the I_n and I_n' curves merge into the lines $\sigma = \lambda$ and $\lambda = 0$. Beyond j_n, I_n lies below $\sigma = \lambda$ for λ between 0 and 1 and goes to $-\infty$ as λ approaches zero. The I_n'-curve remains, throughout the reflection of I_n in the origin. As $r_0 \to \infty$, I_n tends to the line $\lambda = 1$, I_n' to $\lambda = -1$. No I_n curves ever enter the region $\lambda > 1$, $\sigma < 0$; no I_n' curves enter $\lambda < -1$, $\sigma > 0$. It is also important to relate the I_n, I_n' curves to the boundaries of the Polder regions. I_n curves cut the Polder boundary $\sigma = \lambda - p$, of the first quadrant in at most one point. As r_0 increases from 0 to j_n, this point moves from $\sigma = \sigma_0$ to $\sigma = \infty$. Thereafter, no intersection occurs at fixed p until r_0 equals $j_n/\sqrt{1 - p^2}$; it here reappears at $\sigma = 0$ and moves steadily to $\sigma = 1 - p$ as r_0 increases indefinitely. The only intersection with the other Polder boundary $\sigma = 1/\lambda$, is at $\lambda = 1$, $\sigma = 1$, regardless of r_0.

The 0_n, $0_n'$ curves are given by

$$\sigma = \frac{1}{\lambda}\left[1 - r_0^2 \frac{1 - \lambda^2}{(F^{-1}(\lambda))^2}\right]$$

if the n^{th} branch of $F^{-1}(\lambda)$ is used. Thus, as r_0 increases, the successive curves either all pass through a fixed point (which can only be $\lambda = \pm 1$, $\sigma = \pm 1$, $n > 0$) or move steadily up or down without further intersection. An 0_n curve starts from $\sigma\lambda = 1$ at $r_0 = 0$ and falls for $\lambda < 1$, rises for $\lambda > 1$, as r_0 increases. For large λ, since $\sigma \sim j_n^2/r_0^2$ ($\lambda \to 2$), $n > 0$, the 0_n and I_n curves move together with a constant separation. 0_0 is singular, since it does not pass through λ, $\sigma = 1$ and falls steadily for all λ; it tends to $\sigma = 0$ for large λ. The $0_n'$ curves rise from $\sigma\lambda = 1$ at $r_0 = 0$ for $-1 < \lambda$, fall for $\lambda < -1$. They run parallel to I_{n+1}' for $-\lambda$ very large. For small λ there is an expansion

$$\sigma = \left(1 - \frac{r_0^2}{u_n^2}\right)\frac{1}{\lambda} - \frac{2r_0^2}{u_n^2(u_n^2 - 1)} + 0(\lambda)$$

holding for 0_n and for $0_n'$. This indicates that for $r_0 < u_n$, 0_n goes to $+\infty$ and $0_n'$ to $-\infty$ for small λ, but at $r_0 = u_{n+1}$, 0_n and $0_n'$ merge momentarily at

$$\lambda = 0,$$

$$\sigma = -\frac{2r_0^2}{u_{n+1}^2(u_{n+1}^2 - 1)} < 0.$$

For larger r_0, 0_n goes to $-\infty$ and $0_n'$ to $+\infty$. Since the union of 0_n and $0_n'$ takes place at a negative σ, it is clear that 0_n curves, unlike I_n curves, may cross the line $\sigma = 0$ twice. Intersections of the 0_n, $0_n'$ curves with the Polder boundary are difficult to examine explicitly and this may lead to some obscure situations for $0 < |\lambda| < 1$. However, for $\sigma > \sigma_0$, since 0_n and I_n have a fixed separation for large $|\lambda|$, this pair escape intersection with the boundary at the same value of r_0, namely j_n. Similarly $0_n'$ and I_{n+1} escape together at $r_0 = j_{n+1}$ for $\sigma < -\sigma_0$.

We shall now examine the effect of varying r_0 upon the sequence of modes when $\sigma > \sigma_0$. When r_0 is less than u_1, a case in which the isotropic medium would not propagate, no part of $0_0'$ lies in the upper half plane and there is then no $(0_0')_T$ curve. The solution curve which in the previous discussion of Section 4.12 was assigned to TE_{11}, after passing the intersection $[I_1 - (I_B)_T]$ can no longer escape to infinity and terminates on $[I_1 - (I_A)_T]$. Thus, the TE_{11} mode at this radius has become an incipient mode with cut-off and other properties given by the formulae already quoted for such modes. As r_0 approaches u_1 from below, the $\beta^2 - \sigma$ curve is double valued between $\sigma_{\text{cut-off}}$ and some larger value. This is borne out by the fact that $d\beta^2/d\sigma$ becomes positive at cut-off, and by the observation that the solution curve bulges towards large σ between $I_1 - (I_B')_T$ and its terminus. The part of the $\beta^2 - \sigma$

curve along which $\frac{d\beta^2}{d\sigma} < 0$, will tend smoothly towards the $\beta^2 - \sigma$ curve for r_0 just greater than u_1. The course of the TE_{11} solution curve remains qualitatively unchanged for all $r_0 > u_1$.

When r_0 passes through u_1, and the TE_{11} solution curves escapes discontinuously to infinity, the solution curves below it disengage from their former end points $I_{n+1} - (I_A)_T$ and instead end at the point $I_n - (I_A)_T$. When r_0 exceeds j_1, the curves I_1 and 0_1 escape intersection with $\sigma = \lambda - p$ simultaneously, for $\sigma > \sigma_0$, and the curve $(I_1')_T$ makes its first appearance. From the asymptotic formulae (App. II) the latter runs to infinity between I_1 and 0_1, and now the solution curve which ended for $u_1 < r_0 < j_1$ at $I_1 - (I_A)_T$ is carried to infinity between I_1 and $(I_1)_T$. The asymptotic expression for β^2 versus σ, given in formula (56) indicates that β^2 tends to the isotropic value for the TM_{11} mode. No further qualitative changes will take place in behavior of this mode as r_0 increases.

As r_0 increases through u_2 (the value at which the isotropic medium supports the TE_{12} mode), the $(0_1')_T$ curve makes its appearance, an event accompanied by the escape of the uppermost incipient solution curve (the one ending at $(I_A)_T - I_2$) to infinity. The escape takes place in the same way as that of the TE_{11} solution curve as r_0 passed through u_1. The newly escaped curve, of course, represents the TE_{12}-limit mode. The end points of the remaining incipient solution curves also jump discontinuously to their next higher neighbors as they did at $r_0 = u_1$. The course of events as r_0 is increased further should now be abundantly clear, and is summarized in Table I on page 642.

We now turn to the region $0 < \sigma < \sigma_0$ and consider first the situation $0 < r_0 < u_1$. It is clear that in the area bounded by 0_∞, 0_0, $(I_A')_T$ and $(I'_B)_T$ both G functions are negative. There is no simple geometrical argument which determines the existence of a solution curve in this region. It is therefore necessary to use a type of analytic argument, which is useful in a number of other cases, although fully discussed only in the present instance.

We show that the least value attained by $G(\lambda_1, \sigma)$ in the admissible region for $p = 0$ (which contains all regions admissible for other p-values) is greater than the maximum value of $G(\lambda_2, \sigma)$ in the range $-1 < \lambda_2 < 0$, $\sigma > 0$. Consider the variation of $G(\lambda_1, \sigma)$ as the point $\lambda_1 = 1$, $\sigma = 1$ is approached along a line of constant χ^2 in the admissible region for $p = 0$ (see Fig. 4). We have the relation

$$G(\lambda,\sigma) = \frac{1}{\chi^2}\left[\frac{1}{\lambda} F(r_0\chi) - 1\right].$$

For χ^2 negative, $F(r_0\chi)$ is positive and thus, as λ approaches unity from above G decreases. Again for χ^2 positive and $r_0 < u_1$, $F(r_0\chi)$ is positive and thus, as λ approaches unity from below, G also decreases. Thus for any χ^2, $G(\lambda, \sigma)$ takes on its least value at $\sigma = 1, \lambda = 1$ and this value is

$$\frac{1}{\chi^2}\,[F(r_0\chi) - 1].$$

The minimum value of this limit in this region is $F(r_0) - 1$ and is greater than -1. In the region $-1 < \lambda_2 < 0$, $\sigma > 0$, χ^2 is between 0 and 1, and the χ^2 curves run from $\sigma = 0$ to $\sigma = \infty$. G will clearly decrease as σ increases from zero on any one of these curves. Thus G attains its maximum on $\sigma = 0$, where its value is

$$-\frac{1}{1-\lambda^2}\left[\frac{F(r_0\sqrt{1-\lambda^2})}{|\lambda|} + 1\right].$$

Since $F(r_0\sqrt{1-\lambda^2})$ is positive for $r_0 < u_1$ and $|\lambda| < 1$, G is clearly less than -1. In passing we note that for $r_0 = u_1$, both G functions may attain the value -1.

As r_0 passes through u_1, the $(0_0')_T$ curve appears in the region under discussion and together with $(I_B')_T$ delimits the region carrying the TE_{11}-solution curve already discussed at length. No qualitative changes occur in that curve as r_0 is increased indefinitely. When r_0 exceeds j_1, the $(I_1')_T$ curve appears between $(0_0')_T$ and $(I_A')_T$. Between $(I_A')_T$ and $(I_1')_T$ the G functions have a region of common sign, yet no solution curve arises there for a given p until r_0 reaches $j_1/\sqrt{1-p^2}$.* From then on, the I_1 curve cuts $(I_A')_T$, see Fig. 9(c), and a solution curve exists between $(I_1')_T$ and I_1. It is cut off at the intersection $(I_A')_T - I_1$; there, $\beta^2 = 0$ and σ, $\dfrac{d\beta^2}{d\sigma}$ are given by the same parametric formulae (46–8) applying to the cut-off of incipient modes, the parameter θ being negative. The curve begins at $\sigma = 0$, where it satisfies the usual equation, which for this radius has two solutions. The solution with the smaller λ, belonging to the present curve, tends to the isotropic TM_{11}-limit as $p \to 0$. At a fixed r_0, sufficiently below u_2, this mode does not exist at

* There are some exceptions to this statement. When $4.82 < r_0 < u_2 = 5.33$ and p exceeds $\sqrt{1 - j_1^2/r_0^2}$, a double-valued $\beta^2 - \sigma$ curve exists between two positive σ values. For values of r_0 still closer to u_2 further regions of common sign may arise as a result of the interplay of the $(0_1')T$ and $(I_A')_T$ curves. We have not examined these regions closely. Such dubious regions are confined to the immediate neighborhoods below the u_n.

all when

$$p > \sqrt{1 - \frac{j_1^2}{r_0^2}}.*$$

If r_0 is greater than u_2, the $(0_1')_T$ curve has appeared. A new region of like signs of the G's arises between it and $(I_1')_T$, see Fig. 9(e), and contains a solution curve. This ends at σ_0, λ_{10} and begins at $\sigma = 0$ at a value of λ_1 pertaining to the TM_{11}-mode. Thus, it is clear that as r_0 passed u_2, the end-point of the TM_{11} curve jumped discontinuously from $(I_A')_T - I_1$ to σ_0, λ_{10}. This jump is anticipated as r_0 approaches u_2; the $\beta^2 - \sigma$ curve first bulges beyond $(I_A')_T - I_1$ towards its later course and returns to that point with positive slope. As r_0 increases further no change occurs in the qualitative behavior of the mode. It may be noted that above u_2 the mode exists for all p.

Beyond $r_0 = u_2$, at least part of the area between I_1 and $(I_A')_T$ is an admissible region and does in fact contain the TE_{12} solution curve. It begins at $\sigma = 0$ and λ_1 given by that solution of eqn. (39) which is, in the limit $p = 0$, the TE_{12} solution. It is cut off with $\beta^2 = 0$ at $(I_A')_T - I_1$, the end point relinquished by the TM_{11}-solution curve. As r_0 passes j_2, the TE_{12} solution retains its cut-off point, but, beyond $r_0 = u_3$, it will transfer this point discontinuously to σ_0, λ_{10}. Thereafter its course remains essentially unaltered. Tables I, II and III show the progression of cut-off points of the various modes.

It may be recalled that in the analysis of $u_1 < r_0 < j_1$, the modes in $\sigma < -\sigma_0$ followed essentially the same course as in $\sigma > \sigma_0$. This is also true of their progress with changing radius and of the escape process. The singular character of the $(0_0)_T$ curve and the presence of I_B lead to some local changes in the progress of the modes but have no effect on their more salient features in this particular range of σ. The scheme of progression of the end points is shown in Table I.

In contrast with the state of affairs in the region just discussed, the mode structure in the area between $\sigma = 0$ and $\sigma = -\sigma_0$ is very markedly affected by the presence of $(0_0')_T$ and I_B'.

When $r_0 < u_1$, a solution curve exists between $\sigma = -1 - p$, and $\sigma = -\sigma_0$. It starts with $\beta^2 = 0$ at the intersection of $(I_A)_T$ and (I_B') with a slope given by (41). For sufficiently small r_0, β^2 tends to infinity as $\sigma \to \sigma_0$, since the solution curve approaches the line $0_c'$ or $(0_\infty)_T$. Its shape is then given by (52), see Section 4.17. As r_0 increases, 0_0 falls steadily. Eventually, for sufficiently large p, its minimum falls below

* See footnote on page 628.

$-\sigma_0$. $(0_0)_T$ now has two branches for $\sigma > -\sigma_0$, which pass through the point $\sigma = -\sigma_0$, $\lambda_2 = -\frac{1}{\sigma_0}$ making there a finite angle with each other. $(0_0)_T$ is completed by a loop in $\sigma < -\sigma_0$, Fig. 9(g), which does not affect the incipient modes appreciably. The mode in question now has two branches. The first starts as before and ends at $\sigma = -\sigma_0$, where the associated β^2 is given by $\beta_a{}^2 = \lambda_a/\sigma_0$ and λ_a is the smaller root of

$$F\left(r_0\sqrt{\frac{1-\lambda_a{}^2}{1-\sigma\lambda_a}}\right) = \lambda_a . \tag{42}$$

It resumes at $\sigma = -\sigma_0$ and $\beta^2 = \beta_b{}^2 = \lambda_b/\sigma_0$, where λ_b is the larger root of the above equation, progresses to smaller $|\sigma|$-values and then back to $\sigma = -\sigma_0$ where β^2 tends to infinity again in accordance with (52). Beyond $r_0 = u_1$, where 0_0 rises steadily from $\sigma = -\infty$ to $\sigma = 0$ with increasing λ, one branch of $(0_0)_T$ in $-\sigma_0 < \sigma < 0$ disappears and only the second branch of the mode remains. Neither branch has an analogue in ordinary waveguides; as $p \to 0$ each lies in a smaller and smaller neighborhood of $\sigma = 1$, and finally vanishes into $\sigma = 1$, $\lambda_2 = -1$.

For r_0 between u_1 and j_1 there is a single solution curve starting at $\sigma = 0$ and ending with $\beta^2 = 0$ at $(I_A)_T - I_B'$. This may be identified in the limit $p = 0$, with the TE_{11}-limit mode, and has already been fully discussed for $u_1 < r_0 < j_1$. No change in the formula for its cut-off point occurs up to $r_0 = u_2$. A useful spot-point $(I_B' - (I_1)_T)$ along its course can be found when

$$0 < p < 1 - \sqrt{1 - \frac{j_1{}^2}{r_0{}^2}}$$

and is given by (60).

In the range $j_1 < r_0 < u_2$, a further solution curve (corresponding to the TM_{11}-limit mode) can arise, provided

$$p < \sqrt{1 - \frac{j_1{}^2}{u_2{}^2}}$$

The radius at which it will then first appear is

$$r_0 = \frac{j_1}{\sqrt{1-p^2}} .$$

It begins on $\sigma = 0$, according to (39) and is cut off, with $\beta^2 = 0$, at $(I_A)_T - I_1'$.

As r_0 passes u_2 , the cut-off point of the TE_1 solution curve moves dis-

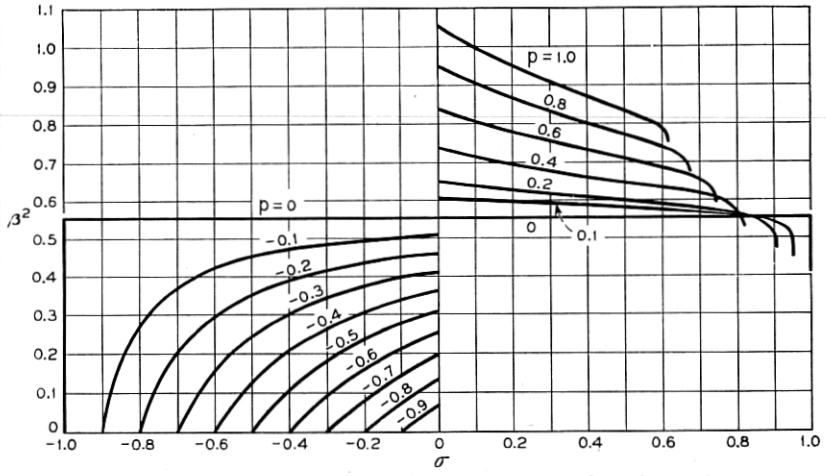

Fig. 13 — Approximate course of modes in the $\beta^2 - \sigma$ plane for various p values and at two values of r_0. Fig. 13(a), above, $r_0 = 2.75$, TE_{11}-limit modes; $-1 < \sigma < 1$. Fig. 13(b), $r_0 = 2.75$, TE_{11}-limit mode and incipient TM_{11}-limit mode, $\sigma > 1$. Fig. 13(c), $r_0 = 2.75$, TE_{11}-limit mode, $\sigma < -1$. Fig. 13(d), (e) and (f), $r_0 = 5.75$, TE_{11}-limit and TE_{12}-limit modes; Fig. 13(d), $-1 < \sigma < 1$; Fig. 13(e), $\sigma > 1$; Fig. 13(f), $\sigma < -1$. Fig. 13(g), 13(h) and 13(i), $r_0 = 5.75$, TM_{11}-limit modes; Fig. 13(g); $-1 < \sigma < 1$; Fig. 13(h), $\sigma > 1$; Fig. 13(i), $\sigma < 1$. It should be noted that a scale linear in $\frac{\beta^2}{1+\beta^2}$ is used for convenience when $|\sigma| > \sigma_0$.

continuously to $\sigma = -\sigma_0$, $\lambda_2 = -\frac{1}{\sigma_0}$ and, simultaneously, the cut-off point of the TM_{11} curve occupies the position relinquished by the former. The TM_{11} mode now exists for all p. A new solution curve (TE_{12}) appears in the region bounded by $0_1'$, $(0_1)_T$ and I_1', if p is not too large, terminating at $(I_A)_T - I_1'$, the point left by the TM_1 terminus. (If p exceeds $\sqrt{1 - j_1^2/u_3^2}$ this curve will not exist at all.)

Figs. 13(a) to (i) and 14 show the approximate course of the $\beta^2 - \sigma$ curves for the TE_{11} mode at $r_0 = 2.75$ and for the TE_{11}, TM_{11} and TE_{12} modes at $r_0 = 5.75$. The incipient TM_{11} mode at $r_0 = 2.75$ is shown for positive σ, p only. They were computed by the methods outlined above.

4.14. *Guides of large radius.* It is of some interest because of the high dielectric constant of ferrites to examine the behavior of the modes as the radius, r_0, is allowed to become very large. The two sides of the G-equation will remain determinate for unlimited r_0 provided

$$r_0 \sqrt{\frac{1 - \lambda_1^2}{1 - \sigma\lambda_1}} \left(\text{or } r_0 \sqrt{\frac{1 - \lambda_2^2}{1 - \sigma\lambda_2}} \right)$$

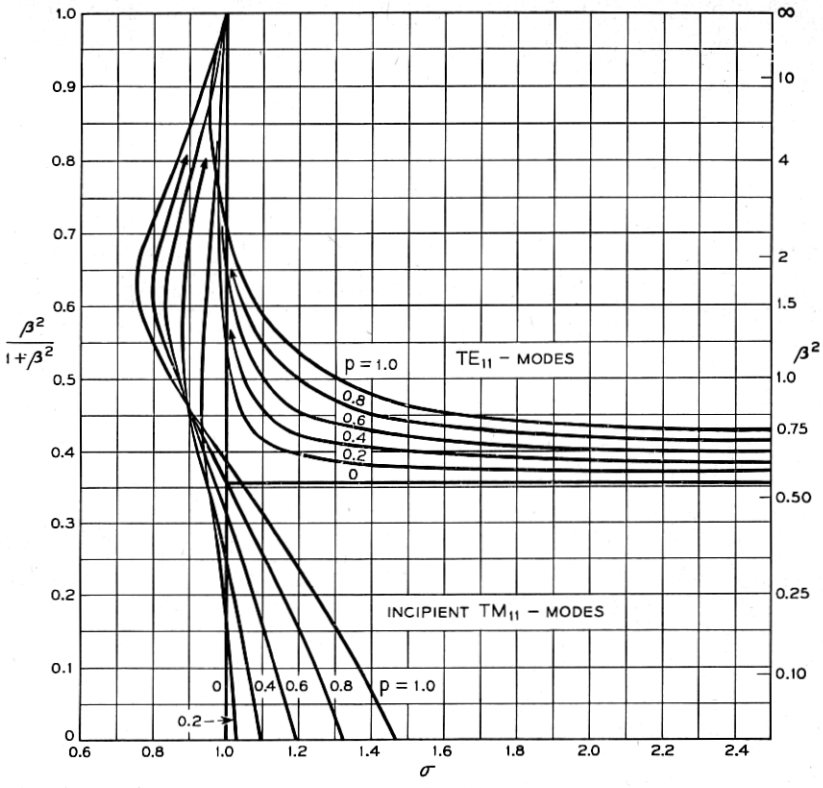

Fig. 13(b) — See Fig. 13.

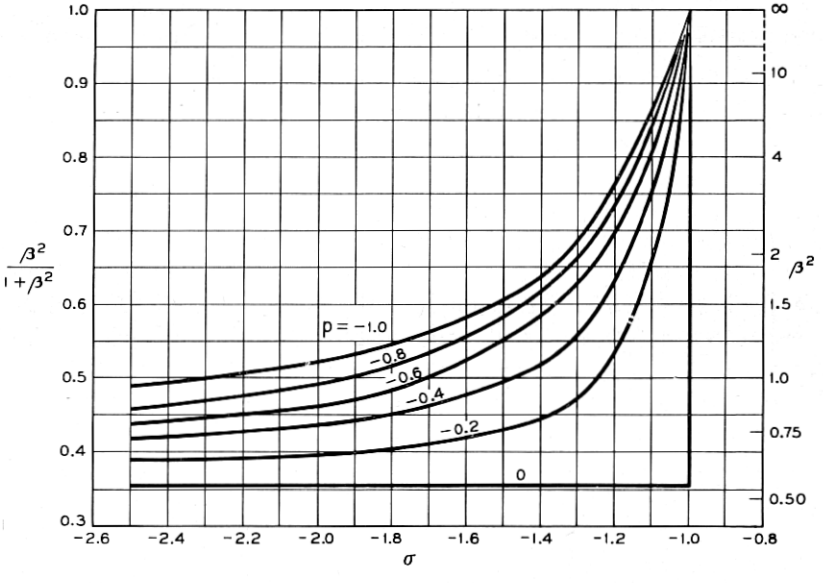

Fig. 13(c) — See Fig. 13.

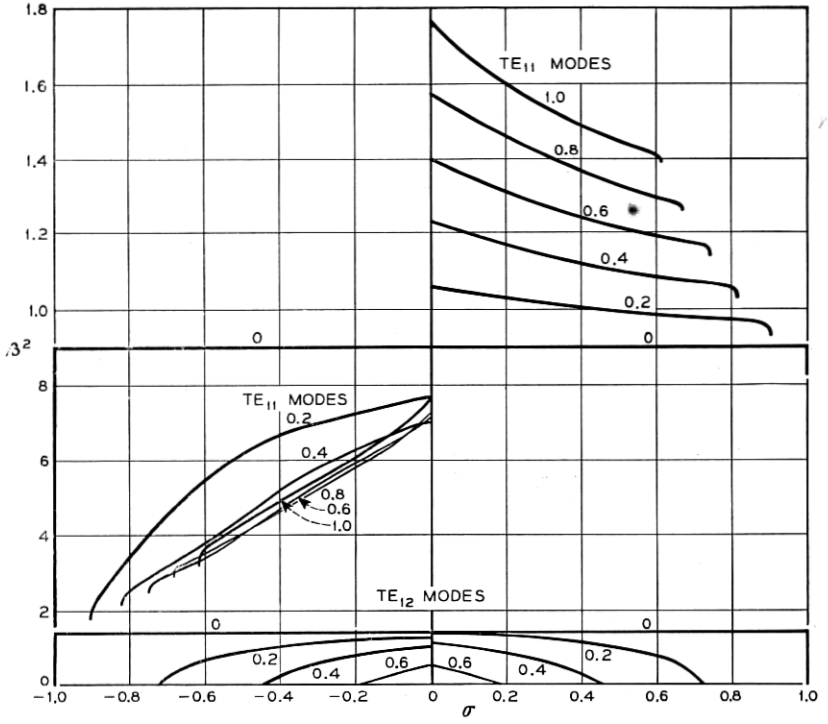

Fig. 13(d) — See Fig. 13.

remains finite, while

$$r_0 \sqrt{\frac{1 - \lambda_2^2}{1 - \sigma\lambda_2}} \left(\text{or } r_0 \sqrt{\frac{1 - \lambda_1^2}{1 - \sigma\lambda_1}} \right)$$

becomes infinite imaginary. Examining the solutions obtained under these conditions it is possible to find expansions for β^2 in inverse powers of r_0^2. These are as follows:

$$\text{for } p > 0, \sigma > 1 \text{ or } p < 0, -\sigma_0 < \sigma < 0$$

$$\beta^2 = 1 + \frac{p}{\sigma - 1} - \left(1 + \frac{p/2}{\sigma - 1}\right) \frac{x_n^2}{r_0^2}, \tag{43a}$$

where the x_n are the successive roots greater than zero of $F(x_n) = 1$ and the modes are associated with the x_n by the scheme: $TE_{11} \rightarrow x_1$, $TM_{11} \rightarrow x_2$, $TE_{12} \rightarrow x_3$, etc:

$$\text{for } p > 0, 0 < \sigma < \sigma_0 \text{ or } p < 0, \sigma < -1$$

$$\beta^2 = 1 + \frac{p}{\sigma - 1} - \left(1 + \frac{p/2}{\sigma + 1}\right) \frac{y_n^2}{r_0^2}, \tag{43b}$$

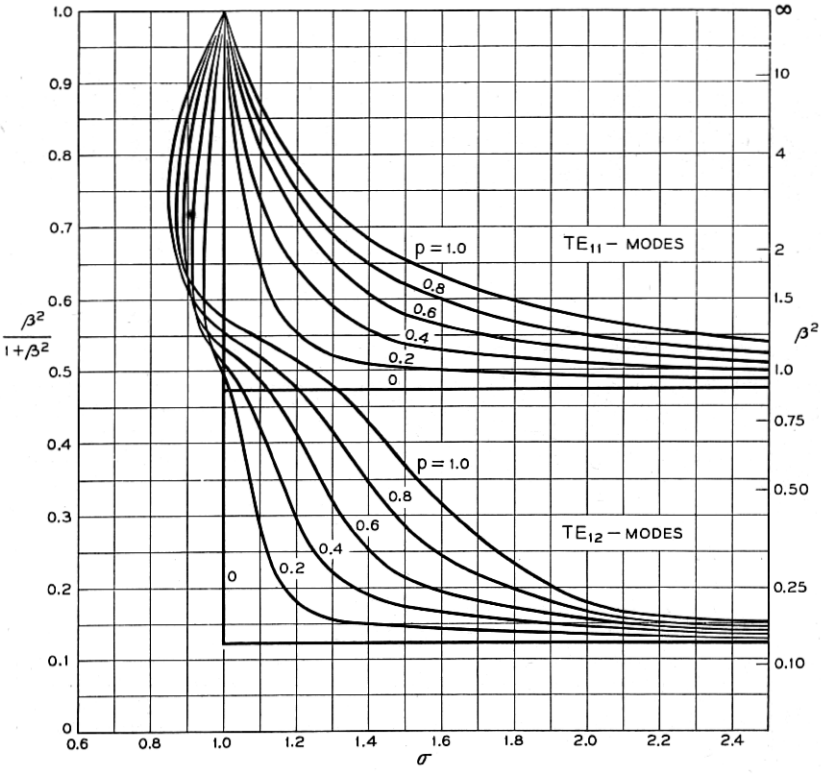

Fig. 13(e) — See Fig. 13.

with $F(y_n) = -1$ and $TE_{11} \rightarrow y_1$; $TM_{11} \rightarrow y_2$; $TE_{12} \rightarrow y_3$, etc.

$$\text{for } p > 0,\ \sigma_0 < \sigma < 1 \text{ and } p < 0,\ -1 < \sigma < -\sigma_0,$$

there are no solutions.

These formulae are valid for any p which is not itself so small as to be of order $1/r_0^2$. If they are applied to modes varying as $e^{jn\theta}$, where $n = \pm 1$ and σ, p are positive, they indicate the following results: for $\sigma > 1$, $n = \pm 1$, $\beta^2 \rightarrow 1 + \dfrac{p}{\sigma - 1}$; for $\sigma_0 < \sigma < 1$, no $n = \pm 1$ modes; for $0 < \sigma < \sigma_0$, $n = \pm 1$, $\beta^2 \rightarrow 1 + \dfrac{p}{\sigma + 1}$. These, in turn, may be classified in the following way. For $\sigma > 1$, $n = -1$, and for $0 < \sigma < \sigma_0$, $n = +1$ which correspond to μ and κ both positive, the propagation constant tends to the value for a plane wave whose direction of circular polarization coincides with that of the wave guide pattern. For $\sigma_0 < \sigma < 1$,

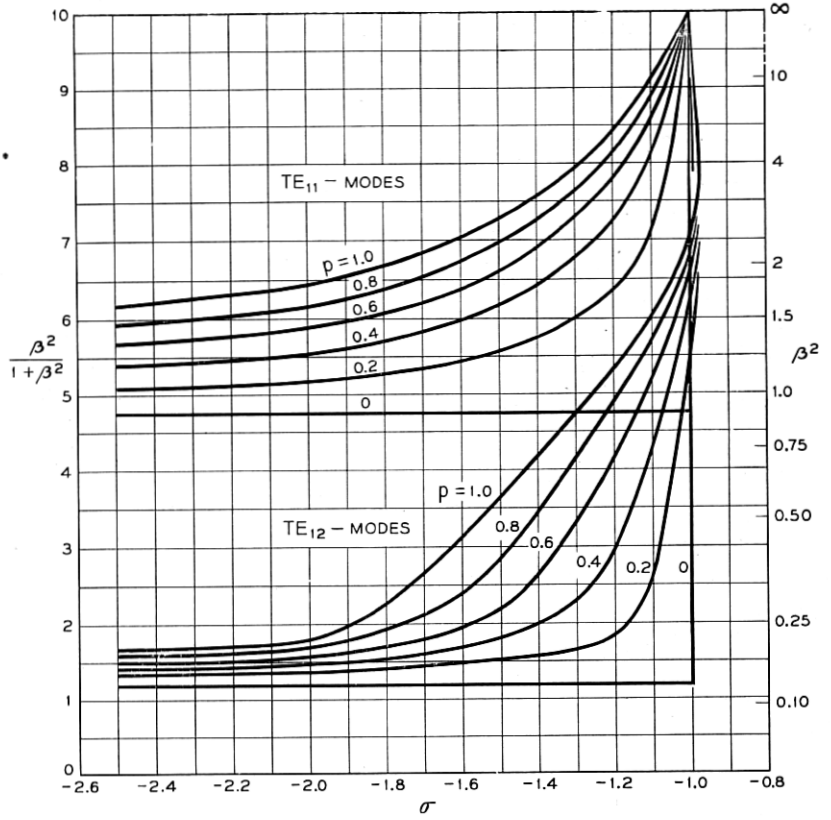

Fig. 13(f) — See Fig. 13.

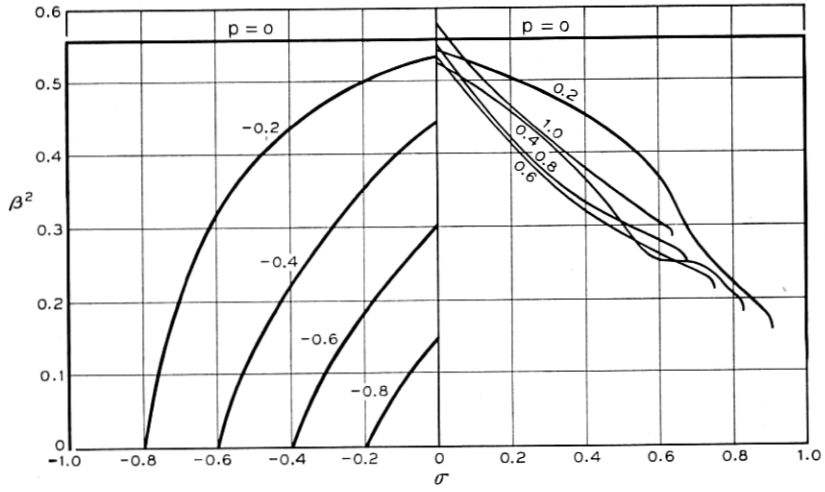

Fig. 13(g) — See Fig. 13.

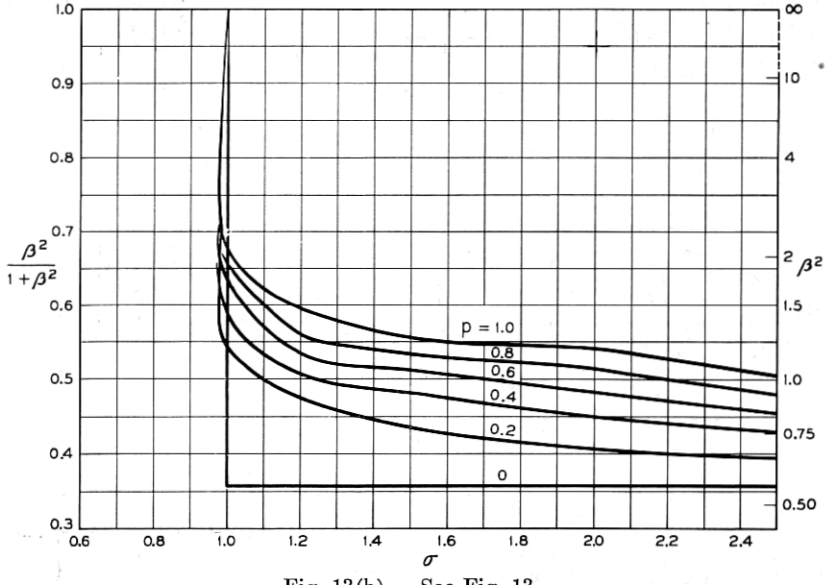

Fig. 13(h) — See Fig. 13.

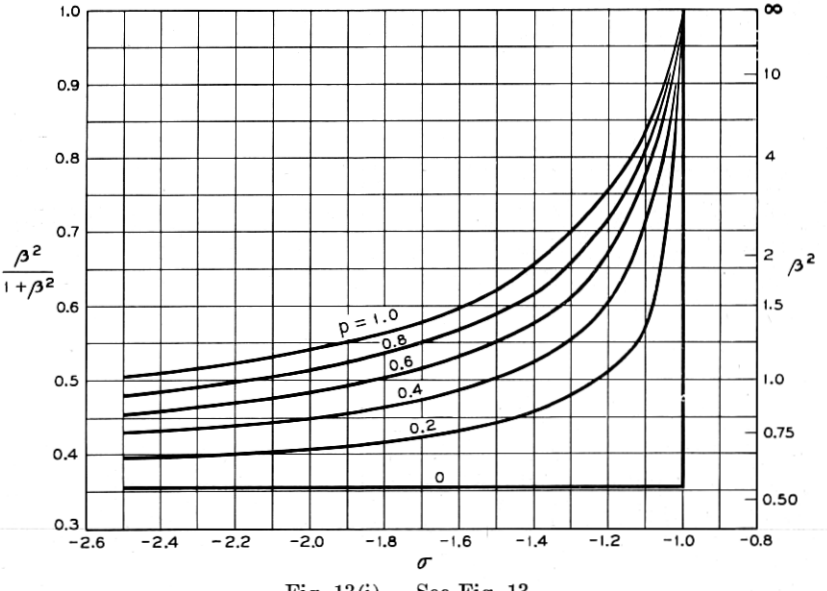

Fig. 13(i) — See Fig. 13.

where μ is negative, $n = \pm 1$, no modes exist for large enough guide. For $0 < \sigma < \sigma_0$, $n = -1$ and $\sigma > 1$, $n = +1$, the propagation constant tends to that for a plane wave whose polarization is in the opposite sense to that of the field pattern and here μ is positive, but κ is negative. An examination of the field pattern in this last case shows that most of the field energy is indeed associated with a circular polarization opposite to that of the pattern as a whole.

The discussion of the preceding sections shows that the complete structure of the mode spectrum for a guide filled with lossless ferrite is very complex. It is also clear that for some combinations of guide size and magnetic parameters the course of an individual mode in the $\beta^2 - \sigma$ plane may be quite involved. In particular, two values of β^2 associated with the same mode often occur at a given σ. The extent to which the complexity of the spectrum will be observed in practice will depend principally upon the loss of the real ferrite and upon the guide radius. The effect of loss near $\sigma = 1$, where the incipient modes are crowded will be to cause simultaneous excitation of many of these and consequently a confused z dependence of the guide excitation. For values of r_0 just below j_n, the point of escape of the TE modes, the latter exist over considerable ranges of σ, see Fig. 12(a), and would probably be observable. The TE modes near u_n also persist over a wide range, but are double-valued. Concerning such double-valued waves it may be observed that from the results of the subsequent treatment of losses, it is clear that if $\dfrac{d\beta^2}{d\,|\,\sigma\,|} > 0$, it is necessary to put the source of power at the opposite end of the guide.

4.15. *Losses, Faraday rotation and merit figure.* So far the analysis has been concerned with the loss-free medium. It is of some interest to determine the attenuation constant (the imaginary part of β) that arises when losses are taken into account. As long as these are small, this can be done rather easily; in fact, sufficiently far from resonance ($\sigma = 1$), for each formula giving β^2, we can establish one giving the attenuation constant.

If the losses are of magnetic origin we utilize the fact (already demonstrated in section 2) that to first order in α, the permeabilities μ, κ are functions of $\sigma + j\alpha \operatorname{sgn} p$, and of no other combination of σ, α. Since σ, α enter Maxwell's equations only through μ and κ, β^2, which is derived from them, must likewise depend on σ through $\sigma + j\alpha \operatorname{sgn} p$. Any formula for β^2 derived for the loss-free medium can, therefore, be generalized to the lossy case by replacing σ with $\sigma + j\alpha \operatorname{sgn} p$, to first order in α. To this order, then, we find

$$\beta^2 = \beta'^2 + ja \operatorname{sgn} p \frac{\partial(\beta')^2}{\partial\sigma},$$

where β' is the propagation constant for the loss-free case. Thus

$$j\beta = j\beta' - \frac{\alpha}{2\beta'} \frac{\partial(\beta')^2}{\partial \mid \sigma \mid}, \tag{44}$$

and the last term on the right, (multiplied by our scaling variable $\beta_0 = \omega\sqrt{\mu_z\epsilon_0}$) is the attenuation in nepers per meter. The present convention is that the waves propagate in the positive z direction, as exp $(-j\beta z)$. It follows that they will decrease in that direction only if $\partial(\beta')^2/\partial \mid \sigma \mid < 0$. Occasionally this is not the case, and presumably indicates that the direction of the power flow opposes that of the phase velocity.

For small dielectric loss, too, it is possible to derive formulae for the attenuation constant from those already obtained; obviously the latter depend on ϵ only through $\epsilon = \epsilon_0 - j\epsilon_1$, and can therefore be expanded. But it must now be remembered that β was defined as $\beta_{\text{actual}}/\omega\sqrt{\mu_z\epsilon}$. and r_0 as $r_{\text{actual}}\ \omega\sqrt{\mu_z\epsilon}$ so that the scaling parameter $\omega\sqrt{\mu_z\epsilon}$ will make contributions to the imaginary part. It is then readily verified that

$$\frac{\beta_{\text{actual}}}{\omega\sqrt{\mu_z\epsilon_0}} = \beta' - j\frac{\epsilon_1}{2\epsilon_0}\frac{1}{\beta'}\frac{\partial}{\partial(r_0^2)}(r_0^2\beta^2). \tag{45}$$

A few words may be said about the relation of Faraday rotation to the $\beta^2 - \sigma$ curves. A linearly polarized plane wave traveling in the unbounded medium along the magnetizing field can be regarded as the

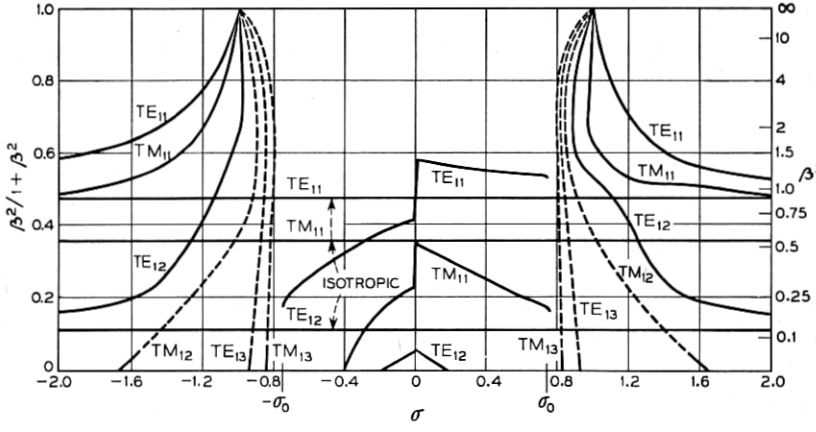

Fig. 14 — The course of the fully developed modes (solid lines) and of some of the lower incipient modes (dotted lines) as a function of σ for $r_0 = 5.75$ and $\mid p \mid = 0.6$.

sum of right and left circular components which travel with different propagation constants. If these are β_+ and β_- (measured in units of β_0) the plane of polarization of the resultant will appear to rotate by $(\beta_+ - \beta_-)/2$ radians per reduced wavelength $\frac{\lambda}{2\pi} = \frac{1}{\beta_0}$.

In the filled waveguide, on the other hand, it is no longer true that right and left circularly polarized modes add up to a plane polarized mode, as is readily seen by reference to the field components given in Appendix IV. To define Faraday rotation in a simple way it is therefore necessary to neglect changes in the field pattern due to the magnetization and consider only the changes in the propagation constants. Then the rotation of a mode with azimuthal mode number n will be $\frac{1}{2n}(\beta_+ - \beta_-)$. In the present case $n = 1$, and the β_+, β_- are found from the curves of β^2 versus σ, Figs. 13(a) to (i), for positive (σ, p) and negative (σ, p) respectively.

The merit figure is defined as the ratio — radians rotation per neper loss — and is independent of path-length. For small losses, (neglecting terms $0(\alpha^2)$), this ratio is

$$\frac{Rl(\beta_+ - \beta_-)}{Im(\beta_+ + \beta_-)} = \frac{1}{\alpha} \frac{\beta_+' - \beta_-'}{\frac{\partial \beta_+'}{\partial |\sigma|} + \frac{\partial \beta_-'}{\partial |\sigma|}},$$

in the notation of the present Section.

4.16. *Formulae for the ferrite.*

I. *Cut-off points*

Cut-off points will be classified into three types, 1, 2 and 3, according to the nature of the intersecting curves which generate them. All points of a given type may be assigned an index which further identifies the generating curve. This will be written as a subscript.

Type 1. Intersections of $I_n - (I_A')_T$, $\sigma > 0$, written as 1_n and of $I_n' - (I_A)_T$, $\sigma < 0$, written as $1_n'$

$\beta^2 = 0$

There is a parametric representation:

$$\begin{aligned} |\lambda_{1,2}| &= e^{\theta}, \\ |p| &= 2 \sinh \theta \left(1 - \frac{r_0^2}{j_n^2}\right) \text{ and} \\ |\sigma| &= \frac{r_0^2}{j_n^2} e^{\theta} + \left(1 - \frac{r_0^2}{j_n^2}\right) e^{-\theta}. \end{aligned} \tag{46}$$

The slope at cut-off:

$$\left(\frac{\partial\beta^2}{\partial\sigma}\right)_p = \frac{\frac{j_n^2}{r_0^2}\left(\frac{j_n^2}{r_0^2} - 1\right)\coth\theta}{\left[\frac{j_n^2}{r_0^2} - 1 + \frac{2}{F(r_0)}\right]e^{-\theta} - e^{\theta}} \cdot \operatorname{sgn}\sigma, \tag{47}$$

and

$$\left(\frac{\partial\beta^2}{\partial p}\right)_\sigma = -\frac{\sigma}{p\coth\theta}\left(\frac{\partial\beta^2}{\partial\sigma}\right)_p. \tag{48}$$

Type 2. Intersections of

$$(0_n')_T - 0_c \text{ at } \sigma = \sigma_0 = \sqrt{\frac{p^2}{4} + 1} - \frac{p}{2}\text{ ; type } 2_n'$$

$$(0_n)_T - 0_c' \text{ at } \sigma = -\sigma_0\text{ ; type } 2_n.$$

$\beta^2 \neq 0$

Define λ_0 as a root of

$$\sigma_0 = \frac{-1}{|\lambda_0|}\left[1 - (1 - \lambda_0^2)\left(\frac{r_0}{F^{-1}(\lambda_0)}\right)^2\right], \tag{49}$$

with the following convention: for $2_n'$, λ_0 is negative and the n^{th} branch of $F^{-1}(\lambda_0)$ is used; for 2_n, λ_0 is positive and the n^{th} branch of $F^{-1}(\lambda_0)$ is used. Now

$$\beta^2 = \frac{|\lambda_0|}{\sigma_0}. \tag{50}$$

Near cut-off

$$\beta^2 = \frac{|\lambda_0|}{\sigma_0} + \frac{r_0}{A}\sqrt{\sigma_0\frac{1+\sigma_0^2}{1-\sigma_0^2}}\sqrt{\frac{\sigma_0 - |\sigma|}{1 + |\lambda_0|\sigma_0}}. \tag{51}$$

with

$$(1 - \lambda_0^2)A = \frac{1}{2|\lambda_0|}\left(1 - \frac{r_0^2}{1 + |\lambda_0|\sigma_0}\right)(\sigma_0 + 2|\lambda_0| + \sigma_0\lambda_0^2) + \frac{1 + \sigma_0|\lambda_0|}{\lambda_0}.$$

For 2_0 a special situation arises for $1 < r_0 < u_1$ where there are two positive solutions for λ_0. We write 2_{01} and 2_{02} for the points corresponding to the smaller and greater of these. A special cut-off point will be labeled $2_{0\infty}$ and arises from $0_c'$ and $(0_0)_T$ as λ_1 goes to infinity. For this point

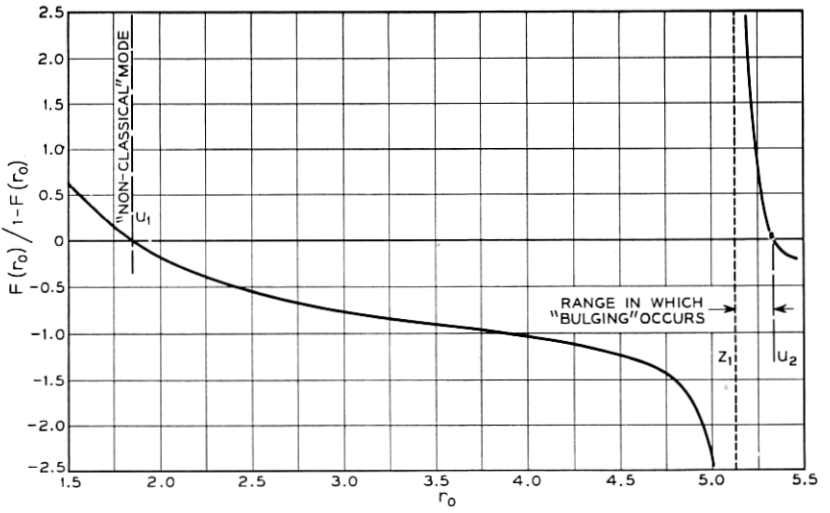

Fig. 15 — The function $\dfrac{F(r_0)}{1 - F(r_0)}$, related to cutoff of Type 3.

$\tau = \sigma_0$, $\beta^2 \to \infty$ and near $-\sigma_0$ we have

$$\beta^2 = \frac{|\, p \,|}{r_0^2(|\, \sigma_0 \,| - |\, \sigma \,|)} \frac{1}{(2 - |\, p \,||\, \sigma_0 \,|)} . \tag{52}$$

Type 3. Intersections of $I_B - (I_A)_\tau$; for $-\sigma_0 < \sigma < 0$ only; no subscript is needed.

$$\beta^2 = 0,$$

$$\sigma = -1 - p,$$

and

$$\frac{(\partial\beta^2)}{(\partial\sigma)_p} = \frac{(\partial\beta^2)}{(\partial p)_\sigma} = \frac{1}{p} \frac{F(r_0)}{1 - F(r_0)} \qquad \text{(see Fig. 15)} \tag{54}$$

The cut-off points of the modes follow various schemes in different ranges of σ as indicated below.

For $\sigma > \sigma_0$ we have Table I. When $\sigma < -\sigma_0$, $1_n'$ replaces 1_n in the Table I. "None" indicates that the mode exists, but has no cut-off.

For $0 < \sigma < \sigma_0$ we have Table II. "N.P." in Table II indicates that the mode is not propagated. For $-\sigma_0 < \sigma < 0$ we have Table III. In this range of σ one has also the mode without classical analogue. For $r_0 < u_1$ this is cut-off at 3 and 2_{01} and may have a second branch from 2_{02} to $2_{0\infty}$. For $r_0 > u_1$ the second branch only exists.

TABLE I

Mode / Radius	TE_{11}	TM_{11}	TE_{12}	TM_{12}	TE_{13} etc.
$r_0 < u_1$	1_1	1_2 ↘	1_3	1_4	1_5
$u_1 < r_0 < j_1$	None	1_1	1_2 ↓	1_3	1_4
$j_1 < r_0 < u_2$	None	None	1_2 ↘	1_3	1_4
$u_2 < r_0 < j_2$	None	None	None	1_2	1_3
$j_2 < r_0 < u_3$	None	None	None	None	1_3
etc.					

II. *Asymptotes, genesis of the modes and spot points*

For $|\sigma| \to \infty$ there are asymptotic formulae:

For TE_{1n}-modes

$$\beta^2 \to \left(1 - \frac{u_n^2}{r_0^2}\right)\left(1 + \frac{p}{\sigma}\right). \tag{55}$$

For TM_{1n}-modes

$$\beta^2 \to \left(1 - \frac{j_n^2}{r_0^2}\right) + \frac{p}{\sigma}. \tag{56}$$

For $|\sigma| > \sigma_0$, all modes have their origin in the points $\sigma = 1, \lambda_1 = 1$ or $\sigma = -1, \lambda_2 = -1$, where $\beta^2 \to \infty$. The variation of β^2 with σ in the neighborhood of these points is described by the two expansions:

for $\sigma \sim 1$

$$\beta_n^2 = \frac{p}{a_n + 1}\left[\frac{1}{\sigma - 1} + \left\{\frac{1 - a_n}{p} + \frac{2a_n^2}{x_n^2}\left(\frac{2}{p} + 1\right) + \frac{a_n^2}{2}\right\} + 0(\sigma - 1)\right], \tag{57}$$

where

$$\frac{a_n}{a_n + 1} = \frac{x_n^2}{2r_0^2},$$

and

$$F(x_n) = 1 \qquad x_n > 0,$$

with the scheme

n	1	2	3	4 etc.
Mode	TE_{11}	TM_{11}	TE_{12}	TM_{12} etc.

TABLE II

Mode / Radius	TE_{11}	TM_{11}	TE_{12}	TM_{12}	TE_{13} etc.
$0 < r_0 < u_1$	N.P.	N.P.	N.P.	N.P.	N.P.
$u_1 < r_0 < j_1$	$2_0'$	N.P.	N.P.	N.P.	N.P.
$j_1 < r_0 < u_2$	$2_0'$	1_1 ↘	N.P.	N.P.	N.P.
$u_2 < r_0 < j_2$	$2_0'$	$2_1'$	1_1 ↓	N.P.	N.P.
$j_2 < r_0 < u_3$	$2_0'$	$2_1'$	1_1 ↘	1_2	N.P.
$u_3 < r_0 < j_3$ etc.	$2_0'$	$2_1'$	$2_2'$	1_1	1_2

TABLE III

Mode / Radius	TE_{11}	TM_{11}	TE_{12}	TM_{12}	TE_{13} etc.
$0 < r_0 < u_1$	N.P.	N.P.	N.P.	N.P.	N.P.
$u_1 < r_0 < j_1$	3 ↓	N.P.	N.P.	N.P.	N.P.
$j_1 < r_0 < u_2$	3 ↘	$1_1'$	N.P.	N.P.	N.P.
$u_2 < r_0 < j_2$	2_1	3 ↓	$1_1'$	N.P.	N.P.
$j_2 < r_0 < u_3$	2_1	3 ↘	$1_1'$	$1_2'$	N.P.
$u_3 < r_0 < j_3$ etc.	2_1	2_2	3	$1_1'$	$1_2'$

for $\sigma \sim -1$

$$\beta_n^2 = \frac{p}{a_n + 1}\left[\frac{1}{\sigma + 1} + \left\{\frac{1 - a_n}{p} + \frac{2a_n^2}{y_n^2}\left(1 - \frac{2}{p}\right) - \frac{a_n^2}{2}\right\} + 0(\sigma + 1)\right], \tag{58}$$

where

$$\frac{a_n}{a_n + 1} = \frac{y_n^2}{2r_0^2},$$

and

$$F(y_n) = -1,$$

with the same identification as above.

For $\sigma > \sigma_0$ a spot-point is given by $I_n - (I_B)_T$ with

$$\beta^2 = \lambda_1 = 1 + \frac{p}{1+\sigma},$$

and (59)

$$\frac{1-\lambda_1^2}{1-\sigma\lambda_1} = \frac{j_n^2}{r_0^2},$$

The identification scheme is again that shown above.

For $-\sigma_0 < \sigma < 0$ an isolated identifiable point arises from I_B'-$(I_n)_T$ which is expressible in inverse form by the relations

$$\sigma = \frac{1-\frac{r_0^2}{j_n^2}}{\beta^2} + \frac{r_0^2}{j_n^2}\beta^2 \qquad \text{and}$$
$$p = (\beta^2-1)\left[1 + \frac{r_0^2}{j_n^2}\beta^2 + \frac{1-\frac{r_0^2}{j_n^2}}{\beta^2}\right] \tag{60}$$

for

$$1 - \frac{j_n^2}{r_0^2} < \beta^2 < \sqrt{1-\frac{j_n^2}{r_0^2}}.$$

The identification of the modes with n proceeds as in the earlier parts of this section.

III. *Small p.*

To order p^2 there exist the following expansions for β^2: for the TE_{1n}-mode

$$\beta^2 = \beta_0^2 + \frac{\beta_0^2}{1-\sigma^2}\left[\frac{2}{u_n^2-1} - \sigma\right]p + \frac{2\beta_0^2}{(1-\sigma^2)^2} \cdot \frac{\beta_0^2}{(u_n^2-1)^2} + \frac{5+5u_n^2-2u_n^4}{4(u_n^2-1)} \cdot \frac{}{(\beta_0^2-1)(1-u_n^2)} p^2 \ldots, \tag{61}$$

where

$$\beta_0^2 = 1 - \frac{u_n^2}{r_0^2}.$$

For the TM_{1n}-modes

$$\beta^2 = \beta_0^2 - \frac{\sigma}{1-\sigma^2}p + \frac{1}{(1-\sigma^2)^2}\frac{3\beta_0^2-2}{2(1-\beta_0^2)}p^2 \ldots, \tag{62}$$

where

$$\beta_0^2 = 1 - \frac{j_n^2}{r_0^2}.$$

The radius of convergence of these series is not known. It is clear that it will depend on σ and will become smaller as $\sigma^2 \to 1$.

4.2. *The Plasma* ($\rho_H = 0$, $\nu_H = 1$). The characteristic equation (26) may now be written

$$\frac{1}{\chi_1^2}[\lambda_1 F_n(\chi_1 r_0) - n] = \frac{1}{\chi_2^2}[\lambda_2 F_n(\chi_2 r_0) - n], \tag{63}$$

where (in contrast with the ferrite case) $\lambda_{1,2} = \beta\Lambda_{1,2}$. The λ satisfy

$$\lambda_{1,2}^2 - \frac{(\nu_E - 1)(1 - \beta^2/\nu_E) - \nu_E\rho_E^2}{\rho_E}\lambda_{1,2} - \beta^2 = 0, \tag{64}$$

and the χ's are given by

$$\chi_{1,2}^2 = (1 - \beta^2/\nu_H) - \rho_H\lambda_{1,2} \tag{65}$$

From the equations for ρ_E and ν_E in terms of σ, q given in Section 2, equation (64) may be written

$$\lambda_{1,2}^2 - \left(\frac{\sigma}{1 - q^2} - \sigma\beta^2\right)\lambda_{1,2} - \beta^2 = 0, \tag{66}$$

or

$$\lambda_1\lambda_2 = -\beta^2 \tag{67a}$$

$$\begin{aligned}\lambda_1 + \lambda_2 &= \frac{\sigma}{1 - q^2} - \sigma\beta^2, \\ &= \frac{\sigma}{1 - q^2} + \sigma\lambda_1\lambda_2.\end{aligned} \tag{67b}$$

Elimination of β^2 between equations (64) and (65) enables us to express $\chi_{1,2}^2$ solely in terms of $\lambda_{1,2}$, ρ_H and ν_H:

$$\chi_{1,2}^2 = \frac{1 - \lambda_{1,2}^2}{1 - \dfrac{1 - 1/\nu_E}{\rho_E}\lambda_{1,2}},$$

which, from the plasma formulae for ρ_E, ν_E, can be written

$$\chi_{1,2}^2 = \frac{1 - \lambda_{1,2}^2}{1 - \sigma\lambda_{1,2}}. \tag{68}$$

With these expressions for the χ, the characteristic equation (63) takes the form

$$H(\lambda_1, \sigma, r_0) = H(\lambda_2, \sigma, r_0),$$

where

$$H(\lambda, \sigma, r_0) = \frac{1 - \sigma\lambda}{1 - \lambda^2}\left[\lambda F_n\left(r_0\sqrt{\frac{1 - \lambda^2}{1 - \sigma\lambda}}\right) - n\right]. \tag{69}$$

For given σ, and q, equations (67b) and (69) are simultaneous equations for λ_1, λ_2. When λ_1, λ_2 have been found, $\beta^2 = -\lambda_1\lambda_2$ is known. Since β^2 must be positive, λ_1, λ_2 must have opposite signs. As in the ferrite, the convention $\lambda_1 > 0$, $\lambda_2 < 0$ will be adopted. Equation (67b) will hereafter be called the plasma relation. The transformation

$$\lambda_1 \rightarrow -\lambda_2, \qquad \lambda_2 \rightarrow -\lambda_1, \qquad \sigma \rightarrow -\sigma$$

leaves the plasma relation unchanged and changes n to $-n$ in the H-equation. As more fully explained in connection with the ferrite section, it is therefore necessary to consider positive n only if σ is allowed to take on negative as well as positive values. As before, only the first azimuthal mode number ($n = \pm 1$) is considered in this paper.

The method of analysis is the same as that used for the ferrite. Here we shall only sketch the most important steps; the reader will have no difficulty in completing the analysis by referring to Section 4.11. For fixed r_0, a contour map of H is drawn in the λ, σ plane (see Fig. 16 drawn for $r_0 \sim 2.2$). The gross features of this map are determined by the lines $H = 0$, $H = \pm\infty$. For greater detail recourse is had to the lines $\dfrac{1 - \lambda^2}{1 - \sigma\lambda} = \text{constant}$, along which values of H are readily generated. Further help is obtained from a knowledge of the location of the saddle point of H. The infinity curves are given by the same formulae as for the ferrite, except that the line $\lambda = 0$ is no longer an infinity line: along $\lambda = 0$, $H = -1$. Zero curves are given by

$$\sigma = \frac{1}{\lambda} - \frac{r_0^2(1 - \lambda^2)}{\lambda[F^{-1}(\lambda^{-1})]^2}.$$

The branches of $\sigma\lambda = 1$ are also zero curves in the same restricted sense as for the G function. In the same notation as for the ferrite, all I_n curves pass through $\sigma = 1$, $\lambda = 1$; all I_n' curves through -1, -1. The same is true for all 0_n, $0_n'$ curves ($n > 0$). The only exception is denoted by 0_0, it arises from that branch of F^{-1} along which $F^{-1}(1) = 0$.

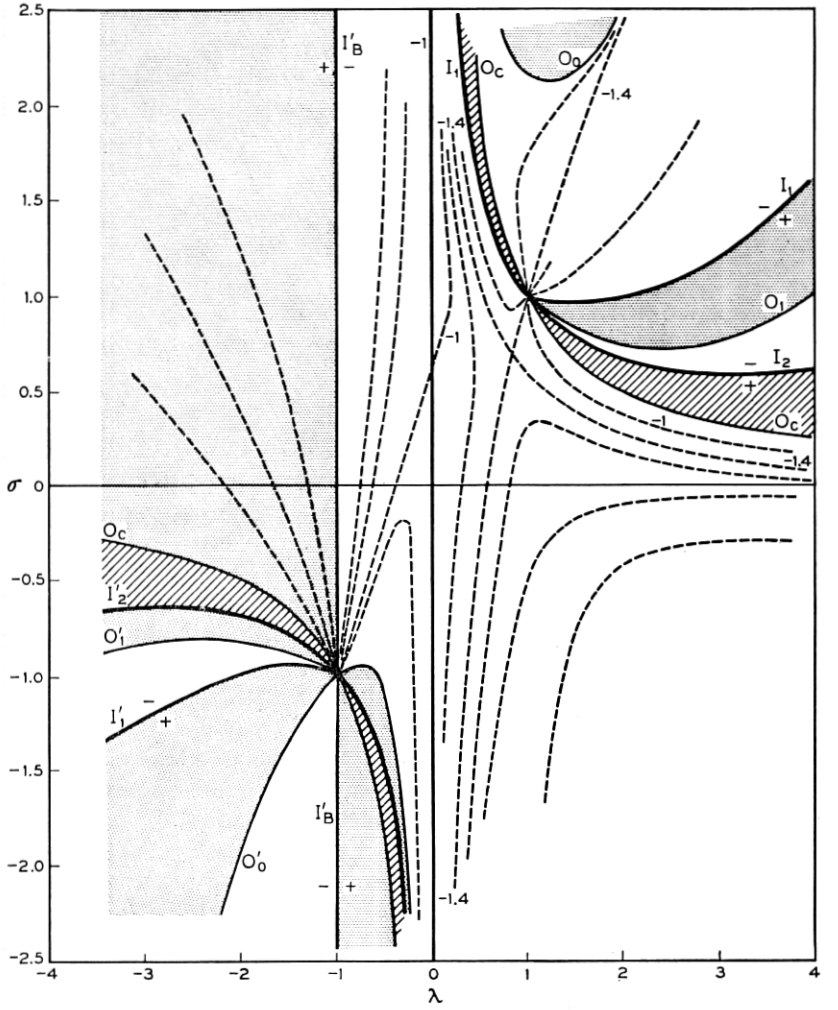

Fig. 16 — The division of the $\lambda - \sigma$ plane into regions of positive and negative H by the first few O and I curves. Dotted regions are positive. Cross-hatched regions contain the higher O and I curves.

Along all lines, $\sigma = \lambda c + d$, H tends to infinity except when $c = r_0^2/u_n^2$ (the slopes of the linear asymptotes of 0 curves). Along $\sigma = \dfrac{r_0^2}{u_n^2}\lambda + d$, H tends to a value depending on d. More about the general behavior of H can be derived by means entirely analogous to those employed in the study of G.

λ-pairs determined from the H-diagram do not necessarily solve the problem, since for a fixed q, they may not satisfy the plasma relation (67b). To take it into account, we interpret it as a transformation of the whole of the second quadrant onto part of the first, and of the whole fourth quadrant on part of the third. Writing (67b) in the form

$$\lambda_1 = \frac{1}{\sigma} + \frac{1}{\sigma}\frac{\dfrac{\sigma^2}{1-q^2} - 1}{1 - \sigma\lambda_2} = T(\lambda_2),$$

we see that the curves $\lambda_2 = \text{const.}$ transform into a bundle of hyperbola passing through the intersection of $\sigma^2 = 1 - q^2$ with $\sigma = 1/\lambda$, that is, through

$$\lambda_{10} = \frac{1}{\sqrt{1-q^2}}, \qquad \sigma_0 = \sqrt{1-q^2}.$$

These hyperbolae have vertical asymptotes $\lambda_1 = -\dfrac{1}{\lambda_2}$, and cut the line $\sigma = 0$ in $-\lambda_2$. For a fixed positive $\sigma < \sigma_0$, λ_1 decreases from $1/\sigma$ to $\sigma/(1-q^2)$ as λ_2 increases from $-\infty$ to 0, but, when $\sigma > \sigma_0$, λ_1 increases from $1/\sigma$ to $\sigma/(1-q^2)$. Thus the second quadrant transforms into the region between $\sigma = \lambda(1-q^2)$ and $\sigma = 1/\lambda$ in the first quadrant. Similarly, the inverse transformation $\lambda_2 = T(\lambda_1)$ transforms the fourth quadrant into the region between $\sigma = \lambda(1-q^2)$ and $\sigma = 1/\lambda$ in the third quadrant. Points outside these regions cannot be site of acceptable solutions of the H equation. In order to locate acceptable solutions, the H = equation is now written in the form

$$H(\lambda_1, \sigma, r_0) = H(T(\lambda_1), \sigma, r_0)$$

when $\sigma > 0$, and in the form

$$H(\lambda_2, \sigma, r_0) = H(T(\lambda_2), \sigma, r_0)$$

when $\sigma < 0$. These equations represent the curves of intersection of the H-surfaces. Along each such curve, both H-equation and plasma relation are satisfied. Their projections onto the first (or third) quadrant give λ_1 (or λ_2) as a function of σ, and hence λ_2 (or λ_1) from the plasma relation. Thus $\beta^2 = -\lambda_1\lambda_2$ is known along each solution curve. The rough locating of the solution curves, and the establishment of precise analytical formulae near special points on them proceeds in complete analogy with the ferrite case. Here we shall consider only the radius $r_0 \sim 2.2$, as typical of radii large enough to permit propagation of the TE_{11} mode

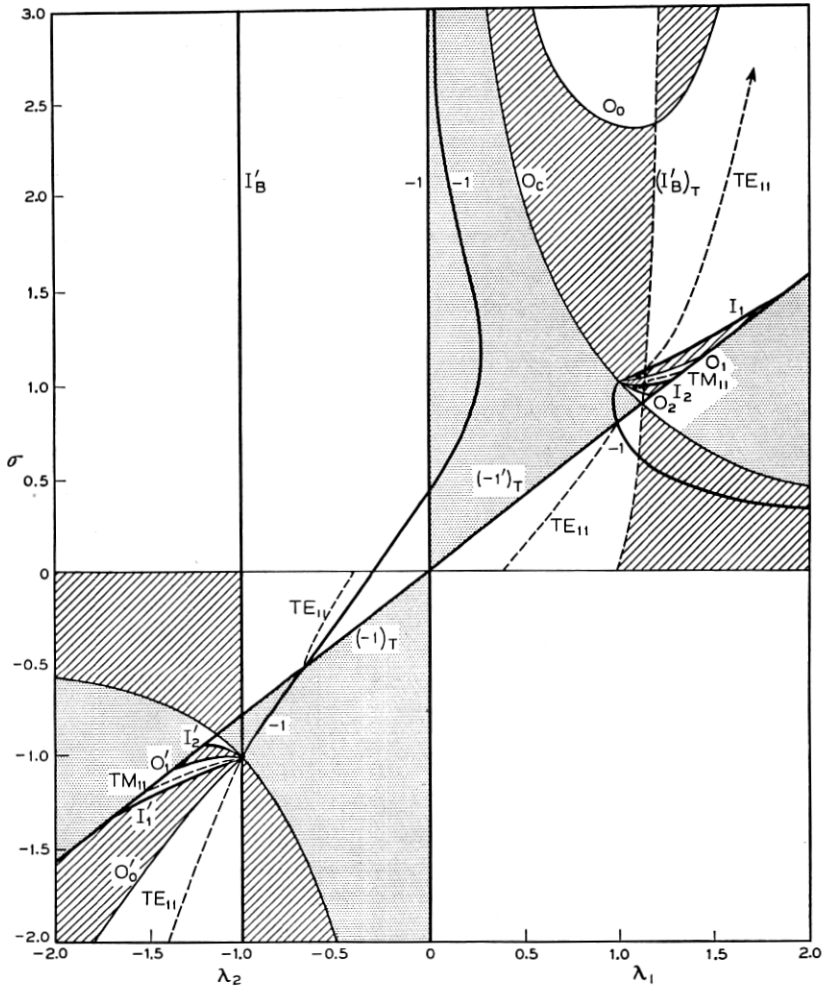

Fig. 17 — Geometrical exploration of solution curves for the plasma. The dotted regions are excluded by the plasma relation; the cross-hatched regions are those in which $H(\lambda, \sigma)$ and $H(T(\lambda), \sigma)$ have unlike sign. Solution curves may lie only in unshaded parts of the 1st and 3rd quadrants. $q^2 = 0.25$, $r_0 \sim 2.0$.

through the unmagnetized plasma, but too small to admit higher modes. The solution curves for $r_0 \sim 2.2$ are indicated roughly in Fig. 17.

In the first quadrant, for $\sigma > \sigma_0$, a solution curve starts at $\lambda_1 = 1$, $\sigma = 1$, passes through the intersection of I_1, $(I_B')_T$ and proceeds to infinity as indicated. The formulae in Section 4.21 describe the corresponding curve near $\sigma = 1$, and at $\sigma \to \infty$, showing that the solution

curve describes the TE_{11}-limit mode. Incipient modes also exist, just as in the ferrite; their end-points on $\sigma = (1 - q^2)\lambda_1$ (or, briefly, on $(\lambda_2 = 0)_T$) are now the points for which $H(\lambda_1, \sigma) = -1$ and, simultaneously, $\sigma = (1 - q^2)\lambda_1$.

Below σ_0, there is only one solution curve for $r_0 \sim 2.2$. It begins at $\sigma = 0$, $\lambda_1 = \beta_{iso}$ $(= -\lambda_2$, by the plasma relation), where β_{iso} is the propagation constant of the TE_{11} mode in the unmagnetized plasma. (In contrast with the ferrite, the plasma becomes isotropic as $\sigma \to 0$). It is cut off at the intersection of the contour $H(\lambda_1, \sigma) = -1$ in that region with $(\lambda_2 = 0)_T$. At that point $\beta^2 = 0$ and σ is best stated, thus:

$$\sigma = (1 - q^2)\sqrt{(1 + y^2)/[1 + (1 - q^2)y^2]},$$

where y is the (unique) real root of

$$F(jyr_0) = \sqrt{(1 + y^2)[1 + (1 - q^2)y^2]}.$$

Alternatively these two equations may (by varying y) be used to generate r_0's and the corresponding cut-off values of σ. Of course, the two equations are merely a re-statement of the equations $H(\lambda_1, \sigma) = -1$, $\sigma = \lambda_1(1 - q^2)$, heed being paid to the fact that the argument of F is imaginary in the region considered for the radius under discussion.

In the third quadrant for $\sigma < -\sigma_0$, we also find the TE_{11}-limit mode. Its solution curve begins at $\lambda_2 = -1$, $\sigma = -1$, and proceeds to $\sigma = -\infty$ without passing through any easily computed intersections of I curves. Formulae pertaining to the TE_{11} mode in this range are stated in Section 4.22. Again the incipient modes are found in their usual region. For $0 > \sigma > -\sigma_0$, the solution curve corresponding to the TE_{11} mode begins at $\sigma = 0$, $\lambda_2 = -\beta_{iso}(= -\lambda_1)$ and is cut off at the intersection of $H(\lambda_2, \sigma) = -1$ with $\lambda_2(1 - q^2) = \sigma$ (or $(\lambda_1 = 0)_T$). At that point $\beta^2 = 0$, and σ is given by

$$\sigma = -(1 - q^2)\sqrt{(1 - y^2)/[1 - (1 - q^2)y^2]},$$

where y is the least real root of

$$F(r_0 y) = -\sqrt{(1 - y^2)[1 - (1 - q^2)y^2]}.$$

Alternatively, this equation can be used to generate r_0, and the associated σ, if y is regarded as a parameter, which for $u_1 < r_0 < j_1$ is between zero and unity.

At a fixed r_0 the higher roots of the last equation with sign reversed and the corresponding σ are associated with the cut-offs of the incipient

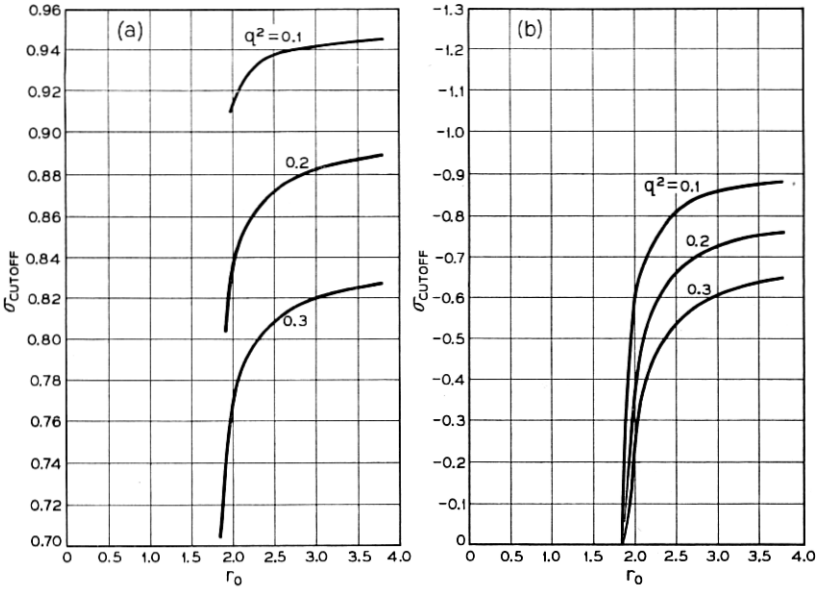

Fig. 18 — Cutoff value of σ for the TE_{11}-limit mode in the plasma as a function of r_0 for various q^2.

modes in the lower half plane. Similarly the real roots of

$$F(r_0 y) = -\sqrt{(1 - y^2)[1 - (1 - q^2)y^2]},$$

and the corresponding

$$\sigma = +(1 - q^2)\sqrt{(1 - y^2)/[1 - (1 - q^2)y^2]},$$

are associated with the cut-offs of the incipient modes in the upper half-plane. These equations have been solved for the TE_{11} mode and their solutions shown in Figs. 18(a) and 18(b).

4.21. *Some formulae relating to the plasma (chiefly for TE-modes).*

The formulas given here employ dimensionless variables (Section 3) except where otherwise stated.

Approximations for extreme values of σ or q^2

(a) small σ, q^2 not near unity

TE_{1m} mode:

$$\beta^2 = \beta_m{}^2 + A_m\sigma + B_m\sigma^2 + \cdots \qquad (70)$$

where

$$\beta_m^2 = 1 - \frac{u_m^2}{r_0^2},$$

$$A_m = \frac{2}{u_m^2 - 1}\frac{q^2}{1 - q^2}, \qquad \text{and}$$

$$B_m = -\frac{q^2}{(1 - q^2)^2}\left[1 + \frac{q^2}{u_m^2 - 1}\left\{\left(\frac{1}{2u_m^2} - 1\right)\beta_m^2 + \frac{4}{(u_m^2 - 1)^2}\left(1 - \frac{1}{2u_m^2}\right)\right\}\right].$$

TM modes show no first order variation with σ.

(b) small q^2, σ^2 not near unity. Here β_a and r_a are the actual propagation constant and radius, without scaling factors:

TE_{1m} mode:

$$\beta_a^2 = (1 - q^2)\omega^2\mu_0\epsilon_0 - \frac{u_m^2}{r_a^2} + \omega^2\epsilon_0\mu_0\frac{\sigma q^2}{1 - \sigma^2}\left(\frac{2}{u_m^2 - 1} - \sigma\right) + 0(q^4). \tag{71}$$

TM_{1m} modes:

$$\beta_a^2 = (1 - q^2)\omega^2\mu_0\epsilon_0 - \frac{j_m^2}{r_0^2} - \omega^2\epsilon_0\mu_0\frac{\sigma^2 q^2}{1 - \sigma^2}\left(1 - \frac{j_m^2}{\omega^2\mu_0\epsilon_0 r_a^2}\right). \tag{72}$$

(c) Approximation for large σ; q^2 not near unity.

TE_{1m} mode:

$$\beta^2 = \frac{1}{1 - q^2} - \frac{u_m^2}{r_0^2} - \frac{2q^2}{\sigma(1 - q^2)}\frac{1}{(u_m^2 - 1)}. \tag{73}$$

All formulae in (a), (b), (c) apply to both positive and negative σ (right and left circular waves). Formulae 70 and 73 show that the first order changes in β^2, whether due to very large or very small σ, have coefficients that differ only in sign.

The TE_{11} mode near resonance ($q^2 < 1$)

Near $\sigma = +1$,

$$\beta^2 = -\frac{q^2}{1 - q^2}\frac{\left(\frac{j_1^2}{2r_0^2} - 1\right)}{\sigma - 1} \tag{74}$$

Near $\sigma = -1$,

$$\beta^2 = \frac{-q^2}{1 - q^2} \frac{1}{1 + \sigma}. \tag{75}$$

Cut-off of the TE_{11} *mode* $(q^2 < 1)$ $(u_1 < r_0 < j_1)$

σ positive:

$$\beta^2 = 0; \qquad \sigma = (1 - q^2) \sqrt{(1 + y^2/[1 + (1 - q^2)y^2]}, \tag{76}$$

where y is the only real root or the smallest imaginary root of

$$F(jr_0y) = \sqrt{(1 + y^2)[1 + (1 - q^2)y^2]}.$$

σ negative:

$$\beta^2 = 0; \sigma = -(1 - q^2) \sqrt{(1 - y^2)/[1 - (1 - q^2)y^2]}, \tag{77}$$

where y is the smallest real root of

$$F(r_0y) = -\sqrt{(1 - y^2)[1 - (1 - q^2)y^2]}.$$

(See section 4.2 for further explanation).

APPENDIX I. THE F-FUNCTION

The function $F(x)$ has been defined by the equation

$$F(x) = x \frac{J_1'(x)}{J_1(x)}.$$

Using the infinite product for $J_1(x)$ and differentiating logarithmically one finds

$$F(x) = 1 - 2 \sum_{n=1}^{\infty} \frac{x^2}{j_n^2 - x^2}, \tag{78}$$

where $J_1(j_n) = 0$. Near one of its poles, j_n, $F(x)$ behaves as $j_n/(x - j_n)$. It is also useful to know the form of $F(x)$ near one of its zeros, u_n, which are also zeros of $J_1'(x)$. Such an expansion may conveniently be found by using the Ricatti equation satisfied by $F(x)$, which is

$$x \frac{dF}{dx} = 1 - x^2 - F^2. \tag{79}$$

The expansion near u_n is then

$$F(u_n + y) = y \left[\frac{1}{u_n} - u_n\right] - \frac{y^2}{2} \left[\frac{1}{u_n^2} + 1\right] + \text{higher terms.} \tag{80}$$

TABLE IV

Equation Number	Asymptote	Polder Transform of Asymptote	Range of Validity
83	$\sigma = -g\left[\lambda + F\left(\frac{r_0}{\sqrt{-g}}\right)\right]$	$\lambda = \frac{1+g}{\sigma} + O\left(\frac{1}{\sigma^2}\right)$	σ large, g finite and not equal to zero or $-r_0^2/j_n^2$
84	$\sigma = \frac{r_0^2}{j_n^2}\left(\lambda - \frac{2}{1 + \frac{j_n^2}{r_0^2} g}\right)$ $n = 1,2,3\cdots$	Not required	σ large, g unrestricted
85	$\sigma = \frac{1}{\lambda} + \frac{g^2}{r_0^2}\lambda$	Not required	Large σ Small λ $g > 0$ for $\lambda < 0$ $g < 0$ for $\lambda > 0$ g finite
86	$\sigma = \left(1 - \frac{r_0^2}{u_n^2}\right)\frac{1}{\lambda} + \frac{2\left(1 + \frac{u_n^2}{r_0^2} g\right)}{1 - u_n^2}\frac{r_0^2}{u_n^3}$ $n = 1,2,3\cdots$	$\sigma = \lambda\frac{r_0^2}{u_n^2} - p - \frac{2\left(1 + \frac{u_n^2}{r_0^2} g\right)}{u_n(1 - u_n^2)}\left(1 - \frac{r_0^2}{u_n^2}\right)$	σ large g finite

The equation may also be used to furnish an expansion near $x = 0$. This is

$$F(x) = 1 - \frac{x^2}{4} - \frac{x^4}{96} + \text{higher terms.} \tag{81}$$

Finally, putting $x = jy$, one finds from Eq. (79) for large y

$$F(jy) = y - \frac{1}{2} + \frac{3}{8}\frac{1}{y} + \text{higher terms.} \tag{82}$$

APPENDIX II. INFORMATION PERTAINING TO THE CONSTRUCTION OF G-DIAGRAMS

The accurate construction of the contours $G = \text{const.}$ is conveniently based on the contours $(1 - \lambda^2)/(1 - \sigma\lambda) = \text{const.}$ along any one of which G is a function of λ alone. These contours are shown in Fig. 4. Their asymptotic properties are almost self-evident.

The curves $G = g = \text{const.}$ have various asymptotes. These, together with their range of validity, and their Polder transforms where needed are stated in Table IV.

The formulas given in Table IV show that the curves $G = \text{const.}$ generally have two kinds of asymptotes; linear and hyperbolic. Formula (83) shows the behavior of G along a line of constant finite slope unequal to r_0^2/j_n^2, the asymptotic slope of the I_n curves. Parallel to a line of slope r_0^2/j_n^2 *all* G contours must be found, not just the restricted range given by the first formula. Writing $\sigma = (r_0^2/j_n^2)\lambda + x$ in the equation $G = g$, and expanding F near its pole j_n, we find x in terms of g and obtain (84) which holds for all g, from $-\infty$ to $+\infty$. When $g = 0$ it also gives the linear asymptotes of 0_n, $0_n'$ curves except 0_0, as is readily verified from the equation

$$\sigma = \frac{1}{\lambda} - \frac{r_0^2(1 - \lambda^2)}{\lambda[F^{-1}(\lambda)]^2},$$

for the zero curves.

Formula (85) shows how the G-contours tend towards $\sigma\lambda = 1$ from the side $\sigma\lambda > 1$ as $\lambda \to 0$.

Formula (86) relates the asymptotic behavior of the curves $G = g$ to the zero curves, $g = 0$, for small λ. All G curves approach zero curves arbitrarily closely as $\lambda \to 0$. The only exceptions are the infinity curves whose form near $\lambda = 0$ is

$$\sigma = \frac{1}{\lambda}\left(1 - \frac{r_0^2}{j_n^2}\right) \tag{87}$$

When $r_0 = u_{n+1}$, the 0_n curve merges with the $0_n'$ curve at

$$\sigma = \frac{-2}{(u_{n+1}^2 - 1)} \frac{r_0^2}{u_{n+1}^3}.$$

Similarly all of the contours $G = g$ of the sheet to which 0_n belongs merge with the corresponding $G = g$ of the sheet to which $0_n'$ belongs, at

$$\sigma = -\frac{2(1+g)}{(u_{n+1}^2 - 1)} \frac{r_0^2}{u_{n+1}^3}. \tag{88}$$

These remarks apply to all 0_n, $0_n'$ curves, 0_0 included.

The 0_0-curve, for large λ, behaves as

$$\sigma = \frac{1 - r_0^2}{\lambda},$$

and so tends to σ from above for $r_0 < 1$ and from below when $r_0 > 1$. (In fact, for $r_0 < 1$, 0_0 lies wholly in the first quadrant; when $u_1 > r_0 > 1$, 0_0 cuts $\sigma = 0$ once.)

The saddle points of G are most easily found by considering G in the coordinate net formed by the curves $\chi^2 = \text{const.}$ and $\lambda = \text{const.}$ At a saddle point

$$\frac{\partial G}{\partial \chi} = \frac{\partial}{\partial \chi}\left[\frac{1}{\chi^2}\left(\frac{1}{\lambda} F(r_0\chi) - 1\right)\right] = 0$$

and simultaneously

$$\frac{\partial G}{\partial \lambda} = 0$$

The only saddle points that might be missed in this way are points at which the two derivatives are not independent, that is points where the χ^2 contours have vertical tangents, and it is easily verified that no saddle points exist there.

Proceeding with the differentiations, we find that $\frac{\partial G}{\partial \lambda} = 0$ gives

$$F(r_0\chi) = 0$$

or

$$r_0\chi = u_n \tag{89}$$

and so $\frac{\partial G}{\partial \chi} = 0$ gives

$$\frac{2}{\chi} + \frac{r_0}{\lambda} F'(u_n) = 0$$

or

$$\lambda_{ns} = \frac{u_n^2 - 1}{2} \tag{90}$$

The corresponding σ_{ns} are given by

$$\frac{1 - \lambda_{ns}^2}{1 - \sigma_{ns}\lambda_{ns}} = \frac{u_n^2}{r_0^2} \tag{91}$$

and are all positive. Thus all saddle points lie in the first quadrant. At a saddle point $G = -r_0^2/u_n^2$ and therefore it is the intersection of two contours $G = -r_0^2/u_n^2$. For $n > 1$, one of these obeys the asymptotic formula (83), the other is asymptotic to I_n and I_{n-1} (see Fig. 5), and obeys (84), with n and $n - 1$, near those curves. For $n = 1$, one of them still follows formula (83), but the two "arms" of the other are asymptotic to $\sigma = 1/\lambda$ and I_1, and so follow (85) and (84) with $n = 1$ respectively.

Three further facts useful in the construction of G-diagrams are:

Along a curve $\dfrac{1 - \lambda^2}{1 - \sigma\lambda} = \dfrac{u_n^2}{r_0^2}$, G equals $-\dfrac{r_0^2}{u_n^2}$; thus the zero curves of F are contours of constant G.

Along $\lambda = +1$,

$$G = \frac{1 - \sigma}{2} - \frac{r_0^2}{4}. \tag{92}$$

As $\sigma, \lambda \to 1$ along $(\sigma - 1) = \alpha(\lambda - 1)$;

$$G \to \frac{\alpha + 1}{2}\left[F\left(r_0\sqrt{\frac{2}{\alpha + 1}}\right) - 1\right] \tag{93}$$

As $\sigma, \lambda \to -1$ along $(\sigma + 1) = \alpha(\lambda + 1)$;

$$G \to -\frac{\alpha + 1}{2}\left[F\left(r_0\sqrt{\frac{2}{\alpha + 1}}\right) + 1\right]$$

As for $G(T(\lambda), \sigma, r_0)$ we have, in addition to the asymptotic formulas in the table:

$$I_B' \text{ transforms into } = 1 + \frac{p}{\sigma + 1}.$$

The intersection of $(I_n)_T$ or $(I_n')_T$ with $\sigma = 0$ is given by

$$\lambda_{1,2} = p \pm \sqrt{1 - \frac{j_n^2}{r_0^2}}.$$

APPENDIX II. THE FIELD COMPONENTS

The field components are given here for the ferrite and for the plasma. They are normalized in such a way that E_z takes a simple form. It should be noted that the λ's appearing in these equations are those defined in Secs. 4.11 and 4.2 for the ferrite and plasma respectively and have a different significance in the two cases.

We write

$$A_1(r) = \frac{J_n(\chi_1 r)}{J_n(\chi_1 r_0)} \qquad A_2(r) = \frac{J_n(\chi_2 r)}{J_n(\chi_2 r_0)}$$

Then, for the ferrite,

$$E_z = [A_1(r) - A_2(r)]e^{jn\theta},$$

$$E_r = -j\beta\left[\frac{A_1(r)}{r}\frac{1}{\chi_1^2}\left\{F_n(\chi_1 r) - \frac{n}{\lambda_1}\right\} - \frac{A_2(r)}{r}\frac{1}{\chi_2^2}\left\{F_n(\chi_2 r) - \frac{n}{\lambda_2}\right\}\right]e^{jn\theta},$$

$$E_\theta = -\beta\left[\frac{A_1(r)}{r}\frac{1}{\chi_1^2}\left\{\frac{F_n(\chi_1 r)}{\lambda_1} - n\right\} - \frac{A_2(r)}{r}\frac{1}{\chi_2^2}\left\{\frac{F_n(\chi_2 r)}{\lambda_2} - n\right\}\right]e^{jn\theta},$$

$$H_z = j\beta\left[\frac{1}{\lambda_1}A_1(r) - \frac{1}{\lambda_2}A_2(r)\right]e^{jn\theta},$$

$$H_r = -\left[\frac{A_1(r)}{r}\frac{1}{\chi_1^2}\left\{n - \frac{1-\chi_1^2}{\lambda_1}F_n(\chi_1 r)\right\} - \frac{A_2(r)}{r}\frac{1}{\chi_2^2}\left\{n - \frac{1-\chi_2^2}{\lambda_2}F_n(\chi_2 r)\right\}\right]e^{jn\theta}, \text{ and}$$

$$H_\theta = -j\left[\frac{A_1(r)}{r}\frac{1}{\chi_1^2}\left\{F_n(\chi_1 r) - \frac{n}{\lambda_1}(1-\chi_1^2)\right\} - \frac{A_2(r)}{r}\frac{1}{\chi_2^2}\left\{F_n(\chi_2 r) - \frac{n}{\lambda_2}(1-\chi_2^2)\right\}\right]e^{jn\theta}$$

and, for the plasma,

$$E_z = [A_1(r) - A_2(r)]e^{jn\theta},$$

$$E_r = -\frac{j}{\beta}\left[\frac{A_1(r)}{r}\frac{1}{\chi_1^2}\{(1-\chi_1^2)F_n(\chi_1 r) + n\lambda_1\} - \frac{A_2(r)}{r}\frac{1}{\chi_2^2}\{(1-\chi_2^2)F_n(\chi_2 r) + n\lambda_2\}\right]e^{jn\theta},$$

$$E_\theta = \left[\frac{A_1(r)}{(r)}\frac{1}{\chi_1^2}\{\lambda_1 F_n(\chi_1 r) + n(1-\chi_1^2)\} - \frac{A_2(r)}{r}\frac{1}{\chi_2^2}\{\lambda_2 F_n(\chi_2 r) + n(1-\chi_2^2)\}\right] e^{jn\theta},$$

$$H_z = -\frac{j}{\beta}[\lambda_1 A_1(r) - \lambda_2 A_2(r)]\, e^{jn\theta},$$

$$H_r = -\left[\frac{A_1(r)}{r}\frac{1}{\chi_1^2}\{\lambda_1 F_n(\chi_1 r) + n\} - \frac{A_2(r)}{r}\frac{1}{\chi_2^2}\{\lambda_2 F_n(\chi_2 r) + n\}\right] e^{jn\theta},$$

and

$$H_\theta = -j\left[\frac{A_1(r)}{r}\frac{1}{\chi_1^2}\{F_n(\chi_1 r) + n\lambda_1\} - \frac{A_2(r)}{r}\frac{1}{\chi_2^2}\{F_n(\chi_2 r) + n\lambda_2\}\right] e^{jn\theta}$$

REFERENCES

1. Goldstein, L., Lampert M. A., and Heney, J. F., Phys. Rev., **82,** p. 956, 1951.
2. Polder, D., Phil. Mag., **40,** p. 99, 1949.
3. Hogan, C. L., B.S.T.J., **31,** p. 1, 1952.
4. Suhl H., and Walker, L. R., Phys. Rev., **86,** p. 122, 1952.
5. Kales, M. L., J. Appl. Phys., **24,** p. 604, 1953.
6. Gamo, H. J., J. Phys. Soc. Japan, **8,** pp. 176–182, 1953.
7. Cook, J. S., R. Compfner and H. Suhl, Letter to the Editor, I.R.E. Proc., to be published.